Process Intensification in Distillation Sequences(Dissertation_全文)

AUTHOR(S):

Jesús Rafael Alcántara Avila

CITATION:

Jesús Rafael Alcántara Avila. Process Intensification in Distillation Sequences. 京都大学, 2012, 博士(工学)

ISSUE DATE:

2012-09-24

URL:

https://doi.org/10.14989/doctor.k17164

Process Intensification in Distillation Sequences

Jesús Rafael Alcántara Avila

2012

Index

Chapter 1

Introduction

1.1 Research background

The two oil crises of the 1970s were turning points in which the world saw to use energy more efficiently. In Japan, since the first oil crisis in 1973, the use of energy has increased remarkably. The energy used in 1970 by the chemical industry represented 29% of the industrial sector which was 5.268 PJ, and in 2007 it increased to 38% which was 6.649 PJ[1]. The increment of energy consumption in the Japanese chemical industry has been steadily growing over the past decades, however, the depletion of fossil fuels, more strict environmental regulations, and the tough competition among enterprises in the international market have urged to use energy more efficiently. To secure a further development in the chemical industry, it is crucial to find novel structures and equipment, which can keep the energy consumption at the minimum while manufacturing goods.

Thorough assessment of the energy utilization in the United States showed that the chemical industry is the largest consumer of energy while the second largest is the petroleum refining industry with a use of 24% and 10%, respectively, of the total U.S. manufacturing energy use. Distillation accounts for 57% of the total energy used in the refining and chemical processing industries with approximately 40,000 distillation columns operating in over 200 different processes[2].

The reason why distillation is the major separation technology used in the chemical, petrochemical and refining industries is that it offers some appealing features:

1. It has good flexibility to cope with changes in production
2. It has relatively low capital investment compared with other separation technologies
3. It has low operational risk
4. It is a well known process that has been widely researched.

Unfortunately, the energy efficiency in a commercial distillation column is low with a thermodynamic efficiency of less than 10 percent being typical in conventional columns. Thus, distillation results in energy-intensive equipment, which further entails a high operation cost.

The low thermodynamic efficiency in conventional distillation is caused by the fact that energy must be supplied to the position in the column with the highest temperature, while energy must be removed from the position in the column with the lowest temperature. In addition, other types of thermodynamic inefficiency results from the mixing of liquid and vapor streams at each stage inside the column. In short, current distillation technologies for conventional columns have three major drawbacks: Large size, high energy consumption, and high operating cost.

1.2 Intensification of distillation columns

To alleviate high costs and energy requirements, process intensification has been suggested as an alternative to the proposal of new equipment structures and operating conditions. Colin Ramshaw, one of the pioneers in process intensification, defined it as a strategy for making dramatic reductions in the size of a chemical plant so as to reach a given production objective[3]. However, the benefits of process intensification have extended far beyond the original goal of reducing size. A later review offers a broader definition of process intensification as follows[4]:

Process intensification consists of the development of novel apparatuses and techniques that, compared to those commonly used today, are expected to bring dramatic improvements in manufacturing and processing, substantially decreasing equipment-size/production-capacity ratio, energy consumption, or waste production, and ultimately resulting in cheaper, sustainable technologies.

In addition, the enforcement of the following seven aspects would guide developments in Process intensification[4]:

1. *Capital investment reduction*
2. *Energy use reduction*
3. *Raw material cost reduction*
4. *Increased process flexibility & inventory reduction*
5. *Ever greater emphasis on process safety*
6. *Increased attention to quality*
7. *Better environmental performance*

Since the first oil crisis, the continuous depletion of fossil fuels along with the need to find energy-efficient sustainable processes have renewed the interest in distillation to find structures and operating conditions that can realize less operating cost and less energy consumption. Some

technologies have been advised to use energy more efficiently in distillation. Among the proposed technologies to intensify distillation columns we can find:

- Thermally coupled distillation
- Distillation with secondary reflux and vaporization (SRV)
- Vapor recompression
- External heat integration
- Heat-integrated distillation column (HIDiC)

Expensive sources of energy from fossil fuels encouraged the research in distillation to use energy more efficiently. Figure 1.1 shows the relation between the oil price[5] (vertical left axis) and the number of research publications in distillation[6] (vertical right axis).

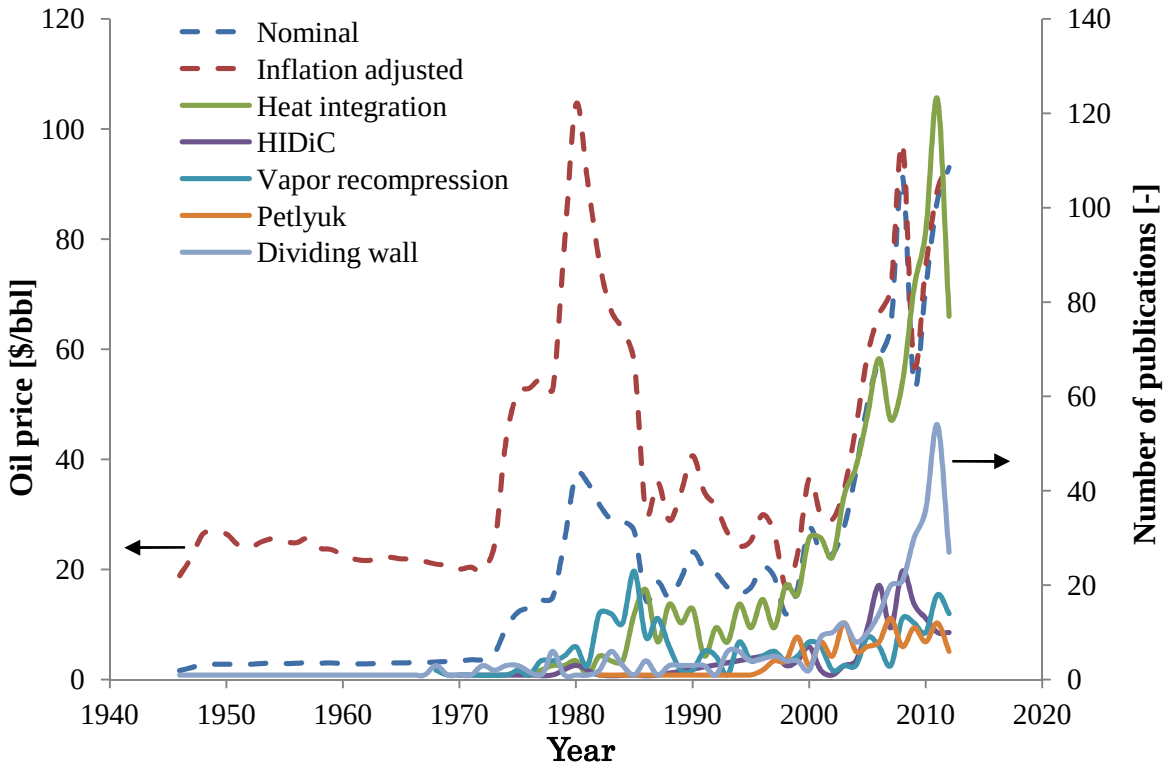

Figure 1.1. Transition of the oil price and the number of research publications in distillation

The blue dashed line in Figure 1.1 denotes the nominal oil prices while the red dashed line denotes the oil prices adjusted for inflation to December 2011. In addition, the solid lines in Figure 1.1 denote the number of published research papers in distillation from 1946 to 2012. These

numbers were obtained from the database Scopus[6] by entering the key words listed in the figure such us "HIDiC", "vapor recompression", etc. and the keyword "distillation".

From Figure 1.1, it becomes evident that the increase of oil prices increased the interest in intensified distillation columns. Also the research in distillation has been very extensive with more than 15,000 researches in distillation during the last 50 years according to a quick survey[6]; nevertheless, there are unexploited researches in distillation which are covered in this thesis. The next subsection will cover the aims for this thesis and explain briefly the unexploited areas in the synthesis problem to find optimal sequences of intensified distillation columns.

1.3 Aims for this thesis

Although many technologies have been used to modify the structure of conventional columns to increase their thermodynamic efficiency, there are some limitations in effectively implementing them in practice. In this thesis the following issues are covered:

1. Although several researches have found optimal solutions with heat integration between condensers and reboilers, there are few which consider heat integration between the intermediate stages in a distillation column. Moreover, when heat integration between stages has been addressed, the case studies have been based on the assumption of infinite number of stages or assumptions based on experience; therefore, a systematic optimization of the total cost has not been assessed.
2. In current researches, heat integration between stages has been limited to the stages between two predetermined sections (columns) because a large number of combinatorial problems arise in the synthesis problem of optimal distillation sequences. To solve the synthesis problem within a practical scope, an optimization procedure to find the optimal sequence among several columns is needed.
3. To reduce thermodynamic inefficiencies in conventional distillation, complex columns with multiple feeds and product streams have been proposed. However, the pressure of the vapor streams flowing between columns is at the same pressure, which drastically restricts the thermal capability to exchange energy within another part in complex columns. Thus, the synthesis problem to enhance the possibility to exchange energy in complex columns remains unsolved.
4. When compressors are included to find optimal solutions, the optimization criteria has been mainly the minimization of the energy consumption at the reboilers. Consequently, the

economic assessment of compressors in distillation columns has been ambiguous because the compressor equipment and electricity cost must not be neglected in the final design.

5. In practice, the economic optimization, which comprises the equipment cost and the operating cost, has been the main criterion to obtain optimal distillation sequences. However, as environmental restrictions become more severe, the minimization of CO_2 emissions or the toxic impact from chemical releases to the environment had been added as optimization criteria. In such circumstances, the optimization of individual criterion has been conveyed; however, the simultaneous optimization of several criteria in a multi-dimensional space remains to be addressed in distillation.

This thesis aims to deal with the unexploited issues in the synthesis problem of distillation sequences and to answer the unsolved synthesis problems when multiple optimization criteria are evaluated simultaneously. Systematic methodologies based on process simulations and optimization through mathematical programming, are adopted to search for optimal solutions.

The answers to issues 1 through 5 in this research lead to new energy-efficient and economical solutions, which have not been considered in previous researches. Thus, the proposed distillation structures and the combination of several energy conservation methods in distillation expand the feasible region to synthesize optimal distillation sequences leading to new research areas in distillation.

1.4 Organization of this thesis

The presented thesis covers the unexploited issues in the synthesis problem of intensified distillation sequences. The organization of this thesis consists of five chapters which are briefly described next. Chapter 1 states the importance of distillation in the chemical, petrochemical and process refining industries, some advantages, and disadvantages in distillation. Secondly, the process intensification, which is a dominant tool in tackling the disadvantages in distillation, is briefly explained. Finally, the aims of this thesis are explained.

Chapter 2 deals with the intensification of conventional distillation columns through internal and external heat integration. In addition to heat integration between condensers or reboilers (external heat integration), heat integration between intermediate stages in a column (internal heat integration) is considered. Any stage in a rectifying section (heat source stage) can supply energy to any stage in a stripping section (heat sink stage) of another column. To assess internal and external heat integration between two columns, a systematic procedure based on rigorous simulations and mathematical programming is developed. Rigorous simulations are executed for several columns

operating at different pressures, next a superstructure between any two columns is formulated through mathematical programming to find the best internal and external heat integration network, and then a superstructure which comprises all the distillation columns and feasible sequences is generated and solved through mathematical programming to find the best distillation sequence. This two-level optimization algorithm answers the two key points in the synthesis problem of distillation columns with internal heat integration: it finds the best heat integration network, and the best sequence of distillation columns. Finally, to obtain reliable results at a fixed number of stages, the concept of "contribution term" is proposed to estimate the changes of condenser and reboiler duties in a distillation column after internal heat integration. The results of the proposed estimation approach are compared with the exact solution obtained by executing rigorous simulations in order to validate its reliability.

Although heat integration is an alternative way to reduce the energy consumption in distillation, conventional columns entail thermodynamic irreversibility owing to the mixing of streams at different composition inside the column. Thus, thermally coupled distillation has been proposed as an alternative to reduce the irreversibility in conventional distillation. Thermal coupling can be realized in two ways: by removing the condenser in one column and connecting, at the top of that column, a side liquid stream from another column, or by removing the reboiler in one column and connecting, at the bottom of that column, a side vapor stream from another column.

Chapter 3 deals with conventional and thermally coupled columns. In addition, the synthesis problem of optimal compressor-aided distillation columns is addressed. Compressor-aided distillation regards the inclusion of compressors in distillation columns. The use of compressors is possible to recompress the top vapor stream of columns having condenser and the vapor streams linking two thermally coupled columns. Vapor recompression in conventional columns has been little researched while vapor recompression in thermally coupled columns remains unexploited. Vapor recompression of top streams to condensers can be beneficial to realize external heat integration between the recompressed vapor stream and the bottom liquid stream of a reboiler. Thus, a comparison between distillation sequences with internal and external heat integration and distillation sequences with external and/or internal heat integration with vapor recompression is conveyed in conventional columns to study the economic and energy attractiveness in each process intensification technology. Later, the inclusion of compressors in thermally coupled columns is considered. Typically, linking vapor streams between columns are at the same pressure; therefore, the resulting sequence operates at the same pressure, however, this restriction drastically limits the heat exchange in thermally couple distillation because energy is added at the highest temperature and removed at the lowest temperature, thus the pressure change of vapor streams to condensers or between thermally couple columns can exploit the heat integration capability in thermally coupled columns. To obtain compressor-aided optimal sequences, a systematic procedure based on rigorous

simulation and mathematical programming is developed. Rigorous simulations are executed for several conventional or thermally coupled columns operating at different pressure. In case of thermally coupled columns, the flow rate of linking streams is optimized. Next a superstructure which is comprised of columns at several discrete pressures with or without vapor recompression is formulated and solved through mathematical programming to find the best distillation sequence which realizes the minimum total annual cost. This simulation-optimization based algorithm answers the key points in the synthesis problem of compressor-aided distillation columns: it finds the best heat integration network with vapor recompression, and more "flexible" thermally coupled sequences with pressure change. Finally, the concept of "contribution term" developed in Chapter 2 is extended to estimate the changes of internal vapor and liquid flow rates in a distillation column after internal heat integration. This estimation approach is compared with the exact solution from rigorous simulation to validate its accuracy.

The synthesis problem of distillation sequences has primarily adopted the total annual cost as the optimization criteria to find optimal solutions; however, the enforcement of more strict environmental restrictions to lower the CO_2 emission and releases of toxic chemicals has urged the consideration of environmental impact as optimization criterion to find optimal distillation processes. When optimization procedures are taken, only one criterion is optimized. Thus, the simultaneous evaluation of multiple criteria in the synthesis problem has not been comprehensibly exploited.

Chapter 4 comprises conventional and thermally coupled columns as distillation candidates where vapor recompression is possible. Because compressor have expensive equipment and electricity costs, they must be included to perform the economic optimization. On the other hand, recompression of vapor streams can result in attractive solutions to reduce the energy consumption; this situation must be considered to perform the optimization of energy requirement. This chapter deals with multi-objective optimization of compressor-aided distillation sequences to readily assess the trade-off between cost and energy consumption, i.e. the cost increase per unit amount of energy consumption reduced in a distillation sequence. To solve multi-objective optimization problems, one way is to adopt a weighted sum of optimization criteria; however, this approach has two major limitations: it cannot find solutions in non-convex regions, and it cannot generate evenly distributed Pareto fronts. To overcome these limitations, a min-max weighted sum combined with and adaptive algorithm was adopted to find Pareto-optimal solutions. At a later part in the chapter, an extension to the simultaneous optimization of three criteria is carried out: the minimization of total annual cost, human toxicity and CO_2 emissions. To obtain compressor-aided Pareto-optimal solutions, and the trade-off between optimization criteria, a systematic procedure based on rigorous simulation and mathematical programming same as the one in Chapter 3, but consideration of several optimization criteria is developed. The proposed procedure answers the key points in the synthesis problem of

Pareto-optimal distillation sequences: It readily finds the trade-off in conflicting objectives, and it can find well-distributed Pareto optimal solutions in non convex regions of the Pareto front.

Finally, Chapter 5 summarizes the conclusions from chapter 2 through 4, and the main results from this thesis. A comparison between optimal solutions in current synthesis problems and optimal solutions in the presented simulation-optimization based synthesis problems is conducted to prove that this work covers regions not considered by previous synthesis problems and to emphasize that this work can effectively find economic and environmental optimal solutions.

Reference literature

(1) **Agency for Natural Resources and Energy, Ministry of Economy, Trade and Industry**, "Energy in Japan 2010",Tokyo, Japan, 2010.

http://www.enecho.meti.go.jp/topics/energy-in-japan/english2010.pdf, visited August 1st 2012.

(2) **U.S. Department of Energy, Office of Energy Efficiency and Renewable Energy**, "Hybrid Separations/Distillation Technology: Research Opportunities for Energy and Emissions Reduction", Washington, D.C., 2005. Visited August 1st 2012.

http://www1.eere.energy.gov/manufacturing/industries_technologies/chemicals/pdfs/hybrid_separation.pdf, visited August 1st 2012.

(3) Ramshaw, C. The incentive for process intensification. *Proceedings, 1st Intl. Conf. Proc. Intensif. for Chem. Ind.* **1995**, 18, BHR Group, London, 1.

(4) Stankiewicz, A.I.; Moulijn, J.A. Process intensification: transforming chemical engineering. *Chem. Eng. Progress* **2000**, 96, 22–34.

(5) **Historical Crude Oil Prices (Table)**, http://inflationdata.com/inflation/inflation_Rate/Historical_Oil_Prices_Table.asp, visited August 1st 2012.

(6) **Scopus document search**, http://www.scopus.com/home.url, visited August 1st 2012.

Chapter 2

Intensification of conventional distillation sequences

2.1 Introduction

Conventional columns (a single feed and two product streams) are dominant in the chemical industry, but they need a large amount of energy resulting in high operating cost. Therefore, recent developments in energy conservation methods have sought out heat integration as an attractive energy-efficient alternative to reduce the energy consumption in conventional distillation although the determination of the best heat integration network is not an easy task. Thus, in this chapter a two-level hierarchical optimization algorithm is proposed to readily synthesize distillation sequences where external and internal heat integration is possible. At each optimization level superstructure representations and mathematical programming formulations are adopted to solve the synthesis problem.

2.2 Internal and external heat integration in conventional columns

The energy conservation method primarily used in the distillation processes has been external heat integration which regards top vapor streams to condensers as heat sources and bottom liquid streams to reboilers as heat sinks. To generate distillation processes with external heat integration, several superstructure-based deterministic approaches[1, 2] and stochastic approaches[3] have been proposed. In those studies, the total annual cost (TAC) was adopted as the objective function to be minimized.

As another alternative to reduce the energy consumption in distillation, recently studies and development efforts have envisioned internal heat integration which regards vapor in rectifying sections as hot streams and liquid in stripping sections as cold streams. The energy exchange between the rectifying and stripping sections in a distillation column can be accomplished either by changing the pressure between sections,[4] i.e. Heat Integrated Distillation Column (HIDiC), or by means of side condensers and/or side reboilers.[5]

Internal heat integration by recompressing a vapor stream between the rectifying and stripping sections has been intensively researched during last two decades and has proven to be an energy-efficient design with less energy consumption, between 30 to 60% compared to its conventional counterparts. Such researches are dominated by simulation-based approaches, for example, those which were applied to the separation of close-boiling binary mixtures,[6] a pilot-scale plant,[7] and ternary mixtures.[8]

The comparison of energy consumption is not enough to show the effectiveness of HIDiC, because the HIDiC needs the high construction cost due to the complex column structure and the high equipment and operation costs in compressors. Thus, TAC has been adopted as the objective function to compare the conventional columns and HIDiCs for close-boiling binary[9] and ternary[10] mixtures. The results showed that HIDiC could reduce the operating cost (utilities and electricity) up to 50%, but increased the fixed cost (vessel, trays, heat exchangers, and compressor) from 10 to 20%. Cabrera-Ruiz et al.[11] studied several ternary mixtures with different feed compositions and volatility ratios between adjacent components based on rigorous simulations in Aspen Plus. After extensive simulations, they concluded that HIDiCs reduced the reboiler duty in most cases, but electricity and compressor cost dominated the operating and fixed cost in several scenarios.

To avoid the use of compressors, Nakaiwa et al.[12] proposed the use of heat exchangers between stages in stripping and rectifying sections operating at different temperatures. This idea was applied to the separation of an ideal ternary mixture[5] by matching the rectifying section of a high pressure column with the stripping section of another lower pressure column; this heat-integrated column was termed as externally heat-integrated double distillation column (EHIDDiC). They performed sensitivity analyses to obtain feasible sequences with minimum TAC and compared EHIDDiC and conventional sequences. They showed that EHIDDiC was the best option for the direct sequence, and external heat integration was the best option for the direct sequence. In the later work[13], they proposed an internal heat integration network which has three side heat exchangers between the sections in EHIDDiC. Their work proposed a sequential procedure having four steps to minimize the TAC. At the first step, a distillation sequence without internal heat integration was generated. Then, one heat exchanger was set between the top stages of the high and low pressure columns, the second between a middle stage of the high and low pressure columns, and the last one between the bottom stages of the high and low pressure columns. At the third step, the location of the top stage in the high pressure column and that of the bottom stage in the low pressure columns were fixed whereas the other four stages were varied to find the best heat integration network. Finally, for the best network, the heat exchangers area was optimized. This procedure was applied to the two column process separating binary mixture. The results showed that the simplified EHIDDiC realized the lowest TAC. In addition, an extension to ternary mixtures was conveyed by including an internally heat integrated column between the columns of the conventional sequence[14]. The synthesis procedure was based on

process simulations and applied to two case studies. The results showed that energy savings around 17% were attained when the entropy production was the minimum.

Most of the papers reviewed in this section selected the best internal heat integration network by trial-and-error or sequential procedures based on general model simplifications such as ideal mixture and 100% tray efficiency. In this research, a systematic procedure based on MILP formulations combined with rigorous simulations is proposed. In the proposed procedure, economically optimal solutions are derived by considering external and internal heat integration simultaneously. A hierarchical optimization algorithm consisting of three levels is adopted. At the first level, for each pair of columns, the best internal heat exchange structure is obtained. At the second level, the best external heat exchange network is derived by taking into account the external heat exchange between top vapor streams and liquid bottom streams of all the candidate columns. For these two levels, the heat transfer area of each exchanger used for internal heat integration is fixed in advance. Thus, at the third level, the heat transfer area is optimized. The effectiveness of the proposed procedure is verified by comparing the TAC in distillation sequences with and without internal heat integration.

2.3 Heat integration of two columns

In conventional distillation, heat is supplied to the reboiler at the highest temperature, and it is removed from the condenser at the lowest temperature in the column. If the heat can be supplied to the intermediate stages in the stripping section, the heat source can be used at lower temperature. By taking this fact into account, recently, many researches have been done to assess the effectiveness of using side reboilers and side condensers[5,13,15-17].

There are two main differences between external heat integration and internal heat integration. Because of these differences, systematic problems have been limited to two columns or sections.

The first difference is related with a remarkably increase of heat integration possibilities in internal heat integration, and it is represented in Figure 2.1. In the case of external heat integration, energy is supplied from the condenser in a rectifying section to the reboiler in a stripping section whereas in the case of internal heat integration, energy can be supplied from all the M stages in a rectifying section to all the N stages in a stripping section, but excluding the condenser-reboiler heat exchange. When the rectifying section consists of ten stages (M = 10) and the stripping section of ten stages (N = 10), the possible matches of internal heat integration are 99 though the external heat integration is restricted to one match.

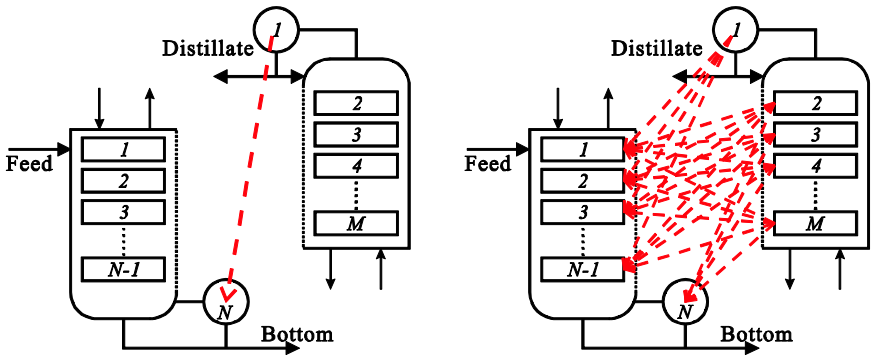

Figure 2.1. Heat integration possibilities: external heat integration (left) and internal heat integration (right)

Figure 2.2 shows a superstructure adopted in this thesis to generate internal heat integration between the rectifying section of column i and the stripping section of column j. M_i is the number of stages in the rectifying section of column i, and N_j is the number of stages in the stripping section of column j. In this research, the stages are numbered downwards from stage 1 (condenser) to M_i in the rectifying section, and from stage 1 (feed) to N_j (reboiler) in the stripping section.

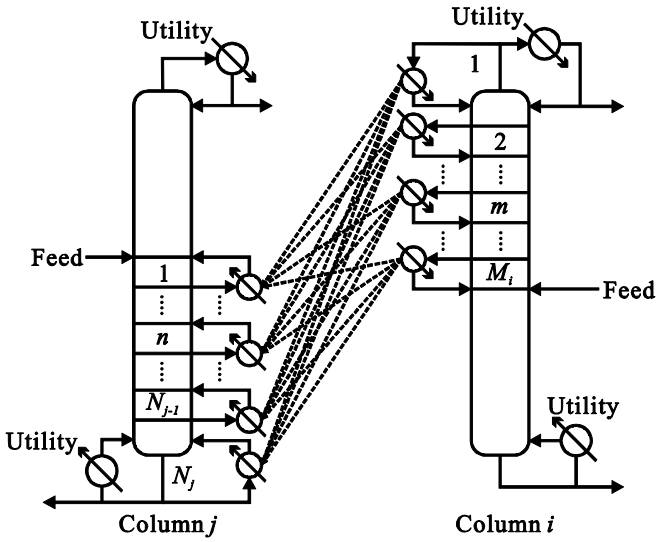

Figure 2.2. Superstructure of internal heat integration

The second difference deals with the effect of changes in condenser and reboiler duties after internal heat integration, and it is represented in Figure 2.3. In the case of external heat integration,

the energy reduced at a condenser and at a reboiler is equal to the energy exchanged by the condenser-reboiler match (Figure 2.3 left side). Contrary, in the case of internal heat integration, the energy reduced at a condenser and at a reboiler is not equal to the energy exchanged by the stage-stage match (Figure 2.3 right side).

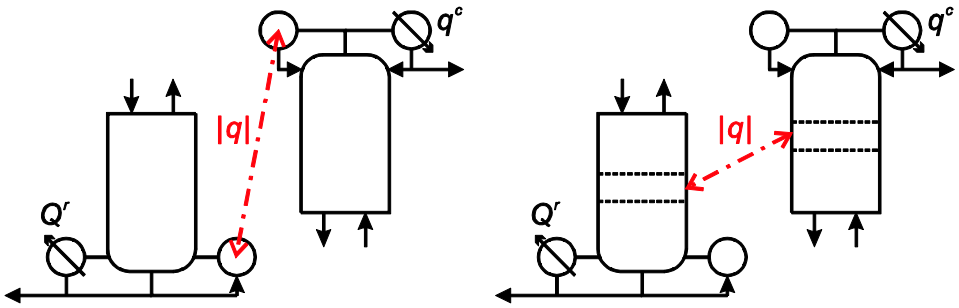

Figure 2.3. External and internal heat integrations

In Figure 2.3, q is the amount of energy exchanged, q^c is the condenser duty, Q^r is the reboiler duty, and 0 means the value prior to heat integration. The reduction of the condenser and reboiler duties by external heat integration depends on the amount of heat exchanged. However, the reduction of the condenser and reboiler duties by internal heat integration depends on two factors: the location of the heat exchange between stages and the amount of energy exchanged. These two aspects will be cover in detail in the following sections.

2.4 Drawback of the CGCC-based approach

The Column Grand Composite Curve (CGCC) gives a useful insight to enhance the thermodynamic efficiency in a distillation column.[18] It has been used to derive the best combination of stages for internal heat integration. [11, 19, 20] Though it is a valuable tool to estimate the amount of heat exchanged between two columns visually, the result is not accurate. Suppose the case where the amount of heat Q_n is supplied to stage n of the stripping section. In the CGCC based approach, the reboiler duty Q^r after the introduction of a side reboiler is calculated by the following equation:

$$Q^r = Q_0^r - Q_n \tag{1}$$

where Q_0^r is the reboiler duty before the introduction of side reboilers.

Similarly, when the amount of heat q_m is removed from a stage m of the rectifying section, the condenser duty q^c after the introduction of a side condenser is calculated by the following equation:

$$q^c = q_0^c - q_m \tag{2}$$

where q_0^c is the condenser duty before the introduction of side condenser.

Figure 2.4 exemplifies the case where internal heat integration between stage m in column i and stage n in column j is realized. In addition, the CGCC for each column and the heat exchanged is shown in a Enthalpy-Temperature diagram.

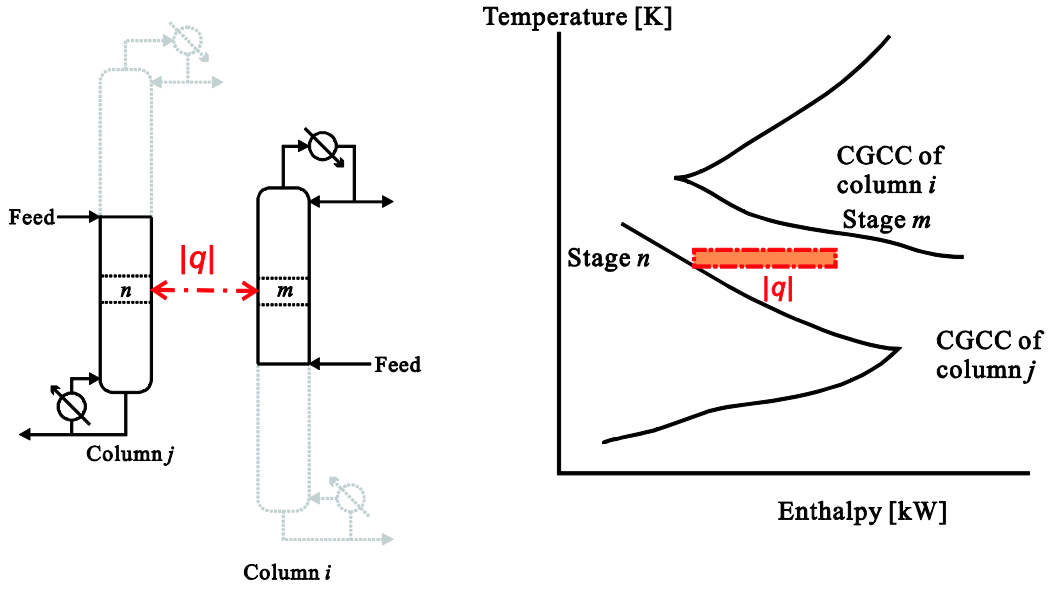

Figure 2.4. Internal heat integration between two columns (left) and its CGCC representation in an Enthalpy-Temperature diagram (right)

The energy balances in Equations 1 and 2 are valid insofar as the column has infinite number of stages and the pinch condition does not occur in the column because the temperature and composition changes approximate to a reversible process, therefore, the energy losses are negligible. When the equipment cost is included in the objective function in addition to the utility cost, the number of stages in each column is treated as a design variable. Hence, the assumption of infinite number of stages is inadequate. When each column takes a finite number of stages, the estimation of Q^r and q^c by Equations 1 and 2 is not longer valid. In the next section, a rigorous simulation-based approach to reliably estimate the relation between the side reboiler or side condenser duty and the reduction of the reboiler and condenser duties is discussed.

2.5 Proposed simulation-based approach

2.5.1 Installation of a single side reboiler or a single side condenser

When a side reboiler is installed in the stripping section, the reboiler duty can be reduced. However, the reduction ratio of the reboiler duty to the unit amount of heat supplied to the side reboiler depends on the design of the column and the location of the side reboiler. [21]

In this subsection, a method to estimate the condenser and reboiler duties after the installment of a side reboiler or a side condenser is explained. It is assumed that the feed and product compositions, number of stages and pressure in each section are given in advance. Then, the reboiler and condenser duties before installing any side reboiler or side condenser, Q_0^r and q_0^c, can be calculated by rigorous simulation. When heat Q_n is supplied to the side reboiler installed at stage n of the stripping section, the reboiler duty Q^r which satisfies the same given product specification can be calculated through rigorous simulation. The reduction of reboiler duty, $Q_0^r - Q^r$, is smaller than Q_n. This difference between Q_n and $Q_0^r - Q^r$ is named as the reboiler compensation term, ΔQ_n^r, and is defined by

$$\Delta Q_n^r = Q_n - (Q_0^r - Q^r) \tag{3}$$

In the same fashion, when heat q_m is removed from the side condenser installed at stage m of the rectifying section, the condenser compensation term, Δq_m^c, can be calculated by the following equation:

$$\Delta q_m^c = q_m - (q_0^c - q^c) \tag{4}$$

where q^c is the condenser duty, which satisfies the same given product specification, after the side condenser is installed.

For two different design conditions shown in Table 1, ΔQ_n^r and Δq_m^c are derived as a function of Q_n or q_m. The feed and product specifications are also shown in Table 2.1. The results from rigorous simulation are shown in Figure 2.5. The reboiler and condenser duties before internal heat integration by side reboiler or side condenser are for case A 607 kW and 548 kW while for case B 690 kW and 631 kW, respectively.

Table 2.1. Feed and product specifications for the case study

Feed condition
Flow rate: 100 kmol/h
Composition [mol%]:
N-pentane/N-hexane/N-heptane = 30/30/40
Temperature: 336 K (Boiling point of the feed mixture)
Pressure: 101.325 kPa
Product specifications:
Distillate: N-pentane : 98 mol %
Bottom product : N-pentane: 0.5 mol %
Number of stages (including reboiler and condenser)
Case A: Rectifying section: 60, Stripping section: 90
Case B: Rectifying section: 10, Stripping section: 10
Stage where side reboiler or side condenser is installed
Case A: Side reboiler: 30, Side condenser: 45
Case B: Side reboiler: 5, Side condenser: 5
Reflux ratio: Case A: 1.43 Case B: 1.79

From Figure 2.5, it becomes clear that ΔQ_n^r and Δq_m^c values are almost zero when the column has a large number of stages. However, these values cannot be neglected at a reasonable design condition such as case B. Moreover, ΔQ_n^r and Δq_m^c depend on the stage where the side reboiler or side condenser is installed. Figure 2.6 shows ΔQ_n^r for different n stages. The simulation condition is the same as case B in Table 2.1.

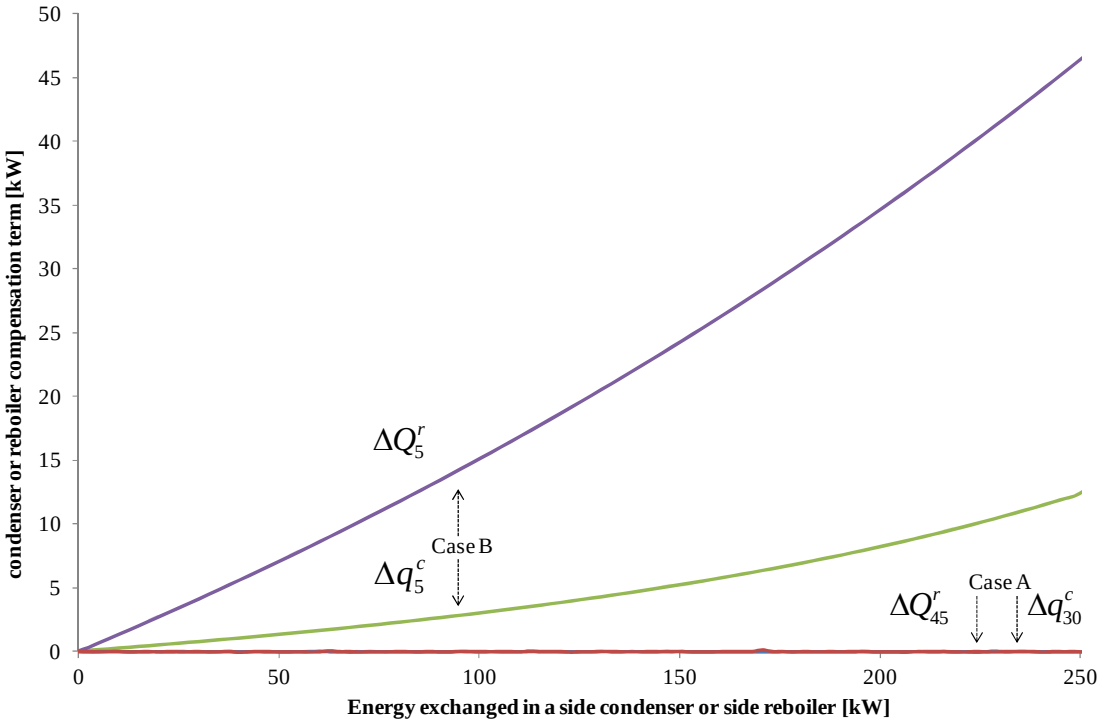

Figure 2.5. ΔQ_n^r and Δq_m^c as a function of Q_n or q_m

From Figure 2.5 it can be observed that as long as the number of stages in each section increases, the compensation term at an intermediate stage *m* or *n* decrease. Hence the number of stages in each section has large value as in Case A, the compensation terms are nearly zero because the composition and temperature of vapor and liquid flows between adjacent stages is similar. Consequently, thermodynamic irreversibility owing to the energy supplied from stage *m* or supplied to stage *n* can be negligible. Contrary, a more realistic situation with fixed number of stages (Case B) exhibit thermodynamic irreversibility owing to the energy supplied from stage *m* or supplied to stage *n* because the composition and temperature difference of vapor and liquid flows between adjacent stages. Thus, the compensation terms in Case B are larger than Case A.

In other words, the thermodynamic irreversibility can be evaluated in terms of energy increase by the compensation terms. Since Case A is an approximation to the minimum reflux condition, the compensation terms are nearly zero.

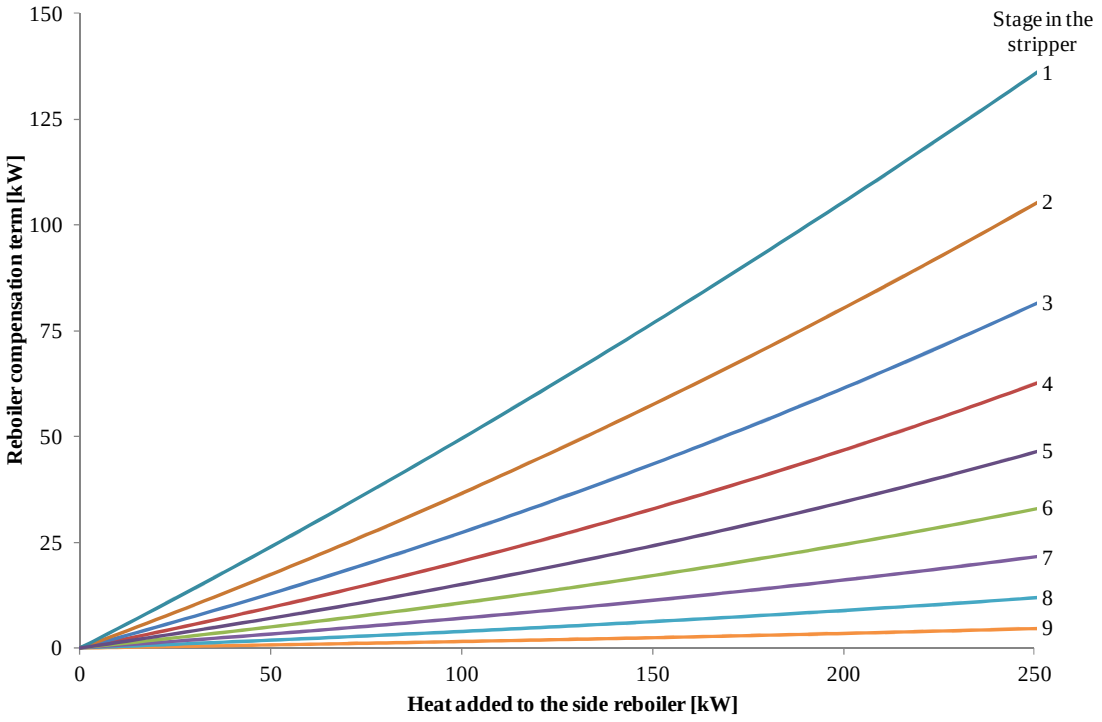

Figure 2.6. Effect of the installed stage on ΔQ_n^r

In order to obtain an explicit mathematical expression which relates Q_n and ΔQ_n^r in the synthesis procedure, each line in Figure 2.6 is approximated by a linear function.

$$\Delta \hat{Q}_n^r = A_n^r Q_n + B_n^r \delta_n^r \qquad (n = 1, 2, ..., N) \tag{5}$$

where A_n^r and B_n^r are the parameters to estimate ΔQ_n^r. $\Delta \hat{Q}_n^r$ is the estimated value of ΔQ_n^r. δ_n^r is a 0-1 variable which takes 0 when $Q_n = 0$, otherwise $\delta_n^r = 1$. N is the number of stages in the stripping section.

In the similar manner, the relation between q_m and Δq_m^c is linearized:

$$\Delta \hat{q}_m^c = A_m^c q_m + B_m^c \delta_m^c \qquad (m = 1, 2, ..., M) \tag{6}$$

where A_m^c and B_m^c are the parameters to estimate Δq_m^c. $\Delta \hat{q}_m^c$ is the estimated value of Δq_m^c. δ_m^c is a 0-1 variable which takes 0 when $q_m = 0$, otherwise $\delta_m^c = 1$. M is the number of stages in the rectifying section.

2.5.2 Effect of side reboiler on condenser duty and effect of side condenser on reboiler duty

The installation of a side reboiler affects not only the reboiler duty but also the condenser duty. This effect can be estimated from the total enthalpy balance, which is expressed by

$$F \cdot h_F + Q_o^r = D \cdot h_D + B \cdot h_B + q_o^c \tag{7}$$

before internal heat integration, and

$$F \cdot h_F + Q^r + Q_n = D \cdot h_D + B \cdot h_B + q^c \tag{8}$$

after a side reboiler is installed at stage *n* in the stripping section. Here, *F*, *D*, and *B* are flow rate for the feed, distillate and bottom product, respectively, and h_F, h_D and h_B are the enthalpies for the feed, distillate and bottom flows, respectively.

Since the feed condition and the product specifications are not changed, it can be assumed that the enthalpy terms of feed, distillate and bottom flows after internal heat integration are the same as those before the introduction of a side reboiler.

From Equations 3, 7 and 8, the following relation can be derived.

$$\begin{aligned} q^c - q_o^c &= Q_n + (Q^r - Q_0^r) = Q_n + (\Delta Q_n^r - Q_n) \\ &= \Delta Q_n^r \end{aligned} \tag{9}$$

Equation 9 indicates that the effect of side reboiler on the condenser duty can be given by the compensation term ΔQ_n^r calculated in Equation 3. In a similar procedure, the following equation can be derived to express the effect of side condenser on the reboiler duty.

$$Q^r - Q_o^r = \Delta q_m^c \tag{10}$$

2.5.3 Installation of multiple side reboilers and/or side condensers

When realizing internal heat integration, the heat can be supplied to multiple stages in the stripping section, and the heat can be removed from multiple stages in the rectifying section. Thus, the effect of multiple side reboilers on the reduction of reboiler duty, and that of multiple side condensers on the reduction of condenser duty are discussed in this subsection. As mentioned in the previous subsection, the introduction of side condenser also affects the reboiler duty. Hence, the reboiler duty Q^r and the

condenser duty q^c for the case where multiple side reboilers and side condensers are installed depend on the locations of those side reboilers and side condensers as well as the amount of heat supplied to or removed from each stage. As general forms, they are expressed by the following equations:

$$Q^r = f^r(Q_1, Q_2, ..., Q_N, q_1, q_2, ..., q_M) \tag{11}$$

$$q^c = f^c(Q_1, Q_2, ..., Q_N, q_1, q_2, ..., q_M) \tag{12}$$

Figure 2.7 is a conceptual representation of Equations 11 and 12 where multiple side condensers and side reboilers are installed in a distillation column. The blue arrows denote the energy removed from the rectifying section and the red arrows denote the energy supplied to the stripping section.

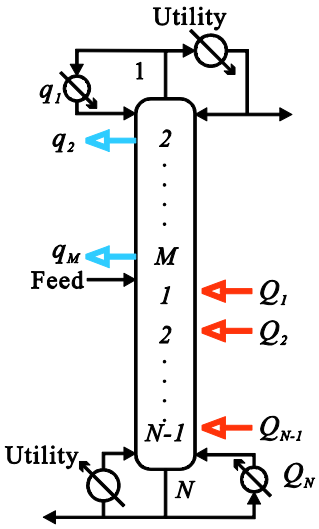

Figure 2.7. Conceptual representation of the installation of multiple side condensers and side reboilers

The overall compensation terms of the reboiler and condenser for the case where multiple side reboilers and side condensers are installed, ΔQ^r and Δq^c, are defined by the following equations:

$$\Delta Q^r = \sum_{n=1}^{N} Q_n - (Q_0^r - Q^r) \tag{13}$$

$$\Delta q^c = \sum_{m=1}^{M} q_m - (q_0^c - q^c) \tag{14}$$

Since Q^r and q^c are expressed by Equations 11 and 12, ΔQ^r and Δq^c are also functions of Q_1, Q_2, ..., Q_N, q_1, ..., q_M. Thus, the rigorous simulation of distillation column is requested to derive the exact values of ΔQ^r and Δq^c for each case of heat supplies and removals. To avoid such a

situation, ΔQ^r and Δq^c are estimated from $\{\Delta \hat{Q}_n^r\}$ and $\{\Delta \hat{q}_m^c\}$ which are obtained by the rigorous simulation for individual assignment of side reboiler or side condenser.

$$\begin{aligned} \Delta \hat{Q}^r = \Delta \hat{q}^c &= \sum_{n=1}^{N} \Delta Q_n^r + \sum_{m=1}^{M} \Delta q_m^c \\ &\cong \sum_{n=1}^{N} \left(A_n^r Q_n + B_n^r \delta_n^r \right) + \sum_{m=1}^{M} \left(A_m^c q_m + B_m^c \delta_m^c \right) \end{aligned} \tag{15}$$

where $\Delta \hat{Q}^r$ and $\Delta \hat{q}^c$ are approximated values of ΔQ^r and Δq^c, respectively.

2.5.4 Effect of side condenser on the reflux ratio and effect of side reboiler on the reboil ratio

If energy is supplied from a rectifying section, some of the vapor will condensate at the stage where a side condenser is installed. Similarly, if energy is supplied to a stripping section, some of the liquid will boil at the stage where a side reboiler is installed. As a consequence, the vapor flow towards the top of a rectifying section and the liquid flow towards the bottom of a stripping section will decrease resulting in changes in the reflux ratio and reboil ratio.

The enthalpy balance at the condenser in a rectifying section is expressed by

$$q_0^c = V_0^c (H_C - h_D) \tag{16}$$

before internal heat integration, and

$$q^c = V^c (H_C - h_D) \tag{17}$$

after side condensers and side reboilers are installed. Here V^c denotes the vapor flow rate towards the condenser after the heat integration, and V_0^c is that before the internal heat integration. H_C is the enthalpy for vapor entering the condenser.

When the column is operated so as to satisfy the product specification, H_C, and h_D after internal heat integration are same as those before the heat integration. If this assumption is valid, the changes in the reflux ratio after the installation of side condensers and side reboilers can readily be estimated by using the concept of compensation terms. From Equations 14, 16 and 17, the reflux ratio before heat integration, R_0^c, and after heat integration, R^c, can be derived:

$$R_0^c = \frac{V_0^c}{D} - 1 = \frac{q_0^c}{(H_C - h_D)D} - 1 \tag{18}$$

$$\begin{aligned} R^c &= \frac{V^c}{D} - 1 = \frac{q^c}{(H_C - h_D)D} - 1 = \frac{q_0^c + \Delta q^c - \sum_{m=1}^{M} q_m}{(H_C - h_D)D} - 1 \\ &= R_0^c - \frac{\sum_{m=1}^{M} q_m}{(H_C - h_D)D} + \frac{\Delta q^c}{(H_C - h_D)D} \end{aligned} \tag{19}$$

Equation 19 shows that the changes of the reflux ratio by the heat integration is calculated if the overall compensation term, Δq^c, can be estimated.

The enthalpy balance around the reboiler can be expressed by the following equation:

$$(V^r + B)h_R + Q^r = V^r H_B + Bh_B \tag{20}$$

where H_B and h_R are the enthalpy terms for vapor leaving the reboiler and the liquid entering the reboiler, respectively. V^r is the vapor flow rate from the reboiler to the column.

By assuming that $h_R = h_B$, the reboil ratio before heat integration, R_0^r, and after heat integration, R^r, can be derived:

$$R_0^r = \frac{V_0^r}{B} = \frac{Q_0^r}{(H_B - h_B)B} \tag{21}$$

$$\begin{aligned} R^r &= \frac{V^r}{B} = \frac{Q^r}{(H_B - h_B)B} = \frac{Q_0^r - \sum_{n=1}^{N} Q_n + \Delta Q^r}{(H_B - h_B)B} \\ &= R_0^r - \frac{\sum_{n=1}^{N} Q_n}{(H_B - h_B)B} + \frac{\Delta Q^r}{(H_B - h_B)B} \end{aligned} \tag{22}$$

where V_0^r is the vapor flow rate from the reboiler to the column before heat integration.

Equation 22 shows that the changes of the reboil ratio by the heat integration is calculated if the overall compensation term, ΔQ^r, can be estimated.

2.6 Validation of the simulation-based approach

To validate the accuracy of Equation 15, the case B in Table 2.1 is used again as an example. Table 2.2 shows several scenarios of multiple heating and cooling. Multiple side reboilers are installed in

cases 1 to 3, multiple side condensers are installed in cases 4 to 6, and the both side reboilers and side condensers are installed in cases 7 to 9.

The simulation results are summarized in Table 2.3. Case 0 in Table 2.3 is the case with no side reboiler nor side condenser are installed. Since $Q_0^r = Q^r$ and $q_0^c = q^c$ for Case 0, the values of the compensation terms calculated from Equations 13 and 14 are zero. Figure 2.8 shows the comparison among the exact value of the reboiler duty, Q^r, the estimated value using Equation 15, $Q_0^r - \sum Q_n + \Delta\hat{Q}^r$, and the estimated value used in CGCC-based method, $Q_0^r - \sum Q_n$, for every case. For the cases where side reboilers and/or condensers are installed close to the feed stage, the estimated values from the CGCC-based method show large errors whereas the results estimated by using Equation 15 show good approximations. The deviations of the values obtained by our proposed estimation method from those obtained by rigorous simulations (exact solution) are between -0.2% (case 3) and 6.5% (case 4). When compensation terms are not considered, the deviations are between 2% (case 2) and 44% (case 9).

Table 2.2. Example cases of side heating and/or side cooling

	Stage in the rectifying section									Stage in the stripping section								
Case	2	3	4	5	6	7	8	9	10	1	2	3	4	5	6	7	8	9
1	50	50	50	50	50	50	50	50										
2			150	100	50													
3	100				100				100									
4										50	50	50	50	50	50	50	50	50
5													50	100	150			
6										150				150				150
7		100	100	100	100									100	100	100	100	
8				75	100	100	75				125	100	125	100				
9		250					250				100					200		

The values in the table are in kW

Table 2.3. Estimation of reboiler and condenser duties

Case	$\sum q_m$	q^c	Δq^c	$\Delta \hat{q}^c$	$\sum Q_n$	Q^r	ΔQ^r	$\Delta \hat{Q}^r$
0	0	631	0	0	0	690	0	0
1	400	267	36	22	0	726	36	22
2	300	344	13	9	0	703	13	9
3	300	369	38	40	0	729	39	40
4	0	733	102	81	450	343	103	81
5	0	683	52	44	300	442	52	44
6	0	743	112	106	450	352	112	106
7	400	294	63	51	400	353	63	51
8	350	455	174	150	450	414	174	150
9	500	234	103	101	300	493	103	101

The values in the table are in kW

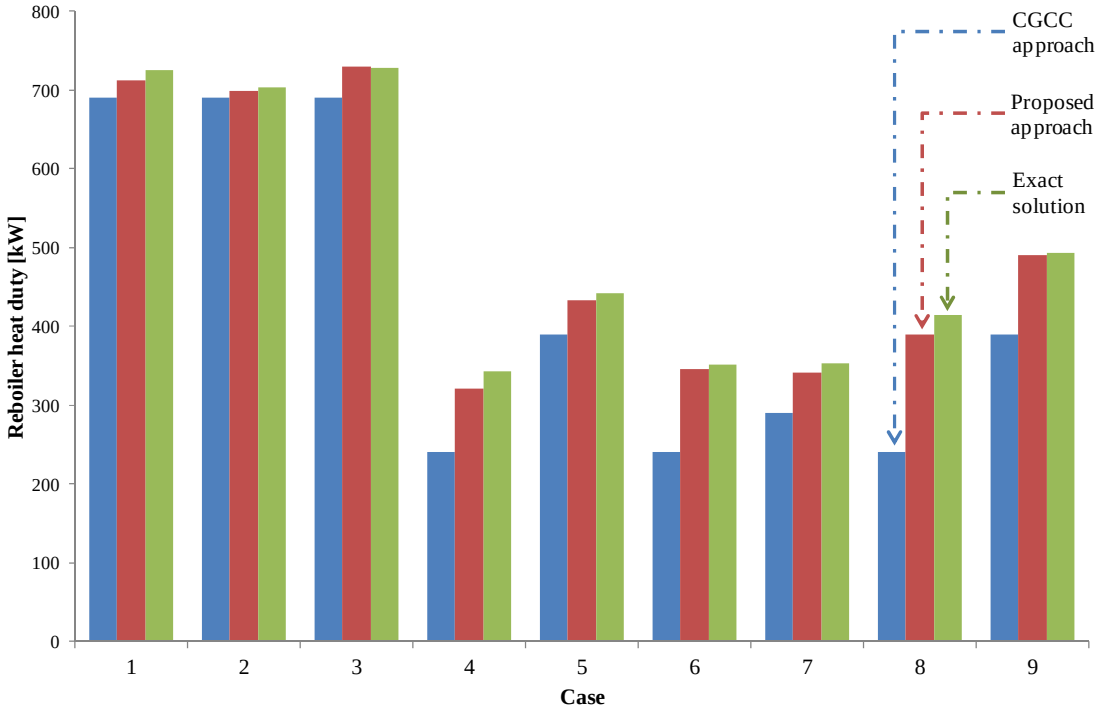

Figure 2.8. Comparison of reboiler heat duties for the three different approaches

2.7 Internal heat integration between two columns

In this section, heat integration of two columns is taken up, and the problem of deciding the optimal heat integration is formulated as a mixed integer linear programming (MILP) problem. It is assumed that the feed and product conditions are given in advance, and that the columns are properly designed to satisfy those conditions.

In order to simplify the explanation, it is assumed that the rectifying section of column *i* is regarded as heat source and the stripping section of column *j* is regarded as heat sink as shown in Figure 2.2. The purpose of this section is to show a general MILP formulation, which derive the best internal heat integration structure.

The connectivity restrictions to generate the matches between stages is determined by the following equation

$$\sum_{n=1}^{N_j} Y_{m,n}^{i,j} \le 1 \qquad (m = 1, 2, ..., M_i) \tag{23}$$

$$\sum_{m=1}^{M_i} Y_{m,n}^{i,j} \le 1 \qquad (n = 1, 2, ..., N_j) \tag{24}$$

$$Y^{i,j} \le \sum_{m=1}^{M_i} \sum_{n=1}^{N_j} Y_{m,n}^{i,j} \tag{25}$$

where $Y_{m,n}^{i,j}$ is a binary variable that becomes one if rectifying stage *m* of column *i* and stripping stage *n* of column *j* is heat integrated and zero otherwise. Equations 23 and 24 restrict that the energy removed from one stage in the rectifying section can only be supplied to one stage in the striping section, and vice versa. $Y^{i,j}$ is the binary variable which become one if heat exchange between columns *i* and *j* is realized, and zero otherwise.

The match coming after (*m*, *n*) can be (*m*-1, *n*+1), (*m*+1, *n*-1), (*m*+2, *n*+3) or so. Such crossed linking streams, however, have practical difficulties. Therefore, in this research, the match after (*m*, *n*) is restricted to (*m*+1, *n*+1). To avoid crossed matches, Equation 26 is introduced to warrant the matches in a cascade way.

$$Y_{m,n}^{i,j} \ge Y_{m+1,n+1}^{i,j} \quad (m = 1, ..., M_i - 1 \; ; \; n = 1, ..., N_j - 1) \tag{26}$$

Suppose the case where $Y_{5,6}^{i,j} = 0$ and $Y_{4,5}^{i,j} = 1$. In this case, $Y_{3,4}^{i,j} = Y_{2,3}^{i,j} = Y_{1,2}^{i,j} = 1$ and other $Y_{m,n}^{i,j} = 0$.

The driving force to generate feasible matches depends on the temperature difference between the stages in the rectifying section of column *i* and the stages in the stripping section of column *j*. Hence feasible matches between stages can take only real positive, Equation 27 denotes the mathematical

expression to calculate the logarithmic mean temperature difference, LMTD. The LMTD for an infeasible match is set equal to zero to eliminate it as candidate match in the MILP problem

$$LMTD_{m,n}^{i,j} = \begin{cases} \dfrac{\left(T_{m+1}^{i} - t_{n}^{j}\right) - \left(T_{m}^{i} - t_{n-1}^{j}\right)}{\ln\left(\dfrac{T_{m+1}^{i} - t_{n}^{j}}{T_{m}^{i} - t_{n-1}^{j}}\right)} & for\ T_{m+1}^{i} - t_{n}^{j} > 0 \\ & T_{m}^{i} - t_{n-1}^{j} > 0 \\ 0 & otherwise \end{cases} \quad (m = 1,...,M_i\ ;\ n = 1,...,N_j) \quad (27)$$

where $LMTD_{m,n}^{i,j}$ is the LMTD for the match between the stage *m* in the rectifying section of column *i* and stage *n* in the stripping section of column *j*. T_m^i is the temperature of the vapor stream at stage *m* in the rectifying section of column *i*, and t_n^j is the temperature of the liquid stream at stage *n* in the stripping section of column *j*. Figure 2.9 shows a detailed representation for the heat exchange between a heat sources stage and a heat sink stage.

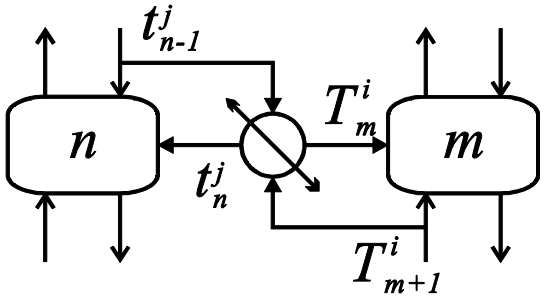

Figure 2.9. Detailed representation of energy transfer between stages.

If a match between stages of different columns has a value of *LMTD* less than a minimum temperature difference, ΔT^{int}, $LMTD_{m,n}^{i,j}$ is set to zero. Thus, some values of LMTD are forced to be zero before performing the optimization. This feature is expressed by the following equation:

$$LMTD_{m,n}^{i,j} = 0 \quad if\ \ LMTD_{m,n}^{i,j} < \Delta T^{int} \quad (28)$$

Finally, the amount of energy transferred between stages is constrained by the energy balance for every match as shown in Equation 29.

$$Q_{m,n}^{i,j} - A^{int}U^{int}LMTD_{m,n}^{i,j}Y_{m,n}^{i,j} \le 0 \qquad (m=1,...,M_i\ ;\ n=1,...,N_j) \tag{29}$$

where A^{int} is the area for the side heat exchanger, and U^{int} is the overall heat transfer coefficient. In this study, these values are assumed to be constant to assure the problem is linear.

The optimization problem, which maximizes the energy exchanged for all the possible matches between two columns, is shown in Equation 30. It is constrained by Equations 23 through 29, and 31 through 35 and it is formulated as follows:

$$\max\ z = Q_{opt}^{i,j} - \alpha S^{i,j} \tag{30}$$

$$Q^{i,j} = \sum_{m=1}^{M_i}\sum_{n=1}^{N_j} Q_{m,n}^{i,j} \tag{31}$$

$$S^{i,j} = \sum_{m=1}^{M_i}\sum_{n=1}^{N_j} Y_{m,n}^{i,j} \tag{32}$$

$$\sum_{m=1}^{M_i}\sum_{n=1}^{N_j} Q_{m,n}^{i,j} \le Q_{UP} \tag{33}$$

$$\Delta Q_{opt}^{i,j} = \sum_{n=1}^{N_j} \Delta\hat{Q}_n^{r,j} \tag{34}$$

$$Q_{opt}^{i,j} = \sum_{m=1}^{M_i}\sum_{n=1}^{N_j} Q_{m,n}^{i,j} - \Delta Q_{opt}^{i,j} \tag{35}$$

where $Q_{opt}^{i,j}$ is the net reduction of the reboiler duty of column j resulted from heat integration between the rectifying section of column i and the stripping section of column j, and $S^{i,j}$ is the number of the side heat exchangers. α is a penalization parameter to avoid a large number of side heat condensers/reboilers in the optimal solution. $Q^{i,j}$ is the amount of energy exchanged between the two columns, and Q_{UP} is the upper bound of the amount of energy exchanged by internal heat integration. It is used to explicitly evaluate the effect of internal heat integration between the two columns. $\Delta\hat{Q}_n^{r,j}$ is the estimated value of ΔQ_n^r for column j. $\Delta Q_{opt}^{i,j}$ is the reboiler compensation term of the column j when there is heat integration between the rectifying section of column i and the stripping section of column j.

Though the condenser duty is not included in the objective function, the following data related to the condenser duty are also obtained for the pair of columns i and j by solving the above problem.

$$\Delta q_{opt}^{i,j} = \sum_{m=1}^{M_i} \Delta \hat{q}_m^{c,i} \tag{36}$$

$$q_{opt}^{i,j} = \sum_{m=1}^{M_i} \sum_{n=1}^{N_j} Q_{m,n}^{i,j} - \Delta q_{opt}^{i,j} \tag{37}$$

where $\Delta q_{opt}^{i,j}$ is the condenser compensation term of the column i when there is heat integration between the rectifying section of column i and the stripping section of column j. $\Delta \hat{q}_m^{c,i}$ is the estimated value of Δq_m^c for column i. $q_{opt}^{i,j}$ is the net reduction of condenser duty of column i resulted from heat integration between the rectifying section of column i and the stripping section of column j.

These values are calculated from the optimization results, and are used in the synthesis procedure explained in section 2.9.

2.8 Synthesis of the optimal sequence among columns

Although previous researches[5-8,11-13,15-17] have proposed procedures to obtain the best internal heat integration network only between two sections or columns, the synthesis problem to obtain the best distillation sequence among several columns remains unsolved.

The first step in solving the synthesis problem is to define all candidate distillation sequences. In this work, a superstructure-based approach is adopted to enumerate them. The superstructure of distillation sequences separating a three-component mixture is shown in Figure 2.10. The mixture consists of A, B, and C, being A the most volatile component. The superstructure generated in this work is a state task network representation. Each ellipse in Figure 2.10 is a state having information of the composition and physical conditions. When the amount of feed and its composition as well as the composition of every product are given, the amount of each product can be calculated from material balance equations. Some states in Figure 2.10 have more than one inlet and/or outlet flows. It is assumed that the number of inlet to and outlet from the state is restricted to one or zero for the finally derived structure, i.e., flow split is not permitted. By introducing this assumption, the conditions of intermediate states such as AB or BC in Figure 2.10 are uniquely determined. It is assumed that each state is liquid at its saturated temperature and that the compression and decompression cost of liquid is negligible. Thus, liquids with the same composition are expressed by one state even if the pressure is different. Task A/BC, (P_i) means that mixture ABC is separated into A and BC by a conventional column operated at pressure P_i. The fixed cost and the operating cost depend on the operating

pressure. Thus, the columns with different pressures are treated as different tasks even if the feed and product states are the same.

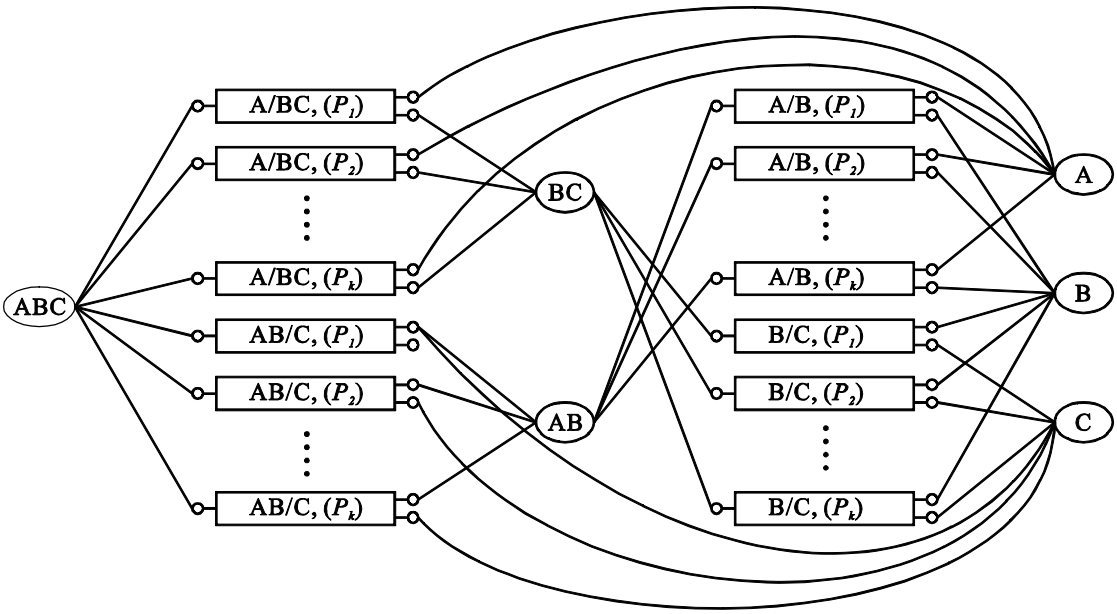

Figure 2.10. Superstructure of a three-component separation problem

2.9 Hierarchical optimization algorithm

In the proposed synthesis procedure, the optimal heat integrated distillation sequence is derived by a hierarchical optimization algorithm. The entire synthesis procedure consists of the following steps:

1) Given the feed and product specifications, the intermediate states conditions are calculated. The pressures, which can be adopted by each column, are discrete. Then, the superstructure such as shown in Figure 2.10 is obtained.

2) For each task, the design and operating conditions are calculated by executing rigorous simulations. At this step, heat integration is not considered.

3) For each task, effects of side reboiler and side condenser on the reboiler and condenser duties are calculated by executing rigorous simulations. The results are summarized as shown in Equation 15.

4) Decide the area of each side heat exchanger (A^{int} in Equation 29) and the upper bound for internal heat integration (Q_{UP} in Equation 33)

5) For every combination of two tasks, the MILP problem explained in section 2.3 is solved, and the values in Equations 34 to 37 are calculated.

6) The synthesis problem to obtain the best sequence is formulated as an MILP problem, and solved by using commercial optimization package. The detail of this step is explained in the next section.

7) Steps 4 through 6 are repeated for new values of A^{int} and Q_{UP} till there is not further improvement of the TAC.

2.9.1 Formulation of the synthesis problem

From step 5) in the synthesis procedure explained above, the best combination of stages for internal heat integration is calculated for each pair of tasks, i.e. the maximum reduction of reboiler duty, $Q_{opt}^{i,j}$, and the total heat transfer area used for internal heat integration. By calculating these values in advance, the synthesis procedure developed for the distillation sequences with external heat integration can be implemented with minor modifications of a proposed procedure[1]. Thus, in this section, the resulting MILP formulation is derived to include internal heat integration as a possibility.

The connectivity constraints between columns to generate feasible sequences are given by

$$\sum_{i \in FEED} Y_{ext}^{i} = 1 \tag{38}$$

$$\sum_{i \in COLF_s} Y_{ext}^{i} - \sum_{i \in COLP_s} Y_{ext}^{i} = 0 \qquad s \in ST \tag{39}$$

where Y_{ext}^{i} is a binary variable assigned to each task in the superstructure of Figure 2.10. If task *i* (column *i*) is selected, Y_{ext}^{i} becomes one; zero otherwise. *FEED* denotes the set of tasks whose input stream is the original feed state. $COLF_s$ and $COLP_s$ are the set of columns, which have state *s* as an output and as an input, respectively. *ST* is the set of states, excepting the feed and product states. Equations 38 and 39 mean that the split of a stream is not permitted.

If task *i* is not used in the sequence, the internal heat integration between task *i* and other task cannot be executed. This constraint is expressed by

$$\sum_j Y^{i,j} \le Y_{ext}^i \tag{40}$$

$$\sum_j Y^{j,i} \le Y_{ext}^i \tag{41}$$

In this research, it is assumed that the heat supply to a stripping section of a column from two or more columns, and the heat supply from a rectifying section of a column to two or more columns are prohibited.

When internal heat integration is not considered, the energy balance equations at the reboiler and condenser of task *i* are expressed by the following equations:

$$\sum_{j\in CU} Q_{ext}^{i,j} + \sum_{j\in TK} Q_{ext}^{i,j} = q_0^{c,i} \cdot Y_{ext}^i \qquad i \in TK \tag{42}$$

$$\sum_{i\in HU} Q_{ext}^{i,j} + \sum_{i\in TK} Q_{ext}^{i,j} = Q_0^{r,j} \cdot Y_{ext}^j \qquad j \in TK \tag{43}$$

where *HU* and *CU* are the sets of heating and cooling utilities, respectively. $Q_{ext}^{i,j}$ is the amount of heat exchanged between the top vapor stream of task *i* and the bottom liquid stream of task *j*. For simplicity, the heating utility is regarded as a task having a top vapor stream, and the cooling utility as a task having a bottom liquid stream. $q_0^{c,i}$ and $Q_0^{r,j}$ are condenser and reboiler duties of task *i* and *j* for the case where neither internal nor external heat integration is considered. Finally, *TK* is set of tasks in the superstructure.

By introducing the internal heat integration as a possibility, the above equations are modified into the following equations:

$$\sum_{j\in CU} Q_{ext}^{i,j} + \sum_{j\in TK} Q_{ext}^{i,j} + \sum_{j\in TK} q_{opt}^{i,j} \cdot Y^{i,j} - \sum_{j\in TK} \Delta Q_{opt}^{i,j} \cdot Y^{i,j} = q_0^{c,i} \cdot Y_{ext}^i \qquad i \in TK \tag{44}$$

$$\sum_{i\in HU} Q_{ext}^{i,j} + \sum_{i\in TK} Q_{ext}^{i,j} + \sum_{i\in TK} Q_{opt}^{i,j} \cdot Y^{i,j} - \sum_{i\in TK} \Delta q_{opt}^{i,j} \cdot Y^{i,j} = Q_0^{r,j} \cdot Y_{ext}^j \qquad j \in TK \tag{45}$$

It should be noted that $\Delta q_{opt}^{i,j}$, $q_{opt}^{i,j}$, $\Delta Q_{opt}^{j,i}$ and $Q_{opt}^{j,i}$ in Equations 34 through 37 are the optimization results at the first optimization level, and they are input as constant parameters at this second optimization level, the difference between the conventional problem and newly proposed problem is the introduction of 0-1 variables, $Y^{i,j}$, to link internal heat integration at the first optimization level and external heat integration at the second optimization level. Thus, by little modifications of the conventional optimization algorithm, the optimization problem which minimize the total annual cost can be formulated as:

$$\min \quad TAC = \frac{FC}{PT} + OH \cdot OC \tag{46}$$

where *PT* is the payout time and *OH* is the annual operation hours. *TAC*, *FC* and *OC* are the values for the total annual cost, fixed and operating costs, which are given by

$$FC = \sum_{i\in TK}\left(C_{col}^{i} + C_{tray}^{i}\right)Y_{ext}^{i} + \sum_{i,j\in TK} CS^{i,j}Y^{i,j} + \sum_{i,j\in TK} C_{ext}^{i,j}Q_{ext}^{i,j} + \sum_{\substack{i\in HU\\ j\in TK}} C_{ext}^{i,j}Q_{ext}^{i,j} + \sum_{\substack{i\in TK\\ j\in CU}} C_{ext}^{i,j}Q_{ext}^{i,j}$$

$$OC = \sum_{\substack{i\in HU\\ j\in TK}} C_{heat}^{i,j}Q_{ext}^{i,j} + \sum_{\substack{i\in TK\\ j\in CU}} C_{cool}^{i,j}Q_{ext}^{i,j} \qquad (47)$$

where C_{col}^{i} and C_{tray}^{i} are the column cost and tray cost of task *i*, respectively. $CS^{i,j}$ is the cost for all the side heat exchangers for internal heat integration between a rectifying section of task *i* and the stripping section of task *j*. C_{col}^{i}, C_{tray}^{i} and $CS^{i,j}$ have been calculated in advance at the first optimization step, which is explained at section 2.7. $C_{ext}^{i,j}$ is the cost of an external heat exchanger per unit amount of heat exchanged between task *i* and task *j*. C_{heat}^{i} and C_{cool}^{j} are the costs of heating utility *i* and cooling utility *j*, respectively. The equipment cost was calculated according to Turton et al.[22]

2.10 Separation of a ternary mixture

The CGCC-based approach and the rigorous simulation-based approach are compared by solving the hierarchical optimization algorithm presented in section 2.8 through the case study in Table 2.1. The aim of this comparison is to assess the deviation in the results between both approaches and to determine whether or not the CGCC-based approach is alike to generate reliable solutions.

Since the components in the case study does not exhibit azeotropic behavior or any major nonlinearity, the Chao-Seader correlation[23] for the liquid phase and the Redlich-Kwong equation[24] of state for the vapor phase were used. The specifications for all the states are shown in Table 2.4, where DS denotes the distillate stream and BS the bottom stream.

Table 2.4. Specifications for all the states in the case study [mol%]

	ABC	AB/C		A/BC		A/B		B/C	
Component	Feed	DS	BS	DS	BS	DS	BS	DS	BS
N-pentane , (A)	10	*	*	99	1	98	*	*	*
N-hexane, (B)	60	*	*	*	*	*	98	98	*
N-heptane, (C)	30	1	99	*	*	*	*	*	98
*Depend on tasks									

Table 2.5 shows additional data for the utilities and overall heat transfer coefficients for the heat exchangers.

Table 2.5. Data for utilities and heat transfer coefficients[25]

Utility	Temperature [K]	Cost [$/MWh]
Chilled Water†, (CHW)	278	14.40
Cooling Water†, (CW)	305	0.914
Steam at 446 kPa, (S1)	420	11.17
Steam at 1135 kPa, (S2)	459	18.93
Steam at 3202 kPa, (S3)	511	29.43
Heat transfer coefficients [kW/(m^{2}K)]		
Condenser: 0.6, Reboiler: 1, Heat exchanger: 0.5		
† 20 K Rise		

All the sequences in the superstructure in Figure 2.10 were simulated at three different pressures: 101, 303, and 506 kPa. The tray efficiency is assumed to be 80%. The Penalization parameter α in Equation 30 is set to 1.0. The payout time is 10 years and the annual operation hours is 8000.

2.10.1 Results and discussion

The hierarchical optimization algorithm was executed in the IBM OPL ILOG by using CPLEX. The optimal solutions are shown in Figure 2.11. All of them correspond to the direct sequence.

Figure 2.11a is the best sequence without heat integration. The first column operates at higher pressure to avoid using chilled water as cooling utility. Figure 2.11b is the optimal solution with internal and external heat integration obtained by the proposed algorithm. The column separating B from C supplied energy to the first column. At five stages, internal heat exchange is executed. The reboiler duty in the first column is drastically reduced because heat is supplied from the second column. Thus, the amount of heat supplied by utility is only 7 kW. The reboiler heat duty of the second column is larger than that of Figure 2.11a. This is due to the higher pressure and the compensation terms by the heat removal from the rectifying section. The rigorous simulation, which satisfies the product specification, is executed for the structure in Figure 2.11b. The result is shown in Figure 2.11c. The differences of reboiler heat duties between Figures 2.11b and 2.11c are 13 % for first column and 1 % for second column.

For the sake of comparison, the CGCC-based method was applied to this case study. Figure 2.11d shows the optimal solution with internal and external heat integration obtained by the CGCC-based method. The column separating A from BC operates at higher pressure and supplies energy to the second column. Though the result seems to be reasonable, this method has failed to estimate the condenser and reboiler duties, i.e. the desired products cannot be obtained by the reboiler and condenser duties obtained by the method. Figure 2.11e shown the feasible operating condition assuming that the number of stages of both columns and the location and the amount heat integration are the same as those in Figure 2.11d. The reboiler duty in both columns is considerably higher than that calculated by the CGCC-based method. The result shown that the sequence obtained by the CGCC based method should be carefully checked when applying real problems.

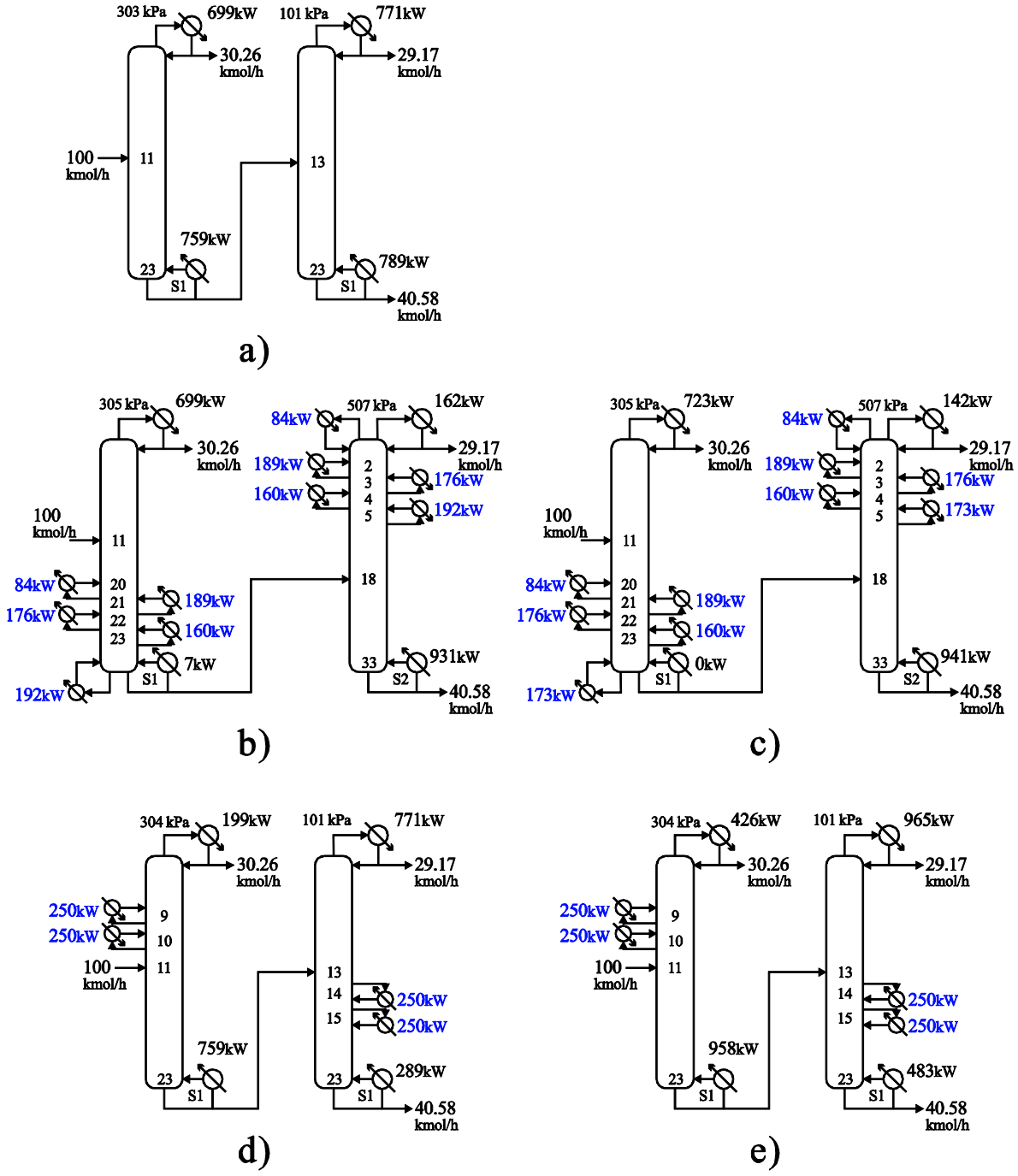

Figure 2.11. Optimal solutions: a) best sequence without heat integration,
b) best sequence with internal heat integration (proposed method),
c) feasible sequence obtained by rigorous simulation of 7b,
d) best sequence obtained by CGCC-based method, and
e) feasible sequence obtained by rigorous simulation of 7d.
blue: internal heat integration, black: utility

Table 2.6 shows the *TAC*, *FC* and *OC* for the solutions reported in Figure 2.11. In addition, the economic and energy savings for the sequences in the figure are compared with a base case, which is the direct sequence at 101 kPa without heat integration.

From the results in Table 2.6 it can be observed that the *TAC* cannot be reduced so much even by considering heat integration. This is because the cost of utilities. For the case of Figure 2.11a, low pressure steam can be used for both columns, though middle pressure steam is requested at the second column of the cases of Figures 2.11b and 2.11c. However, the energy consumption is drastically reduced by adopting the internal and external heat integration. The CGCC-based method is likely to underestimating the *TAC* because it could not update the condenser and reboiler duties increase resulted from internal heat integration.

Table 2.6 Economic and energy savings for the optimal sequences

	TAC [k$/y]	*FC/PT* [k$/y]	*OH·OC* [k$/y]	Economic savings [%]	Energy consumption [kW]	Energy savings [%]	A_{opt}^{int} † [m²]	R^{c} * [-]
Base case	322	115	207	---	1462	---	---	1.716 2.154
Figure 2.11a	278	129	149	14	1548	-6	---	2.344 2.154
Figure 2.11b	277	129	148	14	938	36	23	2.344 0.143
Figure 2.11c	279	130	149	13	941	36	23	2.456 0.048
Figure 2.11d	226	125	101	30	1048	28	45	-0.05** 2.154
Figure 2.11e	320	179	142	1	1469	0	45	1.036 2.949

† A_{opt}^{int} is the optimal value of A^{int} in Equation 29.

* The first line in the column R^{c} defines the value of the reflux ratio for the first column, and the second line the value for the second column.

** The estimated reflux ratio according to Equation 19 yields to an infeasible value

From the results in Figure 2.11 and Table 2.6, it can be observed that sequences with internal heat integration are better than sequences without internal heat integration, however, the solutions obtained from the CGCC-based approach underestimate the TAC because it could not update the condenser and reboiler duties increase resulted from internal heat integration. Because of this, the solutions from both approaches differed.

Internal heat integration realized by side heat exchangers between columns was the most attractive alternative to reduce fixed and operating cost in a distillation sequence. The economic saving was 14%, and the energy saving was 36% for the direct sequence.

2.11. Conclusions

A hierarchical optimization algorithm was proposed to synthesize distillation sequences were internal and external heat integration are possibilities to reduce the energy consumption and cost in distillation.

Two optimization levels were proposed and represented by superstructures. At the first level, all the possibilities for heat integration between the rectifying section of one column and the stripping section of another were comprised while at the second level, all the possible distillation sequences of columns were included.

To deal with all the inherent nonlinearities and nonconvexities in distillation, rigorous simulations were executed, and to obtain optimal heat integration networks and sequences, a mixed integer linear programming (MILP) problem was formulated at each optimization level.

The concept of contribution terms was adopted to estimate the changes in condenser and reboiler duties after internal heat integration so as to obtain the best distillation sequence with the updated values. This approach was able to readily synthesize the best internal heat integrated network between columns as well as to estimate the final condenser and reboiler duties in the distillation sequence.

A case study to separate a ternary mixture was taken. The results showed that the use of side heat exchangers could effectively attain economic savings around 14% and energy savings up to 36%. Furthermore, the use of side heat exchangers could outperform typical external heat integration in terms of TAC and energy consumption.

To determine the reliability of the Column Grand Composite Curve (CGCC), a comparison with our presented approach was assessed. The CGCC approach underestimated the actual total annual cost because was not able to cope with the changes in the condenser and reboiler duty. When the result from the CGCC was executed according our proposed method, the new result yielded to a sub-optimal solution.

The presented methodology can be extended to multicomponent mixtures because it solves one of the main limitations in internal heat integration, which is to find the best sequence of columns; therefore, our future research effort will be in this direction.

Chapter nomenclature

A_n^r (A_m^c) = slope in the estimation equation of reboiler (condenser) compensation term [-]

A^{int} = area for the side heat exchanger [m^2]

B = flow rate of bottom product [kmol/s]

B_n^r (B_m^c) = intercept in the estimation equation of reboiler (condenser) compensation term [kW]

C_{col}^i = column cost of task i [k$]

C_{tray}^i = tray cost of task i [k$]

C_{heat}^i = cost of heating utility i [k$/kWh]

C_{cool}^j = cost of cooling utility j [k$/kWh]

$CS^{i,j}$ = total cost for all the side heat exchangers for internal heat integration between the rectifying section of task i and stripping section of task j [k$]

$C_{ext}^{i,j}$ = heat exchanger cost per unit amount of heat exchanged between the rectifying section of task i and stripping section of task j [k$/kW]

D = distillate flow rate [kmol/s]

$COLF_s$ ($COLP_s$) = set of columns which have state s as an output (as an input) [-]

CU = set of cold utilities [-]

F = feed flow rate [kmol/s]

FC = fixed cost [k$]

$FEED$ = set of tasks whose input stream is the original feed state [-]

h_k = enthalpy of the liquid feed ($k = F$), distillate ($k = D$), bottom product ($k = B$) and to the reboiler ($k = R$) [kJ/kmol]

H_k = enthalpy of the vapor to the condenser ($k = C$) and from the reboiler ($k = B$) [kJ/kmol]

HU = set of hot utilities [-]

L^c = liquid flow rate returning to the column [kmol/s]

$LMTD_{m,n}^{i,j}$ = LMTD for the match between the stage m in the rectifying section of column i and

stage n in the stripping section of column j [K]

M (M_i) = number of stages in a rectifying section (of column i) [-]

N (N_j)= number of stages in a stripping section (of column j) [-]

OC = operating cost [k$/h]

OH = annual operation hours [h/y]

P_i = i-th pressure level [kPa]

PT = payout time [y]

q^c = condenser heat duty after heat integration [kW]

q_0^c ($q_0^{c,i}$) = condenser heat duty before heat integration (for task i) [kW]

q_m = amount of heat removed from stage m of rectifying section [kW]

$q_{opt}^{i,j}$ = net reduction of condenser duty of column i resulted from heat integration between the rectifying section of column i and the stripping section of column j [kW]

Δq^c = overall compensation term of condenser [kW]

Δq_m^c = condenser compensation term defined by Eq. (4) [kW]

$\Delta q_{opt}^{i,j}$ = condenser compensation term of the column i for the internal heat integration between the rectifying section of column i and the stripping section of column j [kW]

$\Delta \hat{q}^c$ = estimated value of Δq^c [kW]

$\Delta \hat{q}_m^c$ ($\Delta \hat{q}_m^{c,i}$) = estimated value of Δq_m^c (for column i) [kW]

Q^r = reboiler heat duty after heat integration [kW]

Q_0^r ($Q_0^{r,j}$) = reboiler heat duty before heat integration (for task j) [kW]

Q_n = amount of heat supplied to stage n of stripping section [kW]

$Q^{i,j}$ = total amount of heat transferred from column i to column j [kW]

$Q_{ext}^{i,j}$ = amount of heat exchanged between the top vapor stream of task i and the bottom liquid stream of task j [kW]

$Q_{m,n}^{i,j}$ = amount of heat transferred from stage m of column i to stage n of column j [kW]

$Q_{opt}^{i,j}$ = net reduction of the reboiler duty of column j resulted from heat integration between the rectifying section of column i and the stripping section of column j [kW]

Q_{UP} = upper bound of the amount of energy exchanged by internal heat integration [kW]

ΔQ^r = overall compensation term of reboiler [kW]

ΔQ_n^r = reboiler compensation term defined by Eq. (3) [kW]

$\Delta \hat{Q}^r$ = estimated value of ΔQ^r [kW]

$\Delta \hat{Q}_n^r$ ($\Delta \hat{Q}_n^{r,j}$) = estimated value of ΔQ_n^r (for column j) [kW]

$\Delta Q_{opt}^{i,j}$ = reboiler compensation term of the column *j* for the internal heat integration between the rectifying section of column *i* and the stripping section of column *j* [kW]

R^c (R_0^c) = reflux ratio after (before) heat integration [-]

R^r (R_0^r) = reboil ratio after (before) heat integration [-]

$S^{i,j}$ = number of side heat exchangers [-]

ST = set of all states [-]

t_n^j = temperature of liquid stream at stage *n* in the stripping section of column *j* [K]

T_m^i = temperature of vapor stream at stage *m* in the rectifying section of column *i* [K]

ΔT^{int} = minimum temperature difference for heat exchange [K]

TAC = total annual cost [k$/y]

TK = set of tasks [-]

U^{int} = overall heat transfer coefficient [kW/(m^{2}K)].

V^c (V_0^c) = vapor flow rate to the condenser after (before) heat integration [kmol/s]

V^r (V_0^r) = vapor flow rate from the reboiler to the column after (before) heat integration [kmol/s]

$Y_{m,n}^{i,j}$ = binary variable that becomes one if rectifying stage *m* of column *i* and stripping stage *n* of column *j* is heat integrated [-]

$Y^{i,j}$ = binary variable which become one if heat exchange between columns *i* and *j* is realized [-]

Y_{ext}^i = binary variable assigned to task *i*. It becomes one when task *i* is selected [-]

z = performance index to be optimized [kW]

Greek letters

δ_n^r , δ_m^c = binary variable in estimation equations of compensation terms [-]

α = penalization parameter to avoid a large number of side heat condensers/reboilers [-]

Reference literature

(1) Andrecovich, M. J.; Westerberg, A. W. An MILP formulation for heat-integrated distillation sequence synthesis. *AIChE J.* **1985,** 31, 1461–1474.

(2) Floudas, C. A.; Paules IV, G. E. A Mixed-Integer Nonlinear Programming formulation for the synthesis of heat-integrated distillation sequences. *Comput. Chem. Eng.* **1988,** 12, 531–546.

(3) Fraga, E. S.; Žilinskas, A. Evaluation of hybrid optimization methods for the optimal design of heat integrated distillation sequences. *Adv. Eng. Software* **2003**, 34, 73–86.

(4) Mah, R.S.H.; Nicholas, J.J.; Wodnik, R.B. Distillation with secondary reflux and vaporization: A comparative evaluation. *AIChE J.* **1977**, 23, 651–657.

(5) Huang, K.; Liu, W.; Ma, J.; Wang, S. Externally heat-integrated double distillation columns (EHIDDiC): Basic concept and general characteristics. *Ind. Eng. Chem. Res.* **2010**, 49, 1333–1350.

(6) Gadalla, MA. Internal heat integrated distillation columns (iHIDiCs)-New systematic design methodology. *Chem. Eng. Res. Des.* **2009**, 12, 1658–1666.

(7) Horiuchi, K.; Yanagimoto, K.; Kataoka, K.; Nakaiwa, M.; Iwakabe, K.; Matsuda, K. Energy saving characteristics of the internally heat integrated distillation column (HIDiC) pilot plant for multicomponent petroleum distillation. *J Chem. Eng. Japan* **2008**, 41, 771–778.

(8) Iwakabe, K.; Nakaiwa, M.; Huang, K.; Nakanishi, T; Ohmori, A.; Endo, A.; Yamamoto, T. Performance of an internally heat integrated distillation column (HIDiC) in the separation of ternary mixtures. *J Chem. Eng. Japan* **2009**, 39, 417–425.

(9) Olujic, Z.; Fakhri, F.; de Rijke, A.; de Graauw, J.; Jansens, P. J. Internal heat integration—the key to an energy-conserving distillation column. *J. Chem. Technol. Biotechnol.* **2003**, 78, 241–248.

(10) Huang, K.; Shan, L.; Zhu, Q.; Qian, J. Design and control of an ideal heat-integrated distillation column (ideal HIDiC) system separating a close-boiling ternary mixture. *Energy* **2007**, 32, 2148–2156.

(11) Cabrera-Ruiz, J.; Jiménez-Gutiérrez, A.; Segovia-Hernández, J. G. Assessment of the implementation of heat-integrated distillation columns for the separation of ternary mixtures. *Ind. Eng. Chem. Res.* **2011**, 50, 2176–2181.

(12) Nakaiwa, M.; Huang, K.; Endo, A.; Ohmori, T.; Akiya, T.; Takamatsu, T. Internally Heat-Integrated Distillation Columns: A Review. *Chem. Eng. Res. Des.* **2003**, 81, 162–177.

(13) Wang, Y.; Huang, K.; Wang, S. Simplified Scheme of Externally Heat-Integrated Double Distillation Columns (EHIDDiC) with Three External Heat Exchangers. *Ind. Eng. Chem. Res.* **2010**, 49, 3349–3364.

(14) Kim, Y. H. Internally and Partially Heat-Integrated Distillation System for Ternary Separation. *Ind. Eng. Chem. Res.* **2011**, 50, 5733–5738.

(15) Zhang, X.; Huang, K.; Chen, H.; Wang, S. Comparing three configurations of the externally heat-integrated double distillation columns (EHIDDiCs). *Comput. Chem. Eng.* **2011**, 35, 2017–2033.

(16) Kiran, B.; Jana, A. K.; Samanta, A. N. A novel intensified heat integration in multicomponent distillation. *Energy* 2012, 41 443–453.

(17) Harwardt, A.; Marquardt, W. Heat-Integrated Distillation Columns: Vapor Recompression or Internal Heat Integration? *AIChE J.* **2012**, Accepted, DOI 10.1002/aic.

(18) Dhole, V. R.; Linnhoff, B. Distillation column targets. *Comput. Chem. Eng.* **1993**, 17 (5/6), 549–560.

(19) Gadalla, M.; Olujic, Z.; Sun, L.; de Rijke, A.; Jansens, P. J. Pinch analysis-based approach to conceptual design of internally heat-integrated distillation columns. *Chem. Eng. Res. Des.* **2005**, 83 (A8), 987–993.

(20) Alcántara-Avila, J.R.; Kano, M.; Hasebe, S. Two-Level Approach for Synthesizing Externally and Internally Heat Integrated Distillation Sequences. *13th APCChE Congress*, Taiwan, **2010**.

(21) Wakabayashi, T.; Hasebe, S. Effect of internal heat exchange rate distribution on energy saving in heat integrated distillation column (HIDiC). *Kagakukogaku Ronbunshu*, **2011**, 37, 499–505.

(22) Turton, R.; Bailie, R.C.; Whiting, W.B.; Shaeiwitz, J.A. *Analysis, Synthesis, and Design of Chemical Processes*; Prentice Hall: Upper Saddle River, New Jersey, **2003**.

(23) Chao, K.C.; Seader, J.D. A General Correlation of Vapor-Liquid Equilibria in Hydrocarbon Mixtures. *AIChE J.* **1961**, 7, 598–605.

(24) Redlich, O.; Kwong, J.N.S. On the Thermodynamics of Solutions V. An Equation-of-state. Fugacities of Gaseous Solutions. *Chem. Rev.* **1979**, 44, 223–244.

(25) Seider, W. D.; Seader, J.D.; Lewin, D.R.; Widagdo, S. *Product and Process Design Principles;* John Wiley and Sons, Inc. 3rd International student edition, **2010**.

Chapter 3

Intensification of compressor-aided distillation sequences

3.1 Introduction

In this Thesis, compressor-aided distillation refers to the inclusion of compressors in the distillation synthesis problem. A compressor can be added in conventional columns between the rectifying and stripping sections in a single column. Such a condition results in the heat integrated distillation column (HIDiC) which has been intensively researched in recent years. Another way to include a compressor in conventional columns is at the top vapor stream before it is fed to the condenser. Though the use of compressors is attractive from the viewpoint of energy conservation, the expensive equipment cost and electricity cost associated with compressors have limited its implementation in real practice.

In addition to conventional columns, there are thermally coupled columns (multiple feed and product streams with or without a condenser or a reboiler) which have increasingly been implemented in the chemical industry because they are thermodynamically more efficient than conventional columns. Sequences of conventional columns exhibit thermodynamic irreversibility owing to the mixing of streams at some stages in the column[1]. At those intermediate stages the molar fraction of a middle component is higher than that in the condenser or reboiler. Petlyuk et al.[1] mentioned that this inefficiency could be reduced by introducing sloppy separations and thermal coupling between columns. In thermal coupling a liquid side stream from a column is fed to the top of the other column to remove the condenser, and/or a vapor side stream from a column is fed to the bottom of the other column to remove the reboiler. Typically, the pressure between thermally coupled columns is kept the same, which can result in two disadvantages:

1. The temperature difference between the reboiler and the condenser increases because more than three components are separated. This feature reduces the possibility of the external heat integration with other columns
2. It is difficult to execute the internal heat integration within the thermally coupled columns because the two columns are operated at the same pressure.

The thermally coupled columns are not *"thermally flexible"* from the viewpoint of heat integration.

Thus, to increase the thermal flexibility in conventional and thermally coupled columns and to generate even more energy-efficient sequences, in this chapter an optimization method to synthesize distillation sequences with internal and external heat integration by means of vapor recompression is proposed.

3.2 Vapor recompression in conventional and thermally coupled columns

Rev et al.[2] showed that in most cases heat integrated sequences are more energy efficient than the Petlyuk column which represents one of the most researched thermally coupled columns. They mentioned that the Petlyuk column was a better alternative only over a small range of relative volatility ratio, feed composition, and price structure. However, they did not include configurations that are partially coupled or thermodynamically equivalent to the Petlyuk column in their comparisons.

The dividing-wall distillation column is thermodynamically equivalent to the Petlyuk column on the condition that no heat transfer is allowed across the dividing wall. However, Suphanit et al. [3] suggested that more energy efficient columns can be generated if heat transfer occurs within a certain part of the wall. Their analysis was based on simulations in HYSYS and CGCC calculations. Their results showed that heat transfer was very limited in the wall and the potential savings for hot utilities were between 4 and 7%.

Usually, the pressures of thermally coupled columns are the same because vapor flow between columns exists. If the pressures of two columns can be selected arbitrarily, more flexible designs with heat integration can be realized. Although less researched, one alternative is vapor recompression to reduce the energy consumption in distillation columns. A vapor stream is recompressed to a higher pressure to increase its temperature, and thereby heat integration becomes possible. Vapor recompression has been primarily applied to distillation of binary mixtures with close boiling points. Fitzmorris and Mah[4] proposed a simulation procedure to explore the thermodynamic efficiency of vapor recompression of the top stream and the vapor stream connecting the rectifying and stripping sections in an ethylene-ethane distillation column. Their results showed that vapor recompression is a valid alternative to reduce energy requirements. Oliveira et al.[5] proposed a simulation procedure for an ethanol-water distillation column with vapor recompression. Their results suggested that vapor recompression was effective in saving energy. It also could be environmentally more attractive than conventional distillation since it uses the own fluids of the column. Finally, our past research[6] focused on the recompression of vapor side streams in thermally coupled columns for a ternary mixture. Our results showed that the pressure change of vapor streams between thermally coupled columns could

yield energy savings. However, the use of compressors made them economically unappealing: the compressor cost exceeded the energy cost savings under some circumstances.

If vapor flows from a low pressure column or a low pressure section of a column to a high pressure column or section, the use of compressors is enforced between them. As a result, a compressor-aided distillation process is realized. Contrarily, if vapor flows from a high pressure column or section to a low pressure column or section, such pressure change is enforced through a throttling valve and the use of a compressor is not enforced. In this case, a compressor-free distillation is realized.

All the papers reviewed in this chapter dealt only with vapor recompression in a single conventional column or thermally coupled columns operating at the same pressure. They have not treated the synthesis problem of the distillation sequence. The aim of this chapter is to propose a systematic procedure based on rigorous simulations and mixed integer linear programming formulations which generate economically optimal sequences of columns by considering vapor recompression, pressure change and internal heat integration simultaneously. A hierarchical optimization algorithm similar to the one in Chapter 2 is proposed.

3.3 Heat integration in conventional and thermally coupled columns

According to the location of compressor, the heat integration of a conventional column can be classified to two types. Figure 3.1 (left) shows the case where the compressor is assigned between the stripping and rectifying sections. In this case, the internal heat integration between the stripping section and the rectifying section of a column can be possible, and the derived structure is HIDiC. The dotted lines in the figure represent the possible heat exchange matches. Superstructure for internal heat integration is conceptually the same as the one in Figure 2.2. The difference is that the stripping and rectifying sections belong to the same column. Figure 3.1 (right) shows the case where the compressor is assigned to the top of the column. In this case, the top vapor is regarded as the heat source and the bottom liquid is regarded as the heat sink.

In the figures, M_i is the number of stages in the rectifying section and N_i is the number of stages in the stripping section of column i. In this research, the stages are numbered downwards from stage 1 (condenser or top stage) to M_i in the rectifying section, and from stage 1 (feed) to N_i (reboiler or bottom stage) in the stripping section.

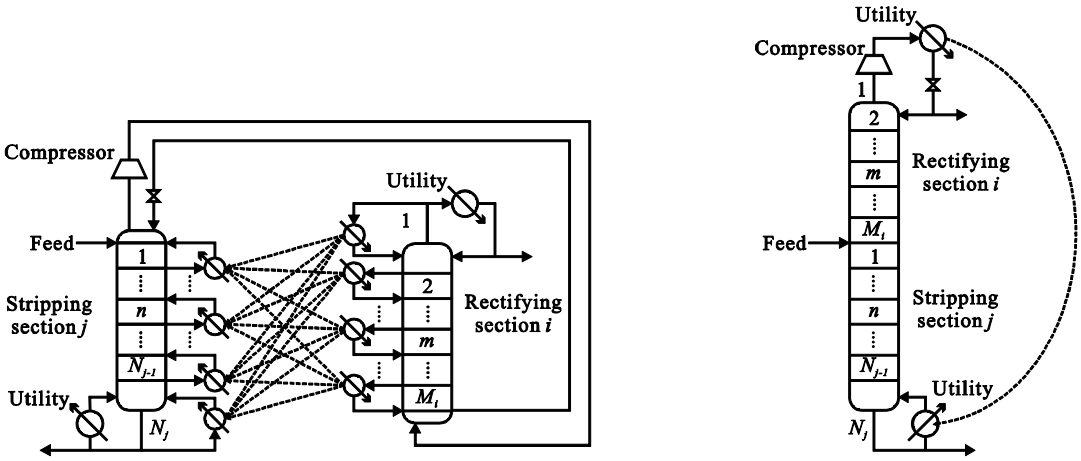

Figure 3.1. Superstructure for heat integration in conventional columns: HIDiC (left), vapor recompression (right).

Figure 3.2 shows vapor recompression in thermally coupled distillation sequences. The figure shows a superstructure to generate heat integration between the rectifying section of thermally coupled column *i* and the stripping section of thermally coupled column *j*.

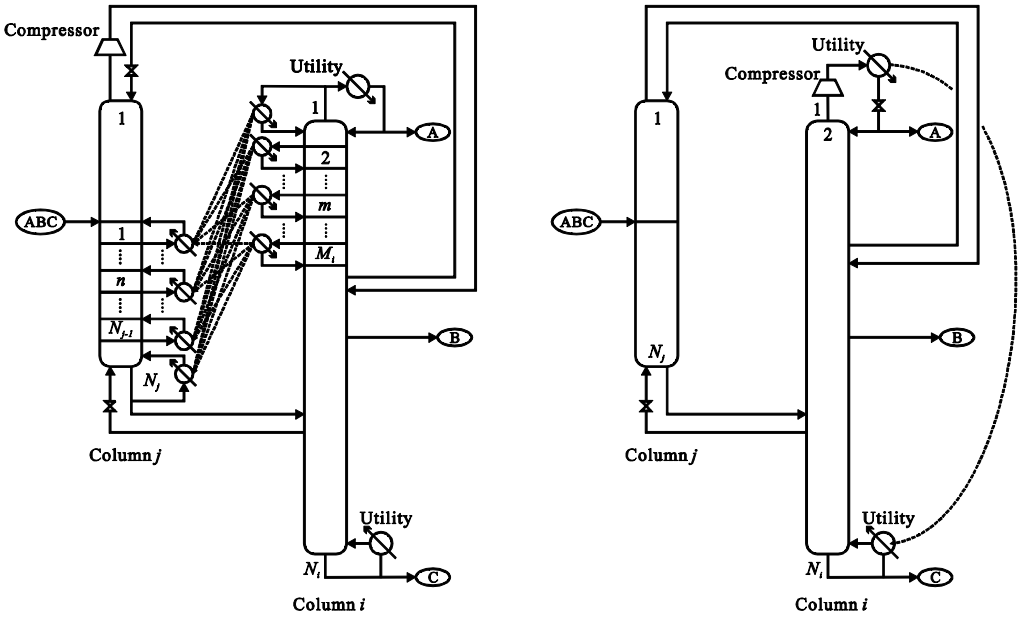

Figure 3.2. Superstructure for heat integration in thermally coupled columns: Compressor-aided sequence (left), vapor recompression (right).

When the pressures of two columns in Figure 3.2 are the same, the temperature of the rectifying section of column *i* is lower than that of column *j*, and the temperature of the rectifying section of column *j* is lower than that of the stripping section of column *j*. To realize heat integration between the rectifying section of column *i* and the stripping section of column *j*, the temperature of the stages in the rectifying section of column *i* has to be higher than that of stages in the stripping section in column *j*. To realize such a condition, the superstructure on the left hand side in Figure 3.2 needs a compressor to increase the temperature of column *i*. For the superstructure at the right hand side of Figure 3.2, a compressor is used to elevate the pressure and temperature of the top vapor stream of column *i*, and the pressurized vapor is used for heat integration.

The Petlyuk column is a fully thermally coupled column that requires lower energy than conventional distillation sequences[7, 8]. The dividing wall column is thermodynamically equivalent to the Petlyuk column when all the sections are operated at the same pressure. When pressure change is permitted, the Petlyuk column is more flexible than the dividing wall column. Thus, in this research, the Petlyuk column configuration is adopted as a candidate sequence.

Agrawal and Fidkowski pointed out that the thermally coupled columns become more operable by reducing the number of interconnections[9]. Thus, the partially coupled Petlyuk column with a reboiler in the first column (PPV), and the partial Petlyuk column with a condenser in the first column (PPL) are considered as candidates. The sequence on the right side in the Figure 3.2 corresponds to the PPL thermally coupled column.

The external and internal heat integration in thermally coupled columns have not been discussed by thoroughly researchers. Thus, the candidate columns in a sequence are limited to those shown in Figure 3.3 for the separation of a ternary mixture where A the most volatile component.

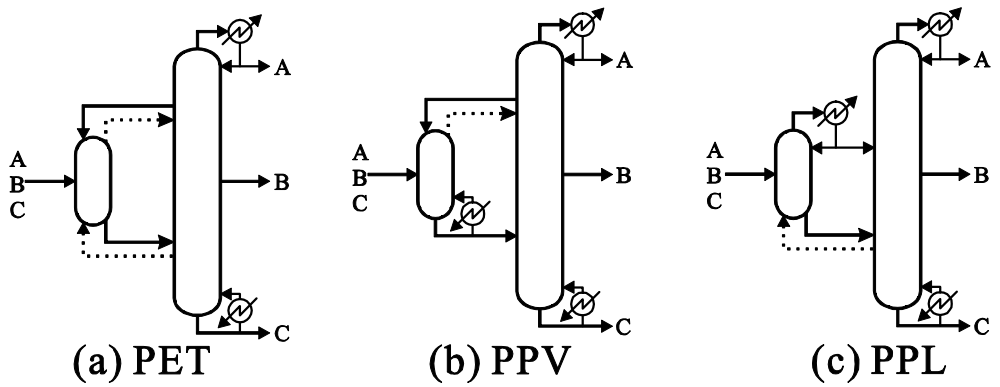

Figure 3.3. Petlyuk-type thermally coupled distillation columns to separate a ternary mixture.

If pressure change is allowed in the thermally coupled columns shown in Figure 3.3, pumps are required to flow liquid streams from low to high pressure, and compressors are required to flow vapor streams from low to high pressure. This situation is exemplified in Figure 3.4.

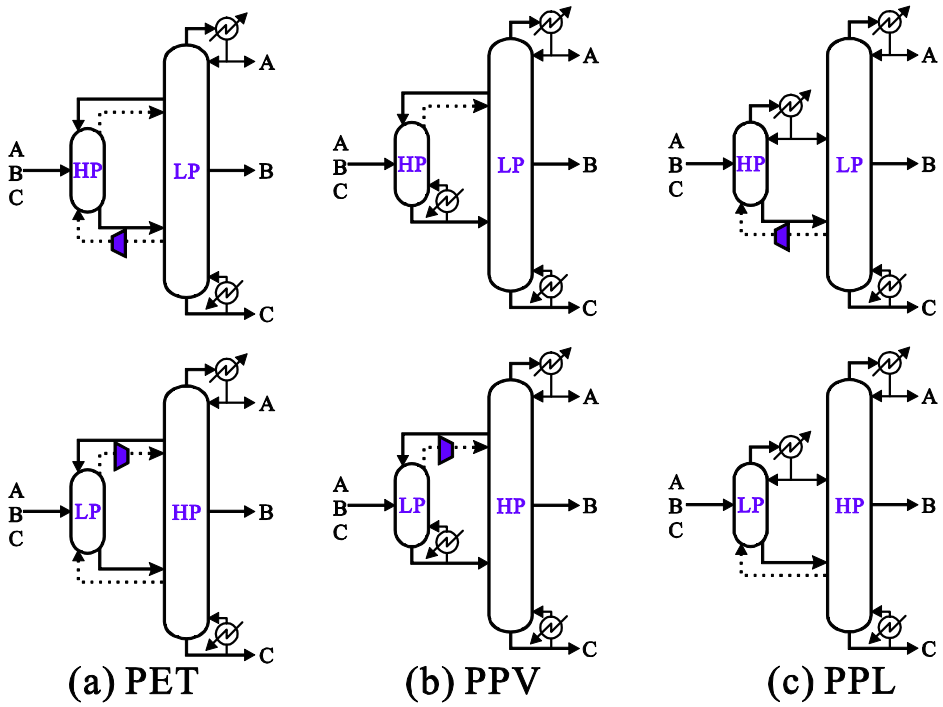

Figure 3.4. Thermally coupled distillation columns with pressure change.

In Figure 3.4, LP denotes low pressure, and HP denotes high pressure. Compressors are depicted by trapeziums. When liquid or vapor flows from high to low pressure columns pumps nor compressors are not needed, but throttling valves to drop the pressure.

3.4 Determination of the number of stages for thermally coupled columns

In the proposed synthesis method, the number of stages for each column is optimized in advance without taking the heat integration into account. In this section the procedure for deciding the number of stages for thermally coupled columns is explained.

For thermally coupled columns, flow rates between the columns can be used as design variables. Thus, compared with conventional columns, the design variables which can be utilized for optimization increases, and the design problem becomes much complicated. In this research, the

number of stages of each column is decided in advance by using an analogy between conventional and thermally coupled columns. Figure 3.5 (a) shows a sloppy split sequence consisting of three conventional columns, and Figure 3.5 (b) shows a decomposed structure of a Petlyuk column, which is shown in Figure 3.5 (c). The design procedure consists of the following steps:

1) For SS sequence in Figure 3.5, it is assumed that the bottom molar composition of section 4 is the same as the distillate of section 5. Under that assumption, the flow rate and its composition are calculated for every stream in the sequence. It is also assumed that the column can take one of the discretized pressures.

2) At step 1), the input and output condition of each column are determined. Thus, the three columns are optimized independently. The rigorous simulation using a process simulator is used to optimize the design condition. Here, the operating pressure of each column is assumed to be the reference pressure, e.g., 304 kPa.

3) The number of stages of each section of thermally coupled columns is determined by using the analogy with the SS sequence, i.e. the sections having the same figure in Figure 3.5 are assumed to have the same number of stages.

4) The rigorous simulation is executed for thermally coupled columns to derive the condition, which minimizes the total energy consumption at the reboilers. Here, the flow rates of thermal linking streams are regarded as optimization variables. The operating pressure is assumed to be at a reference pressure, e.g., 304 kPa. The optimization procedure proposed by Hernandez and Jimenez[10] is adopted to obtain the optimal linking flows.

5) The pressures of two columns composing the thermally coupled column are selected from the available pressures, and the reflux ratio, which satisfies the product specification, is derived. It is calculated by assuming that the flow rates of thermal linking streams are constant at the optimal value obtained in step 4). The assumption of fixing the flow rates of liquid and/or vapor streams between thermally coupled columns can drastically reduce the computation time for optimization.

6) Step 5 is repeated for every combination of the pressures of two columns.

The section analogy is applied to other types of thermally coupled columns, though the section analogy of the SS sequence and the Petlyuk column is shown in Figure 3.5. Furthermore, without losing generality, this section analogy can be applied to cases of more than three components so long as a feasible design of conventional columns exists.

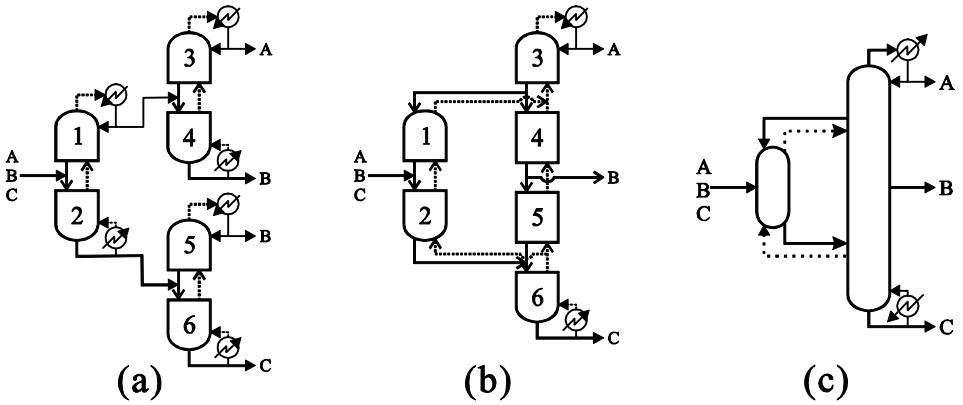

Figure 3.5. Analogy between a sloppy split (SS) sequence (a) and a Petlyuk column (c). The center is the decomposed expression of a Petlyuk column

3.5 Rigorous simulation of vapor recompression

A distillation module in commercial process simulators does not have vapor recompression as a possibility. Thus, the simulation of the vapor recompression part, which is operated at higher pressure (HP) and depicted by the solid lines in Figure 3.6, is executed separately from the main part, which is operated at lower pressure (LP) and depicted by the dotted lines in the same figure. The flow rate and composition of a vapor stream leaving column i, which are obtained by the rigorous simulation, and the pressures before and after the compressor are used to calculate vapor recompression work duty, W_{VR}^{i}, the condenser heat duty, $q_0^{c,i}$, the temperature after vapor recompression, T_{vap}^{i}, and temperature of the liquid leaving the condenser, T_{liq}^{i}.

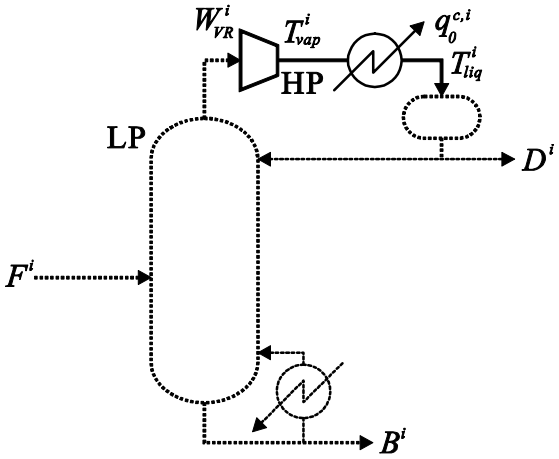

Figure 3.6. Schematic representation of vapor recompression

3.6 Internal heat integration between two sections or columns

In this section the problem of synthesizing optimal distillation sequences with internal and external heat integration will be formulated as a mixed integer linear programming (MILP) problem.

When rectifying sections whose stages are regarded as heat sources and stripping sections whose stages are regarded as heat sinks are given in a set of columns, an internal heat integration network can be obtained. In this subsection, a general MILP formulation is the same as the one in Chapter 2. Therefore, when internal heat integration is realized in a distillation column, changes on the condenser and reboiler duties are estimated as proved in Chapter 2.

If the use of compressors is possible in the synthesis problem, its equipment cost and electricity cost must be included to derive the best distillation sequence. Thus, the calculation of the compressor equipment cost is covered in detail.

Thermally coupled columns can have vapor streams between two columns. A compressor is required when the pressure of the feeding column is lower than that of the receiving column and such cost must not be neglected because compressors entail high equipment and electricity costs. Consider column *i* and column *j* to be the first and second columns (sections) which form thermally coupled columns in Figure 3.2. When the pressure of column *j* is higher than that of column *i*, the vapor flow from column *i* to column *j* must be compressed. This compressor work duty is expressed by $W_{comp}^{i,j}$, and is calculated using the flow rate, composition, temperature and pressure difference. When the pressure of column *i* is equal to or lower than column *j*, $W_{comp}^{i,j}$ is set equal to zero. Here, it should be noted that the flow rates between the columns are determined in advance as explained at section 3.4 when the types of thermally coupled column and the pressures of two columns are selected.

The derived compressor work duty is used to calculate the compressor cost $C_{i,j}^{comp}$ as reported by Turton et al.[11]

$$C_{comp}^{i,j} = f\left(W_{comp}^{i,j}, \phi_{comp}\right) \qquad (i,j) \in CA \tag{1}$$

where ϕ_{comp} is a set of parameters such as a compressor type, construction materials, and pressure factor. *CA* is the set of the pair of columns, which compose a thermally coupled task. Two types of isentropic compressors were investigated in this work: rotary-type compressors, whose work duty is between 18 and 450 kW, and centrifugal-type compressors whose work duty is between 450 and 3000 kW.

The work duty for recompression W_{VR}^{i}, obtained in section 3.5, is used to calculate the compressor cost of vapor recompression for column *i*, C_{VR}^{i}. The cost function of the compressor installed for vapor recompression is generally described by

$$C_{VR}^{i} = f\left(W_{VR}^{i}, \phi_{comp}\right) \qquad i \in VR \subset TK \tag{2}$$

where *VR* is the set of tasks with vapor recompression. It is a subset of the set of all tasks, *TK*.

3.7 Superstructure considering thermally coupling columns and vapor recompression

In order to use the latent heat of the top vapor stream in a distillation column as heating medium of its bottom stream, a compressor is used to increase the pressure of the top vapor stream. In HIDiC, a compressor is used to increase the pressure of the entire rectifying section. For both cases, a compressor is used in one distillation column. For multi-column systems, pumps are used to increase the pressure, because the equipment and operating costs of pumps are remarkably less than those of compressors. Thus, the use of compressors to realize heat integration has not been proposed so far for multi-column systems such as the thermally coupled columns.

In this chapter the synthesis problem of separating ternary mixtures is discussed. To solve the synthesis problem, firstly, it is necessary to define all candidate distillation sequences to separate a given mixture. In this research, a superstructure-based approach is adopted to enumerate the candidate sequences to perform a given separation.

A superstructure, which comprises conventional and thermally coupled distillation columns separating a three-component mixture is shown in Figure 3.7. Here, a sequence consisting of three conventional columns (SS sequence in Figure 3.5a) and thermally coupled sequences PET, PPV and PPL in Figure 3.3 are selected as candidates for the final structure. The mixture consists of A, B, and

C, being A the most volatile component. The superstructure generated is a state task network representation. Each ellipse in Figure 3.7 is a state having information of the composition and physical conditions. When the amount of feed and its composition as well as the composition of every product are given, the amount of each product can be calculated from material balance equations.

States AB and BC are intermediate states of the SS sequence. The output flow rate and composition of the first column of SS is obtained by setting the molar composition of the heavy component, C, in the distillate and the molar composition of the light component, A, in the bottom stream. The enforcement of these two specifications for the intermediate streams, and the assumption of no flow split of intermediate states uniquely defines states AB and BC in Figure 3.7. It is assumed that each state is liquid at its saturated temperature and that the compression and decompression cost of liquid is negligible. Thus, liquids with the same composition are expressed by one state even if the pressure is different. It is also possible to include states as saturated vapor. In such cases, as the compression cost of vapor cannot be neglected, the vapor at different pressure should be treated as different state even if the composition and the flow rate are the same.

Task AB/BC, (P_i) means that mixture ABC is separated into state AB and state BC by a conventional column operated at pressure P_i. The fixed cost and the operating cost depend on the operating pressure. Thus, the columns with different pressures are treated as different tasks even if the feed and product states are the same.

For thermally coupled columns, each column is treated as a task, and the columns operated at different pressures are regarded as different tasks. For example, PET_1, (P_i) means the first column of Petlyuk column operated at pressure P_i, and PET_2, (P_i) means the second column of Petlyuk column operated at pressure P_i. PPV and PPL indicate the column structures shown in Figure 3.3. A pair of first and second columns is hereafter called “an aggregated task.” The pressures of the first and second columns in a sequence are not necessarily the same. If the pressure of the first and/or second column is different, such sequences are treated as different aggregated tasks even when the inlet and outlet states are the same. When a vapor stream flows from a low pressure column to a high pressure column, the use of a compressor is enforced, and when a vapor stream flows from a high pressure column to a low pressure column, compressor is not necessary.

A/B/C_i in Figure 3.7 denotes an aggregated state consisting of the liquid and vapor streams linking two thermally coupled columns. The condition of an aggregated state depends on the selection of the thermally coupled columns in an aggregated task.

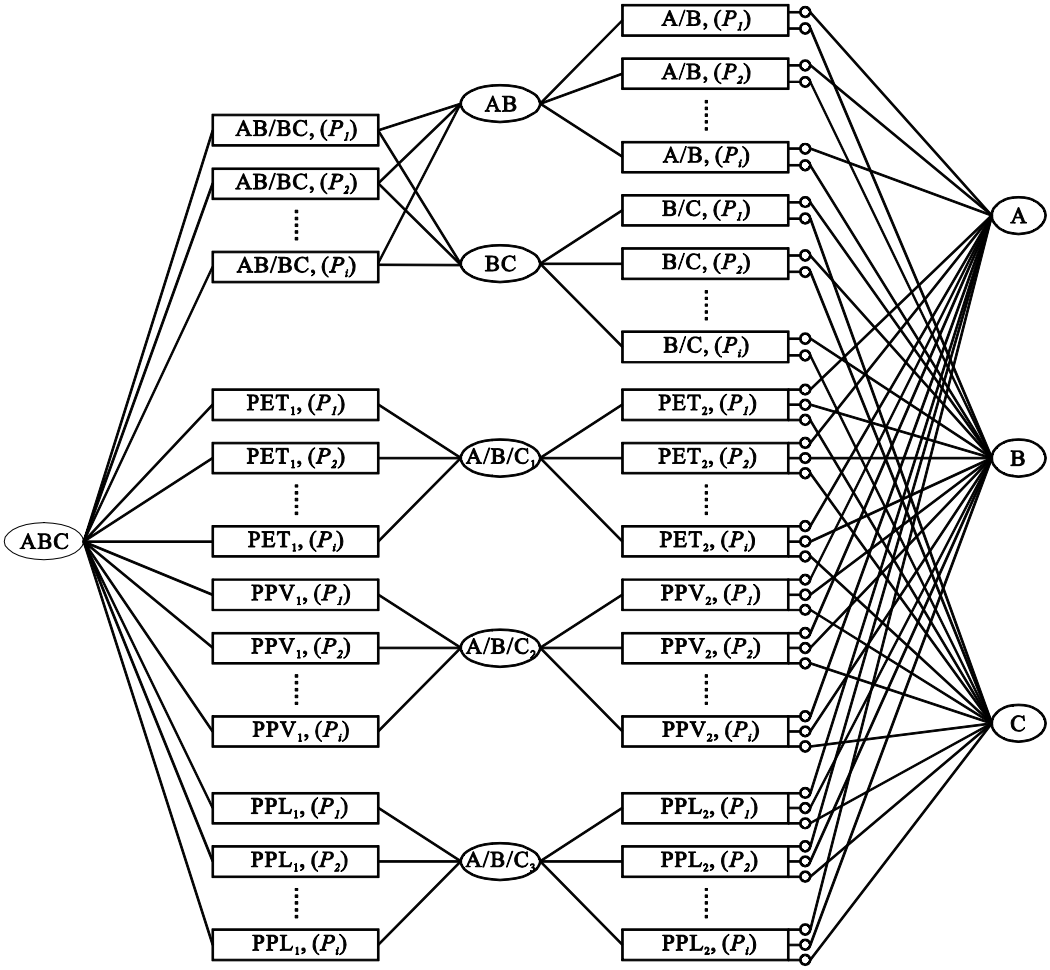

Figure 3.7. Superstructure of a three-component separation problem

3.8 Hierarchical optimization algorithm

In the proposed synthesis procedure, the optimal heat integrated distillation sequence is derived by a hierarchical optimization algorithm similar to the one explained in Chapter 2. The entire synthesis procedure consists of the following steps:

1) For given feed and product conditions, the intermediate states conditions are calculated. The pressures, which can be adopted by each column, are decided. Using this information, the superstructure such as shown in Figure 3.7 is generated.

2) For each task of conventional column, the design and operating conditions are calculated by executing rigorous simulations. At this step, heat integration is not considered.

3) For thermally coupled columns, the number of stages in the first and second columns is optimized using the procedure shown in Section 3.4. Then, the vapor and liquid linking flows are optimized at a reference pressure.

4) For thermally coupled columns, select a pair of tasks to generate an aggregated task. For each of the aggregated tasks, the design and operating conditions are calculated by executing rigorous simulations. At this step, heat integration is not considered.

5) For each task, effects of side reboiler and side condenser on the reboiler and condenser duties are calculated by executing rigorous simulations. The results are summarized as shown in Equation 15 in Chapter 2. For aggregated tasks, the liquid and vapor flow rates of the side streams linking two columns are assumed to be constant.

6) The work duty and the compressor cost for vapor recompression in a task of conventional column, and in an aggregated task of thermally coupled columns is calculated according with the procedures in sections 3.5 and 3.6.

7) Decide the area of each side heat exchanger, A^{int}, and the upper bound for internal heat integration, Q_{UP}.

8) For every combination of two tasks, the MILP problem explained in chapter 2 is solved to derive the optimal structure of internal heat integration. The changes in reboiler and condenser duties are calculated using the compensation terms calculated at step 5.

9) The synthesis problem to obtain the best sequence is formulated as an MILP problem, and solved by using a commercial optimization package. The detail of this step is explained in the next subsection.

10) Steps 7 through 9 are repeated for new values of A^{int} and Q_{UP} till there is not further improvement of the objective function.

3.8.1 Formulation of the synthesis problem with vapor recompression

From step 8 in the synthesis procedure explained above, the best combination of stages, which maximizes internal heat integration, is calculated for each pair of tasks. When internal heat integration is realized, the condenser and reboiler duties as well as the internal vapor and liquid flow will change. With the estimated values of the vapor flows, the compressor work duty and compressor equipment cost can be obtained. By calculating the values of the heat duties, work duty and compressor cost, in advance, the synthesis procedure developed for the distillation sequences with external heat integration proposed by Andrecovich and Westerberg [12] can be implemented with

minor modifications to also consider internal heat integration and vapor recompression. Thus, in this section, the resulting MILP formulation is derived to include internal heat integration and vapor recompression as possibilities.

The connectivity constraints between columns to generate feasible sequences are given by

$$\sum_{i \in FEED} Y_{ext}^{i} = 1 \tag{3}$$

$$\sum_{i \in COLF_s} Y_{ext}^{i} - \sum_{i \in COLP_s} Y_{ext}^{i} = 0 \qquad s \in ST \tag{4}$$

where Y_{ext}^{i} is a binary variable assigned to each task in the superstructure of Figure 3.7. If task *i* is selected, Y_{ext}^{i} becomes one; zero otherwise. *FEED* denotes the set of tasks whose input stream is the original feed state. $COLF_s$ and $COLP_s$ are the set of tasks, which have state *s* as an output and as an input, respectively. *ST* is the set of states, excepting the feed and product states. Here, aggregated states are included in *ST*. Equations 3 and 4 mean that the split of a stream is not permitted.

If task *i* is not used in the sequence, the internal heat integration between task i and other task cannot be executed. This constraint is expressed by

$$\sum_{j \in TK} Y^{i,j} \le Y_{ext}^{i} \qquad i \in TK \tag{5}$$

$$\sum_{i \in TK} Y^{i,j} \le Y_{ext}^{j} \qquad j \in TK \tag{6}$$

In this research, it is assumed that the heat supply to a stripping section of a column from two or more columns, and the heat supply from a rectifying section of a column to two or more columns are prohibited.

When internal heat integration is not considered, the energy balance equations at the reboiler and condenser of task *i* are expressed by the following equations:

$$\sum_{j \in CU} Q_{ext}^{i,j} + \sum_{j \in TK} Q_{ext}^{i,j} = q_0^{c,i} \cdot Y_{ext}^{i} \qquad i \in TK \tag{7}$$

$$\sum_{i \in HU} Q_{ext}^{i,j} + \sum_{i \in TK} Q_{ext}^{i,j} = Q_0^{r,j} \cdot Y_{ext}^{j} \qquad j \in TK \tag{8}$$

where *HU* and *CU* are the sets of heating and cooling utilities, respectively. $Q_{ext}^{i,j}$ is the amount of heat exchanged between the condenser of task *i* (or hot utility *i*) and the reboiler of task *j* (or cold utility *j*). $q_0^{c,i}$ and $Q_0^{r,j}$ are condenser and reboiler duties of task *i* and *j* for the case where neither internal nor external heat integration is considered. Finally, *TK* is set of tasks in the superstructure.

By introducing the internal heat integration and vapor recompression as possibilities, the above equations are modified into the following equations:

$$\sum_{j \in CU} Q_{ext}^{i,j} + \sum_{j \in VR} Q_{ext}^{i,j} + \sum_{j \in TK} Q_{ext}^{i,j} + \sum_{j \in TK} q_{opt}^{i,j} \cdot Y^{i,j} = q_0^{c,i} \cdot Y_{ext}^{i} \qquad i \in TK \tag{9}$$

$$\sum_{i\in HU} Q_{ext}^{i,j} + \sum_{i\in VR} Q_{ext}^{i,j} + \sum_{i\in TK} Q_{ext}^{i,j} + \sum_{i\in TK} Q_{opt}^{i,j} \cdot Y^{i,j} = Q_0^{r,j} \cdot Y_{ext}^{j} \qquad j \in TK \tag{10}$$

where $q_{opt}^{i,j}$ and $Q_{opt}^{i,j}$ are the net reductions of condenser duty of column *i* and the reboiler duty of column *j* resulting from the heat integration between the rectifying section of column *i* and the stripping section of column *j*, respectively. It should be noted that $q_{opt}^{i,j}$ and $Q_{opt}^{i,j}$ are obtained as the optimization results at step 7 of the synthesis procedure, and they are input as constant parameters at step 8. The difference between the conventional problem and newly proposed problem is the introduction of 0-1 variables, $Y^{i,j}$, to link internal heat integration at the first optimization level and external heat integration at the second optimization level.

The inclusion of compressors in the synthesis problem results in a different optimization problem than the one in Chapter 2. Vapor recompression increases heat exchange possibilities between tasks because vapor at higher pressure is available. Equations 9 and 10 include terms, which represent the energy exchange possibilities when vapor recompression is adopted.

When pressure change in aggregated tasks is possible, Equations 11 and 12 are necessary to depict the existence of a compressor in a vapor stream from a low pressure column to a higher pressure column.

$$\sum_{j\in TKP_s} Y_{comp}^{i,j} - Y_{ext}^{i} = 0 \qquad i \in TKF_s, s \in STc \tag{11}$$

$$\sum_{i\in TKF_s} Y_{comp}^{i,j} - Y_{ext}^{j} = 0 \qquad j \in TKP_s, s \in STc \tag{12}$$

where $Y_{comp}^{i,j}$ is a variable that indicates the use of aggregated task, which consists of task *i* and task *j*. *STc* is the set of aggregated states. TKF_s (TKP_s) is a set of tasks whose output (input) stream connects with aggregated state *s*. Since $Y_{comp}^{i,j}$ is determined by binary variables Y_{ext}^{i} and Y_{ext}^{j}, there is no need to define $Y_{comp}^{i,j}$ as a binary variable; it can be defined as a continuous variable between zero and one instead. This definition effectively works to reduce the number of binary variables.

Thus, by little modifications of the conventional optimization algorithm, the optimization problem which minimize the total annual cost, TAC, can be formulated as:

$$\min \quad TAC = \frac{FC}{PT} + OH \cdot OC \tag{28}$$

where *PT* is the payout time and *OH* is the annual operation hours. *TAC*, *FC* and *OC* are the values for the total annual cost, fixed and operating costs, which are given by

$$FC = \sum_{i\in TK}\left(C_{col}^{i} + C_{tray}^{i}\right)Y_{ext}^{i} + \sum_{i,j\in TK} CS^{i,j}Y^{i,j} + \sum_{i,j\in TK} C_{ext}^{i,j}Q_{ext}^{i,j} + \sum_{\substack{i\in HU\\ j\in TK}} C_{ext}^{i,j}Q_{ext}^{i,j} + \sum_{\substack{i\in TK\\ j\in CU}} C_{ext}^{i,j}Q_{ext}^{i,j}$$

$$+\sum_{i\in TK} C_{VR}^{i}Y_{ext}^{i} + \sum_{\substack{i\in VR\\ j\in TK}} C_{ext}^{i,j}Q_{ext}^{i,j} + \sum_{s\in STc}\sum_{\substack{i\in TKF_s\\ j\in TKP_s}} C_{comp}^{i,j}Y_{comp}^{i,j} \qquad (29)$$

$$OC = \sum_{\substack{i\in HU\\ j\in TK}} C_{heat}^{i,j}Q_{ext}^{i,j} + \sum_{\substack{i\in TK\\ j\in CU}} C_{cool}^{i,j}Q_{ext}^{i,j} + C_{elec}\left(\sum_{i\in TK} W_{VR}^{i}Y_{ext}^{i} + \sum_{s\in STc}\sum_{\substack{i\in TKF_s\\ j\in TKP_s}} W_{comp}^{i,j}Y_{comp}^{i,j}\right)$$

where C_{col}^{i} and C_{tray}^{i} are column cost and tray cost of task *i*, respectively. $CS^{i,j}$ is the cost for all the side heat exchangers for internal heat integration between a rectifying section of task *i* and the stripping section of task *j*. C_{VR}^{i} is the cost of the installed compressor to realize vapor recompression. $C_{comp}^{i,j}$ is the cost of the compressor installed between the task *i* and *j* which compose an aggregated task. C_{col}^{i}, C_{tray}^{i}, C_{VR}^{i}, $CS^{i,j}$ and $C_{comp}^{i,j}$ have been calculated in advance at step 7 of the synthesis procedure. W_{VR}^{i}, and $W_{comp}^{i,j}$ are the compressor work duty to realize vapor recompression of top the vapor stream in task *i* and the side vapor streams in thermally coupled columns (task *i* and *j*). $C_{ext}^{i,j}$ is the unit cost of external heat exchanger to execute unit amount of heat exchange. C_{heat}^{i}, C_{cool}^{j}, and C_{elec} are the costs of heating utility *i*, cooling utility *j*, and electricity respectively. The equipment cost was calculated according to Turton et al.[11]

3.9 Separation of a ternary mixture

The hierarchical optimization algorithm presented in section 3.8 is applied to find the best distillation sequence of conventional or thermally coupled columns through the case study of separating ternary components, Benzene (A), Toluene (B) and M-xylene (C). The feed and product specifications are shown in Table 3.1. Since the components in the case study does not exhibit azeotropic behavior, but the mixture is not ideal, the NRTL Equation[13] for the liquid phase and the Redlich-Kwong equation of state[14] for the vapor phase were used. Table 3.2 shows additional data for the utilities and overall heat transfer coefficients for the heat exchangers.

Table 3.1. Specifications of case study

Feed condition
Flow rate: 160 kmol/h
Composition [mol%]:
Benzene/Toluene/M-xylene = 50/19/31
Temperature: 369 K (Boiling point of the feed mixture)
Pressure: 101 kPa
Product specifications:
Benzene (A): 99 mol %
Toluene (B): 92 mol %
M-xylene (C): 99 mol %

Table 3.2. Data for utilities and heat transfer coefficients[15]

Utility	Temperature [K]	Cost [$/MWh]
Chilled Water†, (CHW)	278	14.40
Cooling Water†, (CW)	305	0.914
Steam at 446 kPa, (S1)	420	11.17
Steam at 1135 kPa, (S2)	459	18.93
Steam at 3202 kPa, (S3)	511	29.43
Heat transfer coefficients [kW/(m^{2}K)]		
Condenser: 0.6, Reboiler: 1, Heat exchanger: 0.5		
† 20 K Rise		

In this case study, the compositions of states A, B and C are assumed to be (99/1/0), (4/92/4) and (0/1/99), respectively, where the number in the parentheses are mole fractions of Benzene, Toluene and M-xylene, respectively. From these values, the flow rates of states A, B and C can be calculated. The compositions of states AB and BC are determined by assuming the molar composition of C in the distillate and that of A in the bottom stream. AB was assumed to be (88/11/0.5), and BC (1/28/71). The flow rates of states AB and BC are also calculated from these data.

3.9.1 Decision of number of stages of each column

The input and output condition of all the columns composing the SS sequence are decided. Thus, the each column is optimized using rigorous simulation so as to determine the number of stages of each column. The results are summarized in Table 3.3. To derive these data, the pressure is assumed to be 101 kPa, and the tray efficiency is assumed to be 80 %. The payout time is 10 years and the annual operation hours are 8000 hours.

By using data in Table 3.3, the flow rates between the columns composing a thermally coupled column are optimized.

Table 3.3. Number of stages and reflux ratios at 101kPa

First column
Number of stages of rectifying section: 10
Number of stages of stripping section: 12
Reflux ratio: 0.528
Second column separating Benzene from Toluene
Number of stages of rectifying section: 9
Number of stages of stripping section: 11
Reflux ratio: 0.706
Third column separating Toluene from M-xylene
Number of stages of rectifying section: 12
Number of stages of stripping section: 10
Reflux ratio: 2.825

3.9.2 Derivation of the compensation terms

In order to estimate the condenser and reboiler duties after the internal heat integration, the compensation term given by Equation 15 in Chapter 2 is derived for each of the three columns of the SS sequence. Here, the result for the first column operating at 101 kPa is summarized.

Table 3.4 shows several scenarios of multiple heating and cooling. Multiple side reboilers are installed in cases 1 to 3, multiple side condensers are installed in cases 4 to 6, and the both side reboilers and side condensers are installed in cases 7 to 9.

The results are summarized in Table 3.5 for the estimation of the condenser and reboiler duties. In Table 3.5, q_m is the amount of heat removed from stage m of rectifying section, q^c is the condenser heat duty after heat integration, Δq^c is the overall compensation term of condenser which is defined by Equation 14 in Chapter 2, $\Delta \hat{q}^c$ is the estimated value of Δq^c given by Equation 15 in Chapter 2, Q_n is the amount of heat supplied to stage n of stripping section, Q^r is the reboiler heat duty after heat integration, ΔQ^r is the overall compensation term of reboiler which is defined by Equation 13 in Chapter 2, and $\Delta \hat{Q}^r$ is the estimated value of ΔQ^r given by Equation 15 in Chapter 2.

In Table 3.6 the calculated values of flow rates in top and bottom vapor and liquid streams and their estimation values are shown. Case 0 in Tables 3.5 and 3.6 is the case in which no side reboiler nor side condenser are installed.

Table 3.4. Example cases of side heating and/or side cooling

	Stage in the rectifying section									Stage in the stripping section										
Case	2	3	4	5	6	7	8	9	10	1	2	3	4	5	6	7	8	9	10	11
1	100	100	100	100																
2				50	100	50														
3	100				100				100											
4															50	50	50	50	50	50
5													150	200	150					
6										150				150				150		
7					150	100	100	100								150	150	150	150	150
8	50	50	50	50	50						150	150	150	150						
9	200			200				100			100				200					200

The values in the table are in kW

Table 3.5. Estimation of reboiler and condenser duties

Case	$\sum q_m$	q^c	Δq^c	$\Delta \hat{q}^c$	$\sum Q_n$	Q^r	ΔQ^r	$\Delta \hat{Q}^r$
0	0	1231	0	0	0	1290	0	0
1	400	843	12	12	0	1302	12	11
2	200	1064	33	30	0	1323	33	30
3	300	987	56	58	0	1346	56	58
4	0	1239	8	9	300	998	8	8
5	0	1284	53	41	500	843	53	41
6	0	1299	68	65	450	908	68	65
7	450	906	125	106	750	665	125	106
8	250	1095	114	89	600	805	115	89
9	500	828	97	72	500	887	97	72

* The heat duties are in kW

Table 3.6. Estimation of internal vapor and liquid flows

Case	Vapor flow rate to the condenser	Estimated value of vapor flow rate to the condenser	Liquid flow rate returned to the top of the column	Estimated value of liquid flow rate returned to the top of the column	Vapor flow rate from the reboiler to the column	Estimated value of vapor flow rate from the reboiler to the column	Liquid flow rate to the reboiler	Estimated value of liquid flow rate to the reboiler
0	137.3	137.4	48.2	47.5	140.0	128.1	210.1	198.2
1	94.1	94.1	4.6	4.2	141.4	129.2	211.9	199.3
2	117.6	118.4	20.4	28.5	142.5	131.0	213.3	201.2
3	110.4	110.4	21.5	20.5	146.2	133.8	217.4	204.0
4	138.2	138.4	48.1	48.5	109.1	99.1	179.0	169.2
5	142.9	141.9	51.5	52.1	92.5	82.5	161.1	152.7
6	144.3	144.6	53.1	54.8	99.1	89.8	167.9	160.0
7	101.4	99.0	13.3	9.1	74.3	64.1	146.2	134.3
8	121.8	119.4	29.5	29.5	88.3	77.3	156.1	147.5
9	90.6	89.6	0.9	-0.3[†]	95.7	85.6	166.1	155.7

* The flow rates are in kmol/h

[†] The estimation method yields to an infeasible result.

Our proposed method to estimate the changes in condenser and reboiler duties after internal heat integration proved to be reliable. The average deviation between the values obtained from rigorous simulations (exact solution) and the estimation was -4.2%. In most cases, the proposed equations underestimated the exact solution, however, the obtained values result in a tight lower bound for the exact solution.

3.9.3 Internal and external heat integration in conventional columns

All the sequences in the superstructure in Figure 3.7 were simulated at three different pressures, 101, 202 and 303 kPa. Tray efficiency is assumed to be 80 %. Penalization parameter, α, in Equation 30 of Chapter 2 is set to 1.0. The hierarchical optimization algorithm was executed in the IBM OPL ILOG by using CPLEX to separate the ternary mixture.

Figure 3.8a is the best SS sequence which can realize external heat integration between columns, the column separating B from C operates a higher pressure and supplies energy to the column separating A from B. Figure 3.8b is the feasible result of Figure 3.8a when validated through rigorous simulations. Figure 3.8c is the best sequence with internal and external heat integration for a minimum *LMDT* of 10K. The internal heat integration is executed at the stages indicated by the same "X_i" in the figure. In addition, at the bottom of the figure, the quantitative data of internal heat exchange network are displayed. Internal heat integration is realized between the rectifying section of the columns separating AB from BC supplies energy to the stripping section of the column separating A from B while external heat integration is executed between the condensers in the column separating B from C and the other columns. Figure 3.8d is the feasible result of Figure 3.8c when validated through rigorous simulations. Figure 3.8c and 3.8d show some differences in the internal heat exchange networks because the proposed approach yields to a solution more optimistic than the actual feasible solution 3.8d. This means that the proposed approach underestimates the feasible optimal solution, but still it is a good result because the solution in Figure 3.8c is a tight lower bound.

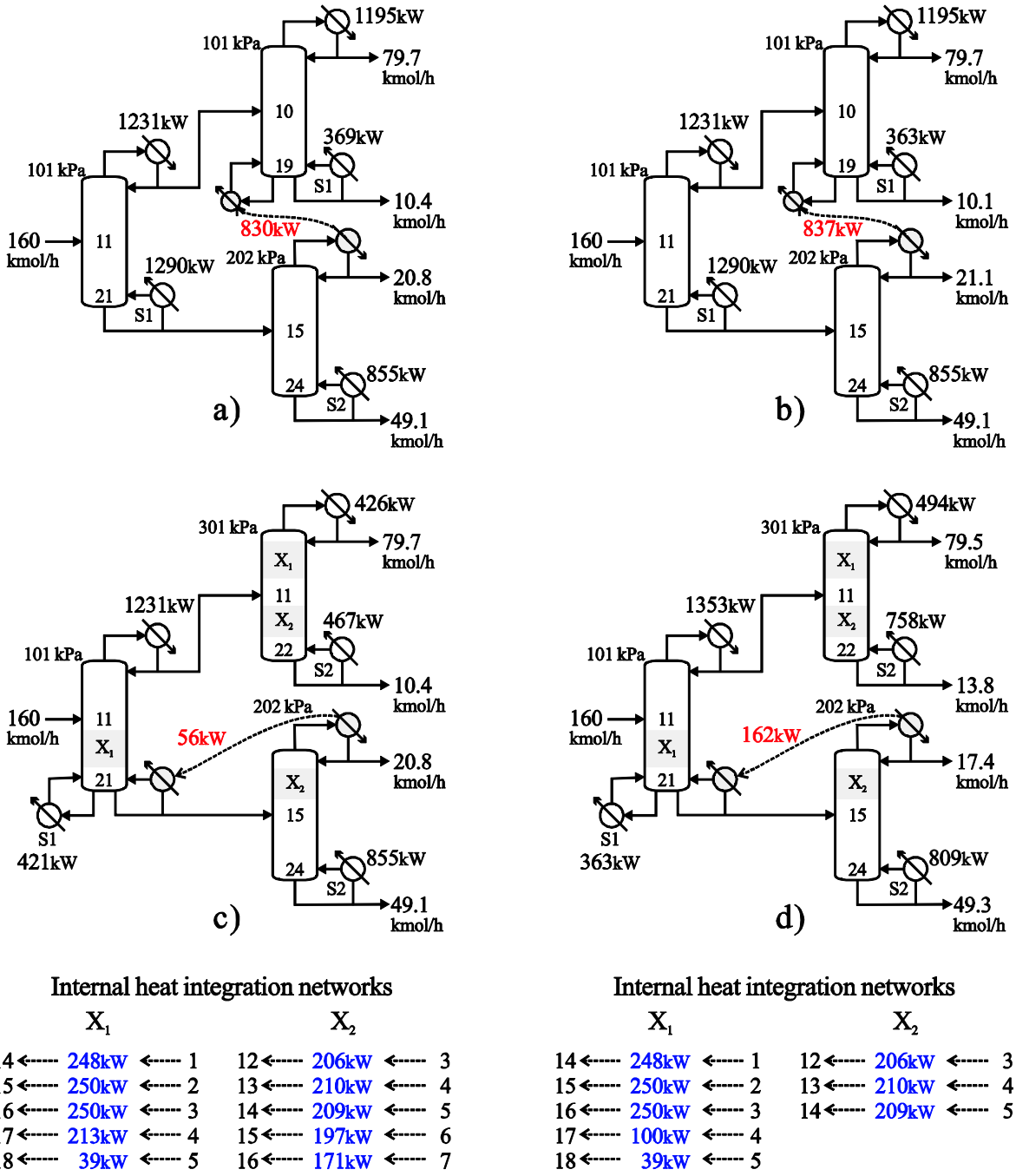

Figure 3.8. Optimal heat integrated distillation sequences for the BTX mixture:
a) sequence with external heat integration (proposed method),
b) feasible sequence obtained by rigorous simulation of solution a,
c) sequence with external and internal heat integration (proposed method), and
d) feasible sequence obtained by rigorous simulation of solution c.
red: external heat integration, blue: internal heat integration, black: utility

For the sake of comparison, the proposed method and the exact solution from rigorous simulations are shown in Table 3.7. When only external heat integration is possible, the results of both approaches did not show large differences. When internal and external heat integration are possible, the results of both approaches show some differences especially in the column separating B from C. Since solution 3.8c underestimates the actual feasible solution, the values of the reflux ratio in the proposed method yielded to a negative value.

Table 3.7 Economic and energy savings for the optimal sequences

	TAC [k$/y]	*FC/PT* [k$/y]	$OH \cdot OC$ [k$/y]	Economic savings [%]	Energy consumption [kW]	Energy savings [%]	A_{opt}^{int} † [m^2]	R^{c*} [-]
								0.528
Base case	534.2	216.7	317.5	---	3292	---	---	0.706
								3.309
								0.528
Figure 3.8a	456.4	161.0	295.4	15	2514	24	---	0.704
								3.307
								0.528
Figure 3.8b	458.0	161.8	296.2	14	2513	24	---	0.706
								3.282
								0.528
Figure 3.8c	420.3	170.4	249.9	21	1743	47	29	-0.39**
								-0.71**
								0.610
Figure 3.8d	451.1	167.6	283.5	16	1931	41	29	0.137
								0.004

† A_{opt}^{int} is the optimal value of A^{int} in Equation 29 of Chapter 2.

* Each line in the column R^c defines the value of the reflux ratio for the first, second, and third column, respectively.

** The estimated reflux ratio according to Equation 19 in Chapter 2 yields to an infeasible value

From the presented results, a combination of external and internal heat integration in conventional columns can be an attractive solution to reduce the fixed and operation cost in distillation. Furthermore, compressors are not necessary to achieve internal heat integration. The use of

compressors in conventional and thermally coupled distillation columns is carried out in the next subsection.

3.9.4 External heat integration and vapor recompression in conventional and thermally coupled columns

Although conventional columns have employ energy conservation methods to reduce their energy consumption, they entail thermodynamic irreversibility due to the mixing of intermediate components. Therefore in this subsection, we deal with the synthesis problem to find optimal distillation columns by adopting vapor recompression in top vapor streams of conventional and thermally coupled columns as well as pressure change between thermally coupled columns.

The optimization algorithm was executed in the IBM OPL ILOG by using CPLEX to separate the ternary mixture. Figure 3.9 shows the optimal solutions of the proposed approach for conventional and thermally coupled columns while Figure 3.10 shows the optimal feasible results from the exact solution obtain through rigorous simulations.

Figure 3.9a is the optimal solution, which can realize the minimum *TAC*, it is a PPV sequence operating at 101 kPa. Figures 3.9b through 9.d are suboptimal solutions when additional constraints are enforced. Figure 3.9b shows the best compressor free thermally coupled column (CF-TCDS), which is a PPV sequence whose first column operates at higher pressure and the second at lower pressure. To obtain this solution, only the aggregated tasks in the superstructure shown in Figure 3.7 were included, and the work duty, $W_{comp}^{i,j}$, for $i = j$ was set to a large value to avoid the selection of aggregated tasks where the first and second column operate at the same pressure. Figure 3.9c shows the best sequence having compressor in the structure (CA-TCDS). It is a PET sequence whose first column operates at higher pressure and the second at lower pressure. Therefore, a compressor in the lower part of the second column is necessary to link the vapor stream. To obtain this solution, only the aggregated tasks in the superstructure shown in Figure 3.7 were included, and the summation of the work duty $W_{comp}^{i,j}$ for all the aggregated tasks was enforced to take a positive value. Figures 3.9a through 3.9c did not realize external heat integration even though pressure change was enforced. Finally, Figure 3.9d is the best sequence with vapor recompression. To obtain this solution, all the tasks in Figure 3.7 were included in the superstructure and the summation of the work duty for vapor recompression, W_{VR}^{i}, in all the tasks was enforced to take a positive value. The top vapor stream in the column separating AB from BC was recompressed up for 303 kPa, which

resulted in heat integration with the reboiler of the column separating A from B. In addition, external heat integration between columns separating B from C and AB from BC was realized.

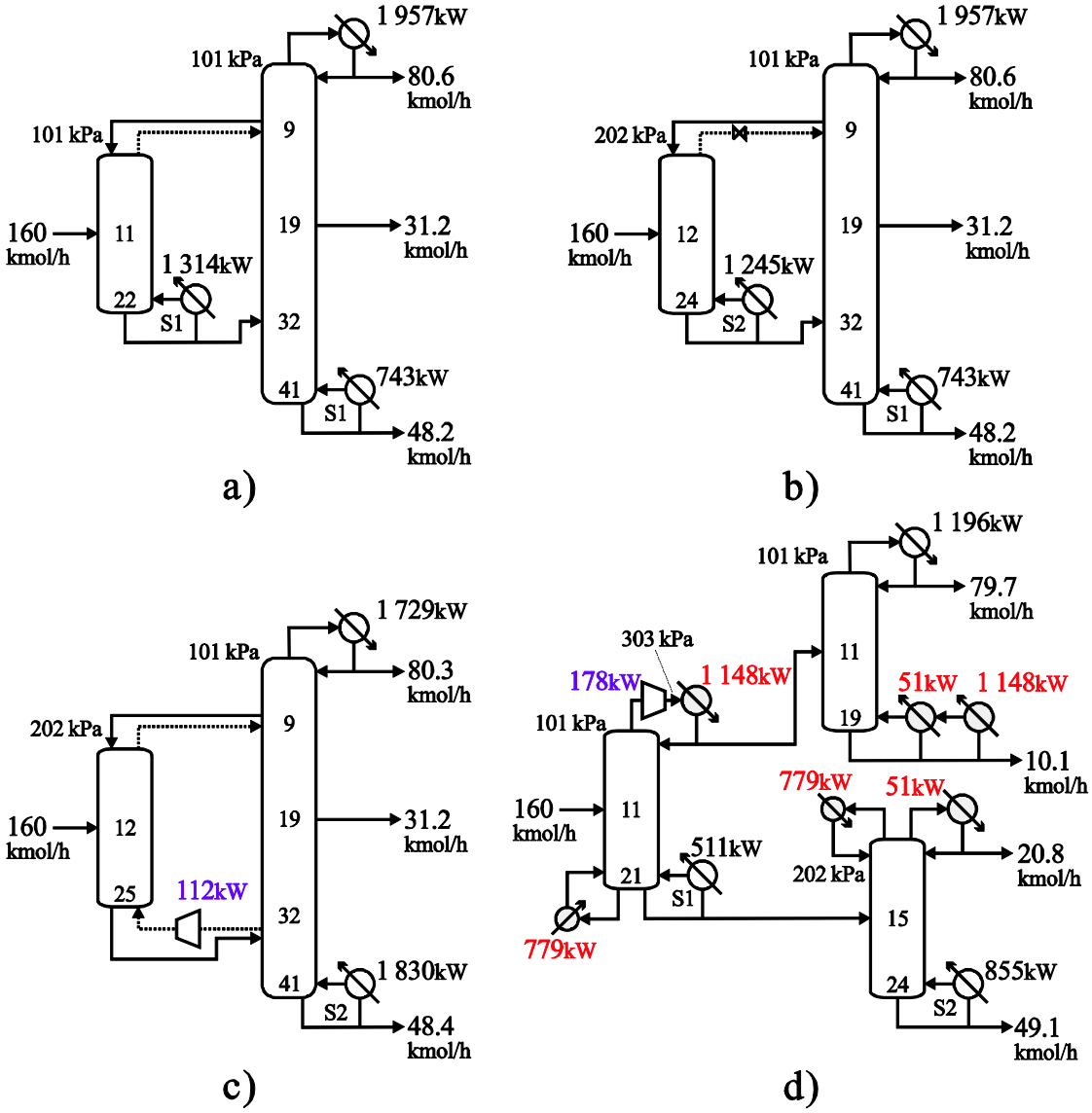

Figure 3.9. Optimal distillation sequences obtain from the proposed method:
a) sequence with the minimum *TAC*,
b) best compressor-free thermally coupled sequence
c) best compressor-aided thermally coupled sequence
d) best sequence when vapor recompression is enforced.
red: external heat integration, purple: work duty, black: utility

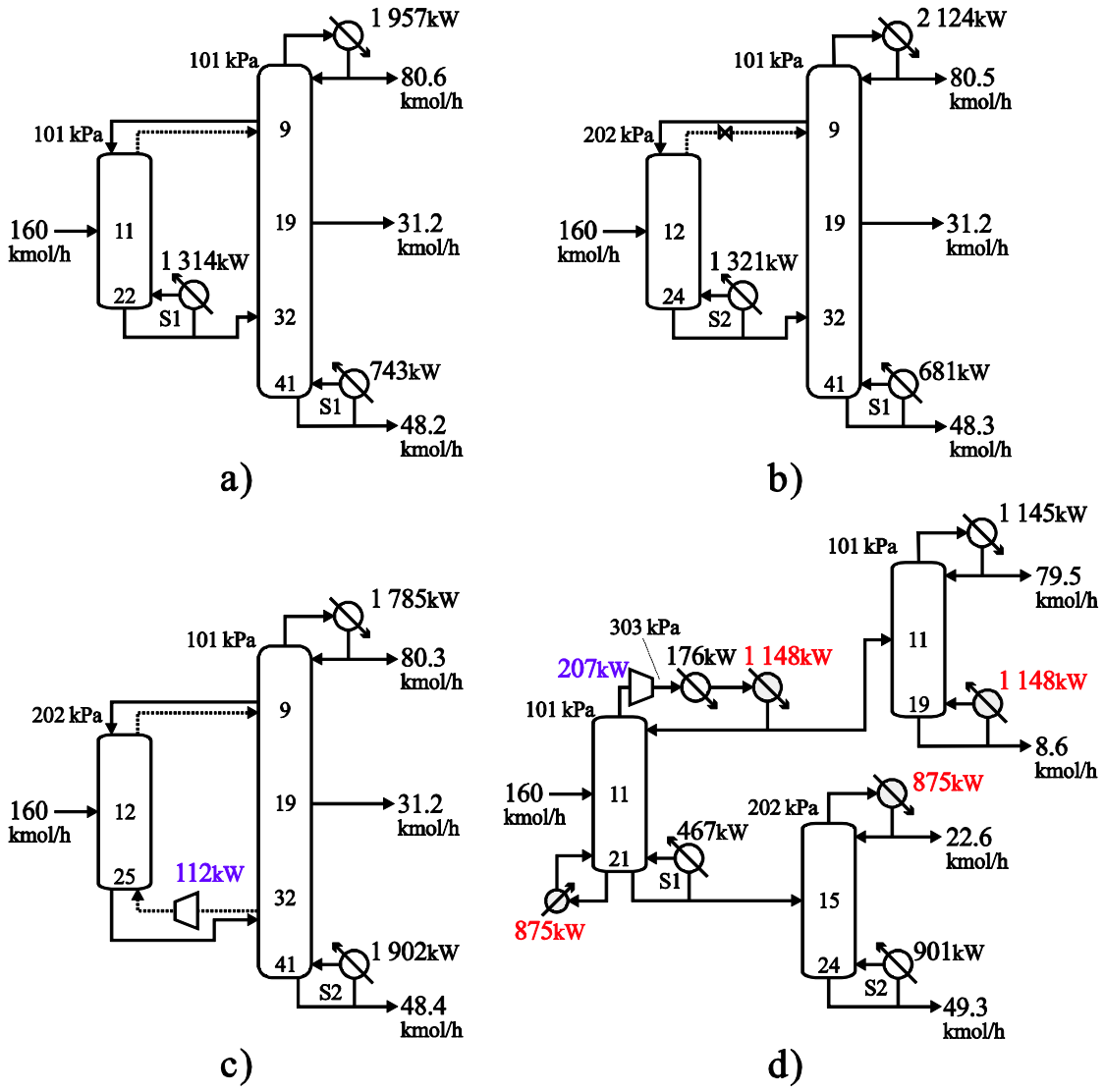

Figure 3.10. Optimal distillation sequences obtain from rigorous simulations:
a) sequence with the minimum *TAC*,
b) best compressor-free thermally coupled sequence
c) best compressor-aided thermally coupled sequence
d) best sequence when vapor recompression is enforced.
red: external heat integration, purple: work duty, black: utility

Each of the results in Figure 3.10 is calculated assuming that the structure of the process is the same as the corresponding structure in Figure 3.9. The results show higher energy consumption than those in Figure 3.9 for each case, which result in higher operating cost. For the case of sequences in Figure 3.9d and 3.10d, the heat integration network is different. Figure3.9d is the result after solving the synthesis problem while Figure 3.10d is the closest feasible solution obtained from rigorous simulation based on the results shown in Figure 3.9d. Figure 3.10d realized vapor recompression in the column separating AB from BC and external heat integration between columns AB/BC and A/B, and columns B/C and AB/BC.

Table 3.8 Economic and energy savings for the optimal sequences

	TAC [k$/y]	*FC/PT* [k$/y]	*OH·OC* [k$/y]	Economic savings [%]	Energy consumption [kW]	Energy savings [%]
Base case	534.2	216.7	317.5	---	3292	---
PET at 101 kPa	376.9	87.2	289.7	29	1 830	44
Figure 3.9a	360.6	162.5	198.1	32	2 057	38
Figure 3.10a	360.6	162.5	198.1	32	2 057	38
Figure 3.9b	415.1	145.8	269.3	22	1 989	40
Figure 3.10b	412.8	136.4	276.4	23	2 002	39
Figure 3.9c	455.1	111.7	343.4	14	2 166	34
Figure 3.10c	469.1	114.3	354.8	12	2 238	32
Figure 3.9d	472.6	203.2	269.4	11	1 900	42
Figure 3.10d	514.4	227.1	287.3	4	1 989	40

For the sake of comparison, the results of the proposed method and the exact solution from rigorous simulations are summarized in Table 3.8. Although the results of both approaches are different, the *TAC* and energy consumption of the sequences validated with rigorous simulations are not very different from those obtained by the proposed method. Figures 3.9d and 3.10d show changes in the *TAC* because the compressor equipment cost and work duty is larger for the later. However, the difference in the energy consumption was not large. For the results presented in this subsection, the solutions obtained by the proposed method are reliable and offer a tight lower bound for a feasible solution.

In addition, the work duty was converted into energy by multiplying its value by 3 because this number is an empirical coefficient that considers the cost electricity in Japan.[16,17]

3.9.5 Internal and external heat integration in thermally coupled distillation columns

In the previous section, CA-TCDS and CF-TCDS were not better alternatives than conventional thermally coupled columns which keep the same pressure in columns (sections) with linking vapor streams. Even when the pressures of two columns are changed, the optimal results are the structures with neither external nor internal heat integration. Therefore, now the synthesis problem of thermally coupled distillation columns, which can realize internal heat integration, is covered in this subsection. For this aim, the superstructure in Figures 3.2 (left side) is solved through the hierarchical optimization procedure proposed in section 3.8.

The hierarchical optimization procedure for CF-TCDS and CA-TCDS with internal heat integration under several values of the LMTD, Q_{UP}, and A^{int} was executed. However, there was not a solution with lower cost than the optimal thermally coupled solution in Figure 3.9a. For comparison purposes, Figure 3.11 shows the best CA-TCDS with internal heat integration obtained by the proposed approach and the solution obtained through rigorous simulations.

Both sequences in Figure 3.11 are the PPV sequence whose first column operates a higher pressure and the second at lower pressure. Therefore, a compressor in the upper part of the first column is necessary to link the vapor stream. At the bottom of the figure, the detailed heat exchange network for the CA-TCDS is shown. This arrangement effectively reduced the amount of energy from hot utilities, but instead it used electricity and a compressor, which resulted in a more expensive fixed and operating cost than the best CA-TCDS without internal heat integration. Table 3.9 shows a comparison between the solutions in Figure 3.11 in terms of economic and energy savings.

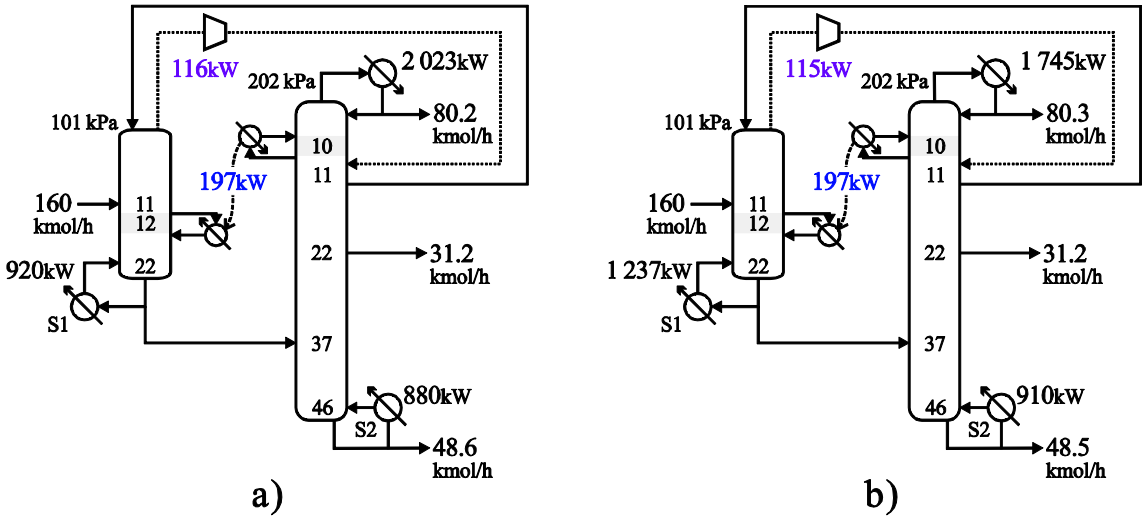

Figure 3.11. Best CA-TCDS with internal heat integration:
a) sequence obtained through the proposed approach, and
b) sequence obtained through rigorous simulations.
red: external heat integration, purple: work duty, black: utility

Table 3.9 Economic and energy savings for the optimal sequences

	TAC [k$/y]	*FC/PT* [k$/y]	*OH·OC* [k$/y]	Economic savings [%]	Energy consumption [kW]	Energy savings [%]	A_{opt}^{int} † [m²]	R^{c} * [-]
Base case	534.2	216.7	317.5	---	3292	---	---	0.528 0.706 3.309
Figure 3.12a	457.1	172.9	284.2	14	2 146	35	20	--- 0.817
Figure 3.12b	473.0	170.9	302.1	11	3 000	9	20	--- 1.157

† A_{opt}^{int} is the optimal value of A^{int} in Equation 29 of Chapter 2.

* Each line in the column R^{c} defines the value of the reflux ratio for the first, second, and third column, respectively.

The comparison between the solutions shows that the proposed approach underestimates the feasible design, especially in terms of energy consumption at the reboilers. In the next section, the main conclusions of this chapter are presented.

3.10 Discussion of results

Conventional columns with compressor-free internal heat integration realized the highest economic and energy savings followed by thermally coupled distillation columns without heat integration. When the use of compressors was enforced, less economic and energy savings were attained. This behavior is because the selected pressure range for these sequences was rather narrow.

From the presented results in Tables 3.7 through Table 3.9, thermally coupled columns are economically more appealing than conventional columns with external heat integration, however, when internal heat integration is enforced; the highest energy savings can be realized.

For the presented BTX mixture, pressure change in thermally coupled columns does not represent an attractive to solution to realize external heat integration.

The results from rigorous simulations were useful to determine the reliability of the proposed approach. Similar results from the rigorous simulations were obtained; however, the proposed approach underestimated the feasible solution in most of the presented sequences.

In some cases, the estimation of the reflux ratio after internal heat integration resulted in negative values, this means, the proposed approach represents an optimistic situation with minimum energy consumption. To avoid negative values in the estimation of reflux ration, this estimation must be included in the optimization mathematical programming problem and to restrict the reflux ratio to positive numbers. If the last statement is enforced, even better solutions might be obtained, which means tighter lower bounds to the synthesis problem can be obtained.

3.11 Conclusions

A hierarchical optimization algorithm was proposed to synthesize compressor aided distillation sequences where internal heat integration, external heat integration and vapor recompression are possibilities to reduce the energy consumption and cost in distillation.

A hierarchical optimization procedure similar to the one presented in Chapter 2 was proposed and represented by superstructures. At the first level, all the possibilities for internal and external heat integration between the rectifying section of one column and the stripping section of another were

comprised while at the second level, external heat integration and vapor recompression for all the possible distillation sequences of columns were included.

The concept of contribution terms was extended to estimate the internal flows in a distillation column at the top and the bottom.

A case study to separate a ternary mixture was taken. The results showed that the use of thermally coupled columns could effectively attain economic savings up to 32% and energy savings around 40%. However, the highest energy savings (47%) were attained by the sloppy split sequence (SS) when internal and external heat integration were adopted simultaneously, and such combination could outperform typical external heat integration in terms of TAC and energy consumption.

As the number of components in the original mixture, and the possible energy conservation methods increase, the complexity of the problem can drastically increase. In addition, as the number of optimal solutions increase, only the economic assessment lacks of reliability, specially for sequences where compressors are added. Therefore the next chapter will deal with not only economic optimization, but also with the assessment of more than one objective function by formulating multi-objective optimization problems.

Chapter nomenclature

A^{int} = area for the side heat exchanger [m^2]

B^i = flow rate of bottom product of column *i* (or task *i*) [kmol/s]

C_{col}^i = column cost of task *i* [k$]

C_{tray}^i = tray cost of task *i* [k$]

C_{heat}^i = cost of heating utility *i* [k$/kWh]

C_{cool}^j = cost of cooling utility *j* [k$/kWh]

C_{elec} = cost of electricity [k$/kWh]

C_{VR}^i = compressor cost to realize vapor recompression in streams to condensers of column *i* (or task *i*) [k$]

$C_{comp}^{i,j}$ = compressor cost which is installed to flow a vapor stream from column *i* (or task *i*) to column *j* (or task *j*) [k$]

$C_{ext}^{i,j}$ = heat exchanger cost per unit amount of heat exchanged between the rectifying section of task *i* and stripping section of task *j* [k$/kW]

CA = set of the pair of columns which compose a thermally coupled task [-]

$COLF_s$ ($COLP_s$) = set of columns which have state *s* as an output (as an input) [-]

$CS^{i,j}$ = total cost for all the side heat exchangers for internal heat integration between the rectifying section of task *i* and stripping section of task *j* [k$]

CU = set of cold utilities [-]

D^i = distillate flow rate of column *i* (or task *i*) [kmol/s]

F^i = feed flow rate of column *i* (or task *i*) [kmol/s]

FC = fixed cost [k$]

$FEED$ = set of tasks whose input stream is the original feed state [-]

HU = set of hot utilities [-]

M_i = number of stages in a rectifying section of column *i* [-]

N_j = number of stages in a stripping section of column *j* [-]

OC = operating cost [k$/h]

OH = annual operation hours [h/y]

P_i = *i*-th pressure level [kPa]

PT = payout time [y]

q^c = condenser heat duty after heat integration [kW]

$q_0^{c,i}$ = condenser heat duty before heat integration for task *i* [kW]

q_m = amount of heat removed from stage *m* of rectifying section [kW]

$q_{opt}^{i,j}$ = net reduction of condenser duty of column *i* resulted from heat integration between the rectifying section of column *i* and the stripping section of column *j* [kW]

Δq^c = overall compensation term of condenser [kW]

$\Delta \hat{q}^c$ = estimated value of Δq^c [kW]

Q^r = reboiler heat duty after heat integration [kW]

$Q_0^{r,j}$ = reboiler heat duty before heat integration for task *j* [kW]

Q_n = amount of heat supplied to stage *n* of stripping section [kW]

$Q_{ext}^{i,j}$ = amount of heat exchanged between the top vapor stream of task *i* and the bottom liquid stream of task *j* [kW]

$Q_{opt}^{i,j}$ = net reduction of the reboiler duty of column *j* resulted from heat integration between the rectifying section of column *i* and the stripping section of column *j* [kW]

Q_{UP} = upper bound of the amount of energy exchanged by internal heat integration [kW]

ΔQ^r = overall compensation term of reboiler [kW]

$\Delta \hat{Q}^r$ = estimated value of ΔQ^r [kW]

ST = set of all states [-]

STc = set of aggregated states [-]

TKF_s *(*TKP_s*)* = set of task whose output (input) flow connects an aggregated state *s* [-]

TAC = total annual cost [k$/y]

TK = set of tasks [-]

VR = set of tasks with vapor recompression [-]

$W_{comp}^{i,j}$ = compressor work duty for the stream from column *i* (or task *i*) to the column *j* (or task *j*) in a thermally coupled column (or an aggregated task) [kW]

W_{VR}^{i} = compressor work duty to increase the pressure of a stream to a condenser in column *i* (or task *i*) [kW]

$Y^{i,j}$ = binary variable which become one if heat exchange between tasks *i* and *j* is realized [-]

$Y_{comp}^{i,j}$ = binary variable which become one if a compressor exists between tasks *i* and *j* [-]

Y_{ext}^{i} = binary variable assigned to task *i*. It becomes one when task *i* is selected [-]

Greek letters

δ_n^r , δ_m^c = binary variable in estimation equations of compensation terms [-]

ϕ_{comp} = parameters to calculate the compressor cost [-]

Reference literature

(1) Peltyuk, F. B.; Platonov, V. M.; Slavinskii, D. M. Thermodynamically Optimal Method of Separating Multicomponent Mixtures. *Int. Chem. Eng.* **1965,** 5, 555-561.

(2) Rev, E.; Emtir, M.; Szitkai, Z.; Mizsey, P.; Fonyo, Z. Energy Savings of Integrated Distillation Systems. *Comput. Chem. Eng.* **2001,** 25, 119-140.

(3) Suphanit, B.; Bischert, A.; Narataruksa, P. Exergy loss analysis of heat transfer across the wall of the dividing-wall distillation column. *Energy* **2007**, 32, 2121–2134.

(4) Fitzmorris, R. E.; Mah, R. S. H. Improving Distillation Column Design Using Thermodynamic Availability Analysis. *AIChE J.* **1980,** 26, 265-273.

(5) Oliveira, S. B. M.; Pitanga Marques, R.; Parise J. A. R. Modelling of an ethanol-water distillation column with vapour recompression. *Int. J. Energy Res.* **2001**, 25, 845-858.

(6) Alcántara-Avila, J. R.; Kano, M.; Hasebe, S. Two-Level Approach for Synthesizing Externally and Internally Heat Integrated Distillation Sequences. *13th APCChE Congress.* **2010**. Taipei, Taiwan.

(7) Fidkowski, Z. T.; Agrawal, R. Multicomponent Thermally Coupled Systems of Distillation Columns at Minimum Reflux. *AIChE J.* **2001,** 47, 2713-2724.

(8) Fidkowski, Z. T. Distillation Configurations and their Energy Requirements. *AIChE J.* **2006,** 52, 2098-2106.

(9) Agrawal, R.; Fidkowski, Z. T. New Thermally Coupled Schemes for Ternary Distillation. *AIChE J.* **1999,** 45, 485-496.

(10) Hernandez, S.; Jimenez, A. Design of energy-efficient Petlyuk systems. *Comput. Chem. Eng.* **1999,** 23, 1005-1010.

(11) Turton, R.; Bailie, R.C.; Whiting, W.B.; Shaeiwitz, J.A. *Analysis, Synthesis, and Design of Chemical Processes;* Prentice Hall: New York, 2003.

(12) Andrecovich, M. J.; Westerberg, A. W. An MILP formulation for heat-integrated distillation sequence synthesis. *AIChE J.* **1985,** 31, 1461–1474.

(13) Renon, H.; Prausnitz, J.M. Local Compositions in Thermodynamic Excess Functions for Liquid Mixtures. *AIChE J.* **1968**, 14, 135–144.

(14) Redlich, O.; Kwong, J.N.S. On the Thermodynamics of Solutions V. An Equation-of-state. Fugacities of Gaseous Solutions. *Chem. Rev.* **1979**, 44, 223–244.

(15) Seider, W. D.; Seader, J.D.; Lewin, D.R.; Widagdo, S. *Product and Process Design Principles;* John Wiley and Sons, Inc. 3rd International student edition, **2010**.

(16) Iwakabe, K.; Nakaiwa, M.; Huang, K.; Nakanishi, T; Røsjorde, A.; Ohmori, T.; Endo, A.; Yamamoto, T. Performance of an internally Heat-Integrated Distillation Column (HIDiC) in separation of ternary mixtures. *J. Chem. Eng. Japan* **2006**, 39, 417–425.

(17) Horiuchi, K.; Yanagimoto, K.; Kataoka, K.; Nakaiwa, M.; Iwakabe, K.; Matsuda, K. Energy saving characteristics of the internally heat integrated distillation column (HIDiC) pilot plant for multicomponent petroleum distillation. *J. Chem. Eng. Japan* **2008**, 41, 771–778.

Chapter 4

Multi-objective optimization of intensified distillation sequences

4.1 Introduction

Multi-objective optimization (MOO), also known as multi-criteria optimization, refers to finding values of decision variables, which correspond to and provide the optimum of more than one objective[1]. Unlike in single objective optimization, which gives a unique solution, MOO can obtain several optimal solutions when two or more objectives conflict each other. Hence, MOO uses special optimization techniques for considering two or more objectives and analyzing the results obtained. To optimize the design and operation of industrial processes, economic assessment has been generally used as the optimization criterion. This strategy is natural for commercial enterprises. However, the economic criterion changes with time and sometimes optimization criteria contradict each other or are not directly related each other. For example, minimizing an environmental stress resulted from CO_2 emissions or minimizing the releases of toxic materials are optimization criteria, which usually conflict with optimizing the economic assessment. The optimization results obtained for different objectives may suggest us essential points of the problem and innovative alternatives. Thus, MOO has gained remarkably importance in the last years because the diversity is requested to the management of the commercial enterprises.

In the case of distillation sequences, minimizing the sum of equipment and operating costs has primarily been chosen as the optimization criterion. However, as environmental restrictions are getting stricter and the price of fossil fuel becomes more uncertain, it becomes more important to design distillation processes by taking several criteria into account. For example, compressors have high fixed cost but can drastically reduce the energy requirements. Thus, even if a structure without compressors is selected as the optimal structure, which minimizes the total annual cost at current energy price, the structure with compressors may be selected in near future when the energy price is drastically increased. In addition, from the environmental viewpoints, the amount of CO_2 emissions may be restricted. In such a case, the structure with less CO_2 emission must be selected even if the total annual cost is higher.

From such situations, there has been an ambiguous economic and environmental interpretation when compressors are included in distillation sequences. Therefore, this chapter aims to derive a meaningful interpretation of vapor recompression in conventional columns, and at the vapor streams from low to high pressure section of thermally coupled columns. Both the total annual cost and the energy consumption are selected as the objective functions, and are optimized simultaneously using the multi-objective optimization technique to separate ternary, four-component, and five-component mixtures. Furthermore, three-objective problem, which minimize the total annual cost, CO_2 emissions and the release of toxic chemicals in the production of anhydrous ethanol from lignocellulosic materials, is discussed.

4.2 Synthesis of conventional and thermally coupled sequences

Caballero and Grossmann[2] proposed a superstructure representation based on short-cut methods to synthesize conventional (a single feed, two product streams, a condenser, and a reboiler) and complex (several feeds and product streams with or without a condenser or a reboiler) distillation sequences with heat integration. Their representation formulated the problem as a generalized disjunctive programming (GDP) problem, and then the derived problem was solved as a reformulated MINLP problem. Their results showed that the best sequence did not have heat integration when the pressure was kept constant; however, the best sequence had heat integration when pressure change in conventional columns was possible. In either case, the resulting sequence, which minimizes the total annual cost (TAC) was a combination of conventional and complex columns. Yiqing et al.[3] utilized a simulated annealing optimization technique based on short-cut methods and pinch analysis to synthesize conventional and thermally coupled distillation sequences with heat integration. The pressure selection was embedded in the short-cut methods, but columns with thermal coupling were operated at the same pressure. Their results showed that a combination of conventional and thermally coupled heat integrated columns yielded the best sequence, which minimized the TAC.

In the following sections, a systematic procedure for synthesizing the optimal distillation sequences is proposed. The proposed procedure explicitly includes many types of thermally coupled distillation columns as candidate sequences, and the vapor recompression of streams to condensers is allowed so as to effectively use the sensible heat of the vapor.

4.2.1 Superstructure generation

Figure 4.1 shows all sub-sequences adopted in this research. The conventional column (CC) is shown in Figure 4.1a, and a structure having a sloppy split (SS) is in Figure 4.1b. The other figures show thermally coupled columns: the Petlyuk column (PET) in Figure 4.1c, the partial Petlyuk column with a reboiler in the first column (PPV) in Figure 4.1d, the partial Petlyuk column with a condenser in the first column (PPL) in Figure 4.1e, a partially coupled sequence with vapor side stream to the second column (PCV) in Figure 4.1f, and the partially coupled sequence with liquid side stream to the second column (PCL) in Figure 4.1g.

The feed streams in Figure 4.1 are not restricted to a ternary mixture. L represents the light component or a set of light components, M represents the middle component or a set of middle components, and H represents the heavy component or a set of heavy components. The final separation structure is the combination of those structures.

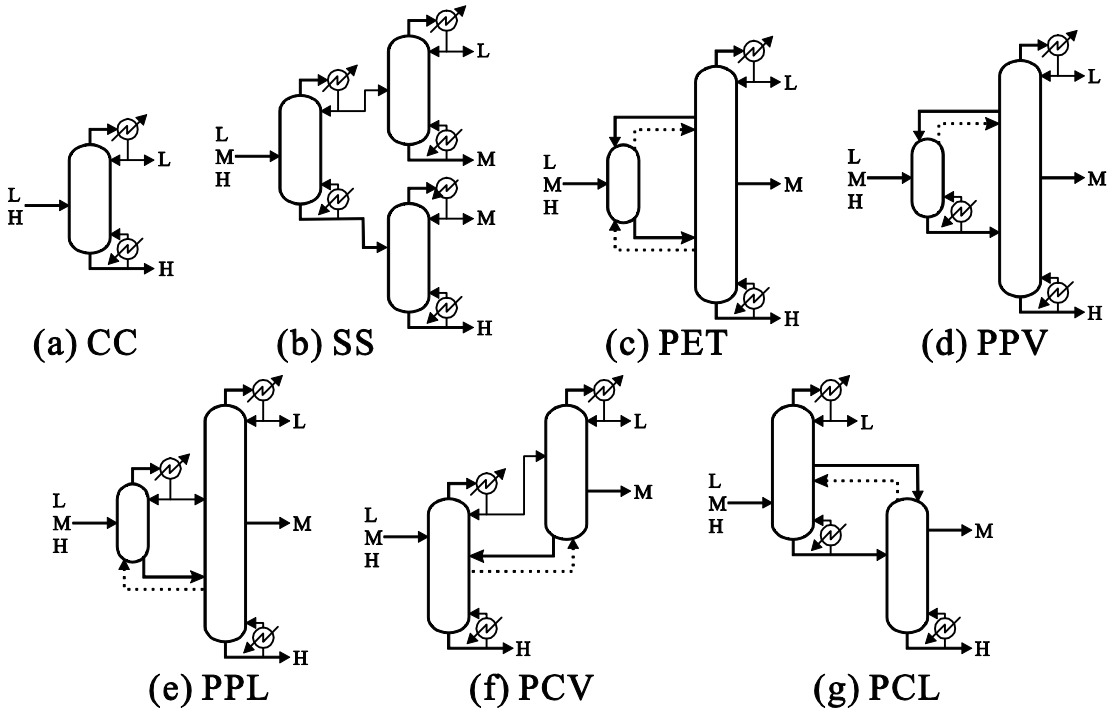

Figure 4.1. Candidate sub-sequences investigated in the research

In addition to the Petlyuk column and its partially coupled alternatives, Agrawal and Fidkowski pointed out that the thermally coupled columns become more operable by reducing the number of

interconnections[4] and adopting unidirectional vapor streams[5]. Thus, the partially coupled sequences (PPV and PPL) and the unidirectional vapor connection sequences (PCV and PCL) are explicitly included in candidate sub-sequences. Complex sequences that can separate a mixture into four or more products (e.g., four-component Petlyuk column[6]) are not treated in this research.

The same mathematical model can express PPV and PCL when the first and second columns operate at the same pressure. These two structures, however, show different separation performance and column cost when the two columns operate at different pressures. Thus, PPV and PCL are treated as different sub-sequences. For the same reason, PPL and PCV are also treated as different sub-sequences.

To enhance the heat integration among the columns, the pressures of two columns in a sub-sequence are not necessarily the same. When the pressures of two columns are different, pumps, compressors and/or valves are installed between them. As the fixed and operating costs of compressors cannot be neglected, they are added to the TAC.

The first step in solving the synthesis problem is to define all candidate distillation sequences. In this chapter as well, a superstructure-based approach is adopted to enumerate them. The complexity of the superstructure greatly depends on the number of candidate sequences and the number of components to be separated. Here, candidate sequences are limited to the combination of sub-sequences shown in Figure 4.1.

The superstructure of distillation sequences separating a four-component mixture is shown in Figure 4.2, where each rectangle represents a sub-sequence in Figure 4.1 and ellipses are the feed, intermediate products and final products. The mixture consists of A, B, C, and D, with A the most volatile component. A/BCD means that mixture ABCD is separated into A and BCD by a conventional column, while AB/C/D means that ABCD is separated into AB, C, and D by a complex sub-sequence in Figure 4.1.

The superstructure generated in this section is a state task network representation. Each ellipse is a state having information of the composition and physical conditions. When the amount of feed and its composition as well as the composition of every product are given, the amount of each product can be calculated from material balance equations. Some states in Figure 4.2 have more than one inlet and/or outlet flows. It is assumed that the number of inlet to and outlet from the state is restricted to one or zero for the finally derived structure, i.e., flow split is not permitted. By introducing this assumption, the conditions of intermediate states such as ABC or BCD in Figure 4.2 are uniquely determined. It is assumed that each state is liquid at its saturated temperature and that the compression and decompression cost of liquid is negligible. Thus, liquids with the same composition are expressed by one state even if the pressure is different. It is also possible to include states as saturated vapor. In such cases, as the compression cost of vapor cannot be neglected, the vapor at different pressure should be treated as different task even if the composition and the flow rate are the same.

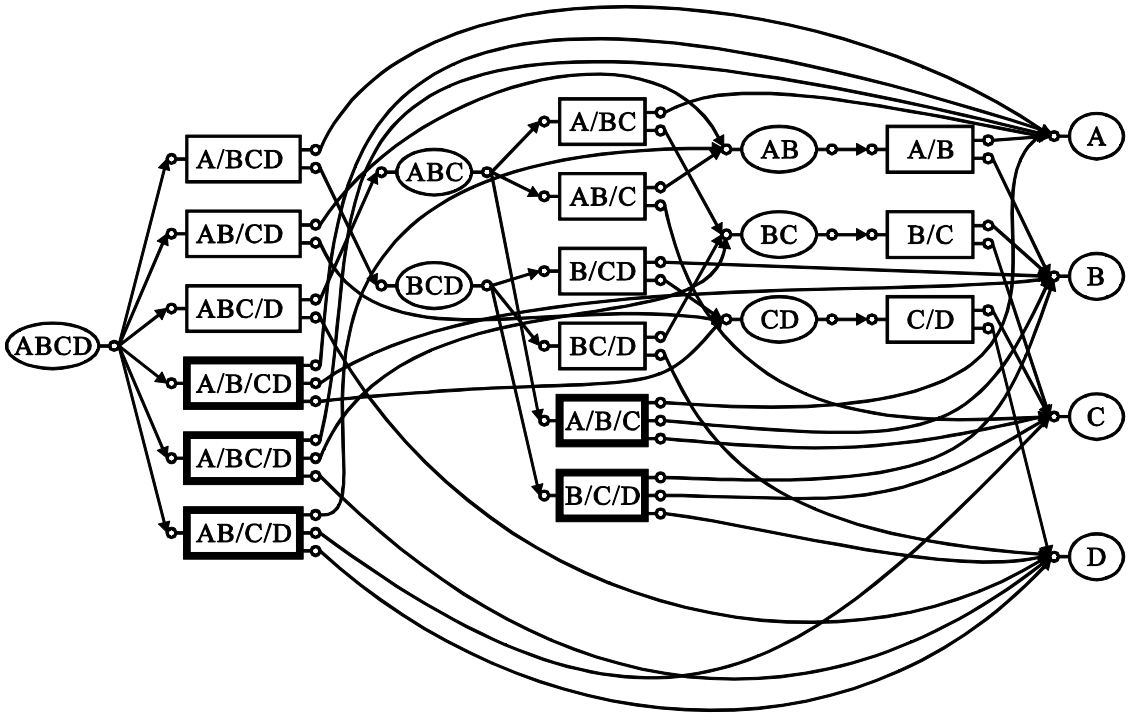

Figure 4.2. Superstructure of a four-component separation problem

The fixed cost and the operating cost depend on the operating pressure. Thus, the columns with different pressures are treated as different tasks even if the feed and product states are the same. A thin rectangle in Figure 4.2 shows a set of simple tasks executed by conventional columns, CC. Tasks executed by sub-sequences in Figure 4.1b through 4.1g are hereafter called aggregated tasks. A set of aggregated tasks having the same inlet and outlet states is expressed by a thick rectangle in Figure 4.2. In this work, the pressures of the first and second columns in a sub-sequence are not necessarily the same. If the pressure of some columns is different, such sub-sequences are treated as different aggregated tasks even when the inlet and outlet states are the same. To avoid complexity, the set of aggregated tasks with the same feed and product states is expressed by one rectangle in Figure 4.2.

An aggregated task is a compacted representation of two or three tasks and intermediate states. Suppose that SS in Figure 4.1 can be used to separate ABCD into AB/C/D. In this case, the aggregated task AB/C/D can be decomposed into three tasks and two intermediate states as shown in Figure 4.3a. It is assumed that each column in the sequence can take one of the predetermined discrete pressures.

The columns with different pressures are treated as different tasks. Thus, each rectangle in Figure 4.3a is a set of tasks. When PET, PPV or PPL in Figure 4.1 is adopted, the aggregated task AB/C/D

can be decomposed into two tasks and one aggregated intermediate state as shown in Figure 4.3b. The aggregated state depicted by a bold ellipse is a virtual state consisting of the liquid and vapor streams linking two columns into a thermally coupled column. Similarly, the aggregated task AB/C/D for PCV and PCL is decomposed to those shown in Figure 4.3c and Figure 4.3d, respectively.

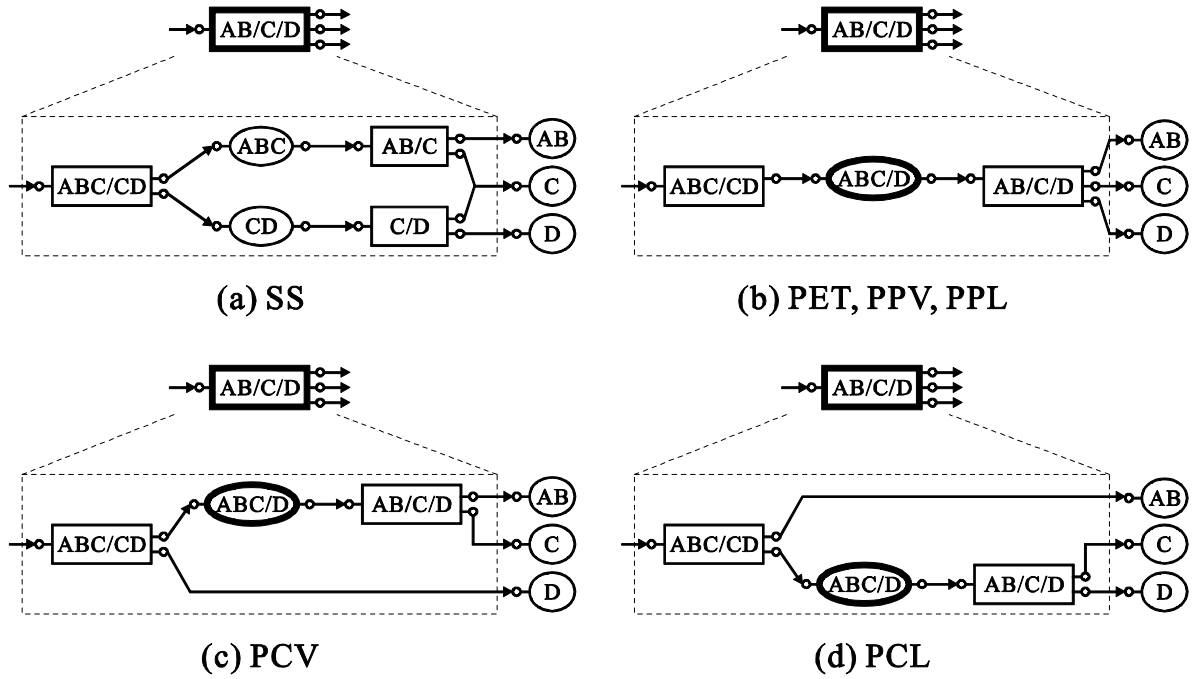

Figure 4.3. Decomposition of aggregated tasks

4.3 Determination of the number of stages in tasks

The calculation the number of stages in a conventional column (CC) and the structure having a sloppy split (SS) can be done by the proposed methodology explained in Chapter 3. For aggregated tasks made of thermally coupled columns, the calculation of the number of stages is based on the section analogy proposed in Chapter 3. This section analogy is applied to other aggregated tasks made of thermally coupled columns. An example of the analogy between SS and two thermally coupled

columns is illustrated in Figure 4.4. Without losing generality, this section analogy is also applied to more than three-component cases so long as a feasible design of SS exists.

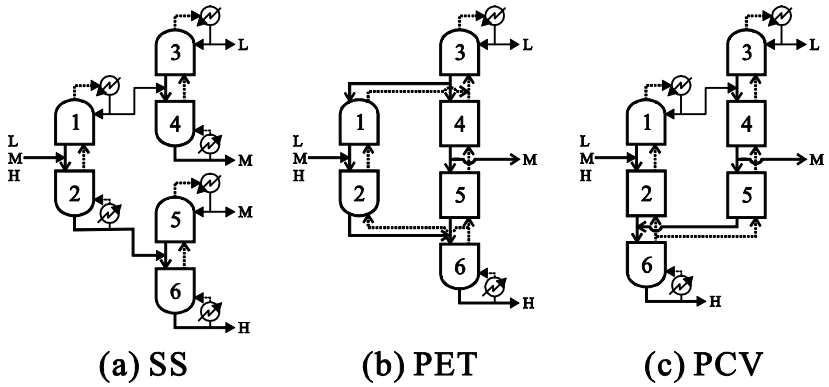

Figure 4.4. Analogy between SS and two thermally coupled columns

The exemplified analogy in Figure 4.4 can be extended to all the thermally coupled columns in Figure 4.1. Moreover, when the sections can be moved from one column to another, different thermally coupled columns can be originated. Figure 4.5 shows the difference between the PPL and PCV for aggregated tasks.

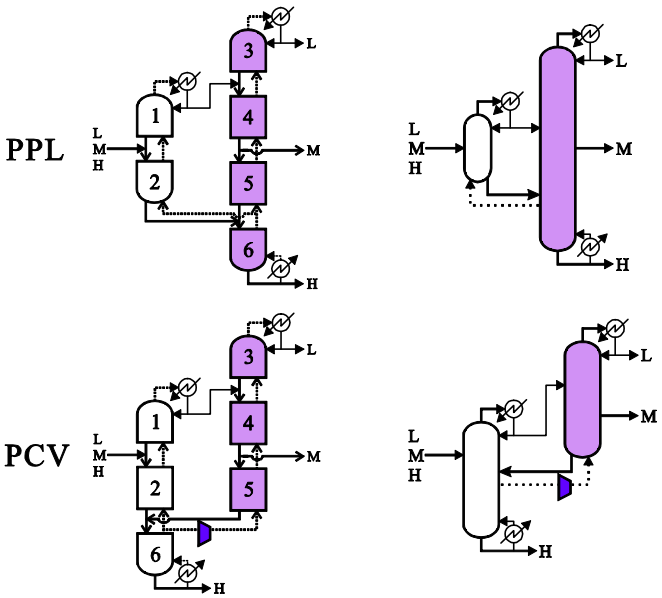

Figure 4.5. Difference between PPL and PCV sequences: section analogy (left), and optimized thermally coupled column (right)

Moving section 6 of the aggregated task PPL from the second column to the first column generates the PCV aggregated task. If the pressure is kept constant in both aggregated tasks, they are thermodynamically equivalent even though the direction of the vapor stream is opposite in each aggregated task. In the PPL aggregated task, vapor flows from the second column to the first column while in the PCV aggregated task, vapor flows from the first column to the second column.

Contrary, if pressure change is allowed as in Figure 4.5, the PPL and PCV aggregated tasks are not thermodynamically equivalent anymore because section 6 operates at a different pressure in each case. Furthermore, to warranty a feasible sequence, vapor and liquid streams must flow from high pressure (sections in purple) to low pressure (sections in white), therefore, compressors, pumps and throttling valves are necessary. Because the equipment cost and electricity cost of compressors cannot be neglected in the synthesis problem, they must be included as decision variables. The compressors in Figure 4.5 are represented by purple trapeziums. In this case, the PPL aggregated task is a compressor-free thermally coupled column while the PCV aggregated task is a compressor-aided thermally coupled column. The same assertion is valid for the PPV and PCL aggregated tasks.

In summary, pressure change results in different thermally coupled columns which are not thermodynamically equivalent, thus, they must be treated as different tasks and be optimized independently from each other during the rigorous simulation step, which is explained in the next section.

4.4 Rigorous simulation of distillation sub-sequences

A short-cut simulation has been widely used to derive information on condenser and reboiler duties as well as the vapor flow rate in the column, which can be used to estimate the cost and energy requirements of each task[2,3]. Since the results based on short-cut simulations are not accurate for non-ideal cases, rigorous models are necessary to obtain reliable results. However, when rigorous models are directly embedded in the synthesis formulation[7], crucial difficulties in solving MINLP problems arise due to nonlinearity and non-convexity of the formulated model. Therefore, their implementations have been mostly restricted to ideal or nearly ideal mixtures. In our proposed method, rigorous simulations are executed to derive the number of stages and to derive the column conditions, and the derived data are used in the synthesis problem formulated as an MILP problem. Thus, more accurate input data can be obtained compared with the short-cut methods, and less time is consumed compared with MINLP formulation.

For simple tasks executed by CC and aggregated tasks executed by SS, data such as the reboiler and condenser heat duties have been optimized after determining the number of stages. For an aggregated task made of thermally coupled columns, the number of stages of each column has been determined

by using the analogy with SS as shown in Figure 4.4. The flow rates of thermal linking streams are optimized as proposed in section 3.4 at the reference pressure. Then, additional simulations at several discrete pressures are executed by fixing the flow rates of thermal linking streams at the optimal value.

4.5 Mathematical formulation

The MILP formulation proposed in this work is based on the transportation problem presented by Andrecovich and Westerberg[4]. The advantage of the proposed formulation is that the following data for each task can be obtained by the prior execution of rigorous simulations:

1. Design parameters:
   Condenser duty, reboiler duty, number of stages, and column diameter.
   Compressor work duty.
   Compressor cost.
   Heat exchangers cost.
2. Flow rate and composition of each input and output streams, and
3. Top and bottom temperatures.

Although these data can be obtained from short-cut methods, rigorous simulations supply more realistic values especially in non-ideal cases. Rigorous simulations of each column implicitly deal with all the non-linearity such as complex thermodynamics and non-convexities such as stage-by-stage bilinear products of flow rate and composition. Thus, at the synthesis stage, the problem can be expressed by an MILP problem, which can be solved easily compared with a non-linear, non-convex MINLP problem, which requires strong and sophisticated mathematical skills and might fail to warranty global optimality. The combination of rigorous simulations and MILP optimization is easier to perform, and can derive the global optimal solution in shorter computation time.

4.5.1 Vapor recompression and external heat integration in sub-sequences

The constraints and the objective function are explained here. The connectivity constraints between columns to generate feasible sequences are given by

$$\sum_{i \in FEED} Y_{ext}^{i} = 1 \tag{1}$$

$$\sum_{i \in TKF_s} Y_{ext}^{i} - \sum_{i \in TKP_s} Y_{ext}^{i} = 0 \qquad s \in ST \cup ST_C \tag{2}$$

where Y_{ext}^{i} is a binary variable assigned to each task. If task *i* is selected, Y_{ext}^{i} takes one; otherwise it takes zero. *FEED* denotes the set of tasks whose input stream is the original feed mixture. *ST* is the set of all states, excepting the feed and product states. ST_C is the set of all aggregated states. TKF_s and TKP_s are the set of tasks, which have state *s* or aggregated state *s* as an output and as an input, respectively.

The energy balance constraints to satisfy the energy demand at the condensers and at the reboilers are described by

$$\sum_{i \in TK} Q_{ext}^{i,j} + \sum_{i \in HU} Q_{ext}^{i,j} = Q_0^{r,j} Y_{ext}^{j} \qquad j \in TK \tag{3}$$

$$\sum_{j \in TK} Q_{ext}^{i,j} + \sum_{j \in CU} Q_{ext}^{i,j} = q_0^{c,i} Y_{ext}^{i} \qquad i \in TK \tag{4}$$

where *TK* is the set of all the tasks in the superstructure and $Q_{i,j}^{ex}$ is the amount of heat exchanged between the top vapor of task *i* (or hot utility *i*) and the bottom liquid of task *j* (or cold utility *j*). An infeasible match (*i*, *j*) is avoided by assigning a very large value, such as 1e6, to its heat exchange cost.

Finally, the following equations are necessary to express the existence of a compressor in a vapor stream from a low pressure column to a higher pressure column.

$$\sum_{j \in TKP_s} Y_{comp}^{i,j} - Y_{ext}^{i} = 0 \qquad i \in TKF_s, s \in STc \tag{5}$$

$$\sum_{i \in TKF_s} Y_{comp}^{i,j} - Y_{ext}^{j} = 0 \qquad j \in TKP_s, s \in STc \tag{6}$$

where $Y_{comp}^{i,j}$ is a variable that indicates the use of aggregated task, which consists of task *i* and task *j*. Since $Y_{comp}^{i,j}$ is determined by binary variables Y_{ext}^{i} and Y_{ext}^{j}, there is no need to define $Y_{comp}^{i,j}$ as a binary variable; it can be defined as a continuous variable between zero and one instead. This definition effectively works to reduce the number of binary variables.

Here, two types of objective functions are introduced: the total annual cost, TAC, and the energy consumption, EC. The optimization problem, which minimizes the total annual cost, TAC, can be formulated as:

$$\min \quad TAC = \frac{FC}{PT} + OH \cdot OC \tag{7}$$

where *PT* is the payout time and *OH* is the annual operation hours. *TAC*, *FC* and *OC* are the values for the total annual cost, fixed and operating costs, which are given by

$$FC = \sum_{i \in TK} \left(C_{col}^{i} + C_{tray}^{i} + C_{VR}^{i} \right) Y_{ext}^{i} + \sum_{i,j \in TK} C_{ext}^{i,j} Q_{ext}^{i,j} + \sum_{\substack{i \in HU \\ j \in TK}} C_{ext}^{i,j} Q_{ext}^{i,j} + \sum_{\substack{i \in TK \\ j \in CU}} C_{ext}^{i,j} Q_{ext}^{i,j} + \sum_{s \in STc} \sum_{\substack{i \in TKF_s \\ j \in TKP_s}} C_{comp}^{i,j} Y_{comp}^{i,j} \quad (8)$$

$$OC = \sum_{\substack{i \in HU \\ j \in TK}} C_{heat}^{i,j} Q_{ext}^{i,j} + \sum_{\substack{i \in TK \\ j \in CU}} C_{cool}^{i,j} Q_{ext}^{i,j} + C_{elec} \left(\sum_{i \in TK} W_{VR}^{i} Y_{ext}^{i} + \sum_{s \in STc} \sum_{\substack{i \in TKF_s \\ j \in TKP_s}} W_{comp}^{i,j} Y_{comp}^{i,j} \right)$$

where C_{col}^{i}, C_{tray}^{i}, and C_{VR}^{i} are the column cost, tray cost, and cost of the installed compressor to realize vapor recompression of task *i*, respectively. $C_{comp}^{i,j}$ is the cost of the compressor installed between the task *i* and *j* made of thermally coupled columns. C_{col}^{i}, C_{tray}^{i}, C_{VR}^{i}, and $C_{comp}^{i,j}$ have been calculated in advance at the first optimization step which is explained at section 2.7. W_{VR}^{i}, and $W_{comp}^{i,j}$ are the compressor work duty to realize vapor recompression of top the vapor stream in task *i* and the side vapor streams in thermally coupled columns (task *i* and *j*). $C_{ext}^{i,j}$ is the unit cost of external heat exchanger to execute unit amount of heat exchange. C_{heat}^{i}, C_{cool}^{j}, and C_{elec} are the costs of heating utility *i*, cooling utility *j*, and electricity respectively. The equipment cost was calculated according to Turton et al.[8]

Compressors have a negative impact on the fixed and operating costs because of their expensive hardware and electricity costs, but they also have a positive impact through reducing the amount of energy used at the reboilers. Thus, a second objective function that explicitly evaluates the energy consumption of a sequence is added to evaluate the positive and negative impacts of compressors.

$$EC = \sum_{\substack{i \in TK \\ j \in HU}} Q_{ext}^{i,j} + 3 \left(\sum_{j \in TK} W_{VR}^{j} Y^{j} + \sum_{d \in IDc} \sum_{\substack{i \in TKF_d \\ j \in TKP_d}} W_{comp}^{i,j} Y_{comp}^{i,j} \right) \quad (9)$$

where *EC* is the value of the energy consumption in distillation sequences. The first term of the right-hand side of Equation 9 is the amount of heat used at the reboilers and the second term is the work duty at the compressors. The work duty is converted into energy by multiplying its value by 3, which is an empirical coefficient estimated from electricity efficiency in Japan[9] because the conversion factor for the compressor duty was determined as 2.85 in 2005 by taking the power

generation efficiency in Japan according to the Ministry of Economy, Trade and Industry of Japan.[10] The energy removed from tasks by cold utilities is not included in *EC*.

The final formulation of the problem is to minimize Equations 7 and/or 9 under the constraint of Equations 1 to 6. The decision variables are $\left\{Y_{ext}^{i}\right\}$, and $\left\{Q_{ext}^{i,j}\right\}$.

4.6 Multi-objective optimization

Multi-objective optimization problems (MOO) involve two or more objective functions, which depend on many decision variables and constraints. Equation 9 presents a general description of a multi-objective optimization problem with two objectives: $f_1(X)$ and $f_2(X)$ where X is the vector of decision variables for a general problem.

$$\begin{aligned} &\min_X f_1(X) \\ &\min_X f_2(X) \\ &s.t. \\ &X^{lo} \le X \le X^{up} \\ &h(X) = 0 \\ &g(X) \le 0 \end{aligned} \tag{9}$$

where the superscripts *lo* and *up* denote the lower and upper bound, respectively, for the decision variables. The lower and upper bounds can be continuous, integer or binary variables. The equality constraints $h(X)=0$ result from mass or energy balances, etc. The inequality constraints $g(X)\le 0$ result from equipment, material, operating conditions, purity specifications and other configurations.

The two objectives, $f_1(X)$ and $f_2(X)$, are often conflicting. In such cases, there will be many optimal solutions to Equation 9. All these solutions are equally good because of one of them is better than the rest in at least one objective. This implies that the worsening of one objective improves the optimal solution another objective. The solutions of an MOO problem are known as *Pareto-optimal solutions*, which are defined as follows:

> *The set:* X^P, $f_1(X^P)$ *and* $f_2(X^P)$ *is said to be a Pareto-optimal solution for the two-objective problem in Equation 9, if and only if, there is no other feasible X such that* $f_1(X) \le f_1(X^P)$ *and* $f_2(X) \le f_2(X^P)$ *with strict inequality valid for at least one objective.*[1]

Although there are several methods for solving multi-objective optimization problems, the most robust approach involves normalizing each term in the objective function.[11] One way to delimit objective functions between zero and one is by normalizing them as shown in Equation 10

$$\overline{f}_k(X) = \frac{f_k(X) - f_k^*}{f_k^N - f_k^*} \quad k = 1...n \tag{10}$$

where n is the number of objective functions, therefore, in a two-objective function n=2. The superscript * and N denote the utopia and the Nadir points. The utopia point of the *k-th* objective function is defined by optimizing the objective function f_k while the Nadir point of f_k is defined by the maximum value of f_k when optimizing each of the other objectives. The mathematic definition of the utopia and Nadir point is shown in Equation 11.

$$\begin{aligned} f_k^* &= \min_X f_k(X) \\ f_k^N &= \max_{k' \neq k} \{\min_X f_{k'}(X)\} \end{aligned} \qquad k = 1...n \tag{11}$$

After normalizing the objective functions, the problem to solve several objectives simultaneously arises. There are several multi-objective optimization techniques, which are reported in literature references[1, 11]. However, in this chapter we will focus on a particular type of techniques termed as Weighted Sums (WS), which is widely used in solving MOO. The WS approach weights the objective functions with a parameter. Equation 12 gives a general description for the WS approach.

$$\begin{aligned} &\min_X WF = \sum_{k=1}^{n} w_k \overline{f}_k(X) \\ &s.t. \\ &X^{lo} \leq X \leq X^{up} \\ &h(X) = 0 \\ &g(X) \leq 0 \\ &\sum_{k=1}^{n} w_k = 1 \end{aligned} \tag{12}$$

where WF is the weighted objective function, which comprises several optimization criteria, and w_k is a weighting parameter given by the user.

Although the WS approach is widely used to solve multi-objective optimization problems, it has two drawbacks. These are:

1. It cannot find Pareto-optimal solutions in concave regions despite the weighting parameters are varied.
2. The Pareto-optimal solutions are not evenly distributed in the solution space. In other words, the Pareto front is not well represented by the derived Pareto-optimal solutions.

To overcome these important limitations in the WS approach, an adaptive algorithm which finds Pareto-optimal solutions in concave regions and better distribution of such solutions along the Pareto front was proposed.[12] The adaptive weighted sum (AWS) performs a refinement between Pareto-optimal solutions as long as the distance between them is larger than a given criterion. Below the steps in the AWS are explained in detail for two-objective optimization problem.

1. Normalize the two objective functions according to Equation 10.

2. Perform multi-objective optimization using the usual weighted-sum approach. The uniform step size of the weighting factor w_k is adopted, and w_k at the i-th optimization is calculated by

$$w_1 = i/(n_{initial}+1), \qquad w_2 = 1-w_1 \qquad (i = 1, 2, ..., n_{initial}) \tag{13}$$

where $n_{initial}$ is the number of initial divisions.

3. Rank the solution obtained at step 2 in ascending order of the first objective function. Then, compute the Euclidean distance between the neighboring solutions. If the Euclidian distance between two adjoining solutions is larger than a prescribed distance (ε), then the pair of solutions is recorded. If there are no recorded solutions, go to step 9.

4. Determine the number of further refinements between each of solutions recorded at step 3. The region among the two adjoining solutions is called a "segment." The length of a segment is the Euclidian distance derived in step 3. The longer the segment lenght is, the more it needs to be refined. The number of refinement of segment i, n_i, is determined based on the length of the segment:

$$n_i = round\left(C \frac{l_i}{l_{avg}} \right) \tag{14}$$

where l_i is the length of the i-th segment, l_{avg} is the average length of all the segments, and C is a constant of the algorithm. The function *'round'* rounds off to the nearest integer.

5. If n_i is less than or equal to one, no further refinement is conducted in the segment. For other segments whose number of further refinements is greater than one, go to the following step.

6. Determine the offset distances from the two end points of each segment. First, a linearized secant line is made by connecting the end points, P_1 and P_2, as shown in Figure 4.6a. Then, the user selects the offset distance, δ, along the linearized Pareto front. The distance δ determines

the final density of the distribution in the Pareto front, because it becomes the maximum segment length during the last phase of the algorithm. In order to find the offset distances parallel to the objective axes, the angle θ in Figure 4.6b is computed as:

$$\theta = \tan^{-1}\left(-\frac{P_1^{\bar{f}_2} - P_2^{\bar{f}_2}}{P_1^{\bar{f}_1} - P_2^{\bar{f}_1}}\right) \tag{15}$$

where $P_k^{\bar{f}_1}$ and $P_k^{\bar{f}_2}$ are the values of end points, P_1 and P_2, of the $\bar{f}_k(X)$ axes, respectively. Then, δ_1 and δ_2 are determined with δ and θ as follows:

$$\delta_1 = \delta\cos\theta \quad and \quad \delta_2 = \delta\sin\theta \tag{16}$$

7. Impose additional inequality constraints in Equation 17, and conduct the optimization with the weighted-sum method given by Equation 12. As shown in Figure 4.6c, the feasible region defined by the distance of δ_1 and δ_2 in the direction of $\bar{f}_1(X)$ and $\bar{f}_2(X)$ is narrower than the original region defined by P_1 and P_2.

$$\begin{aligned}
&\min_X WF = w_1\bar{f}_1(X) + (1-w_1)\bar{f}_2(X)\\
&s.t.\\
&\bar{f}_1(X) \le P_1^{\bar{f}_1} - \delta_1\\
&\bar{f}_2(X) \le P_2^{\bar{f}_2} - \delta_2\\
&X^{lo} \le X \le X^{up}\\
&h(X) = 0\\
&g(X) \le 0\\
&0 \le w_1 \le 1
\end{aligned} \tag{17}$$

The number of necessary refinements is determined from Equation 13 by replacing $n_{initial}$ with the n_i calculated at step 4.

8. Step 7 is repeated every segment recorded at step 3, and return to step 3.

9. Compute the length of the segments between all the neighboring solutions. Delete nearly overlapping solutions. If all the segment lengths are less than a prescribed maximum length, δJ, terminate the optimization procedure.

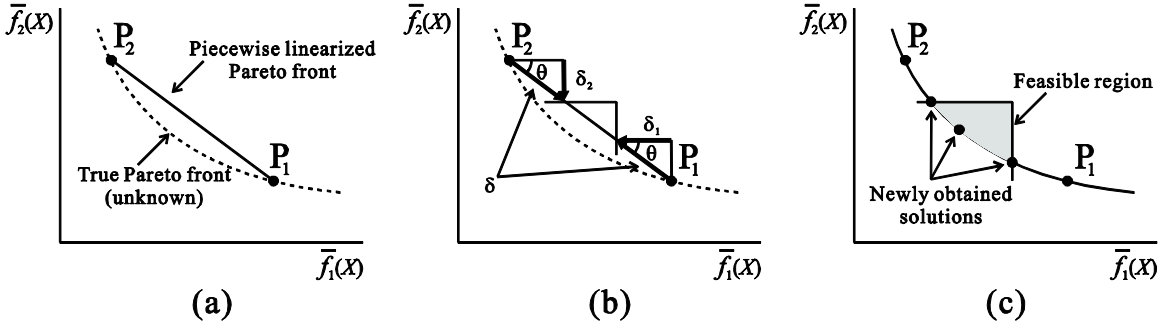

Figure 4.6. Offset distances in the adaptive weighted sum

Although the aforementioned AWS gives a better Pareto front, it requires in many cases several refinements which make this approach time consuming because the MOO has to be solved several times. In addition this approach has not been extended to solve three or more objectives and requires setting several criteria such as $n_{initial}$, ε, C, and δJ.

Another alternative to obtain Pareto-optimal solutions and a better distributed Pareto front without needing any further refinements or iterative procedures is by adopting a min-max weighted sum (MMWS).[12] A general description of MMWS is shown in Equation 18

$$\begin{aligned} &\min_X WF = \max_k \left\{ w_k \bar{f}_k(X) \right\} + \rho \sum_{k=1}^{n} w_k \bar{f}_k(X) \\ &s.t. \\ &X^{lo} \le X \le X^{up} \\ &h(X) = 0 \\ &g(X) \le 0 \\ &\sum_{k=1}^{n} w_k = 1 \end{aligned} \tag{18}$$

where ρ is a parameter typically between 10^{-2} and 10^{-4}.

For the sake of clarity, a comparison between WS, AWS and the MMWS objective functions are compared though a simple case study which has three Pareto-optimal solutions in a non-convex Pareto front as depicted in Figure 4.7.

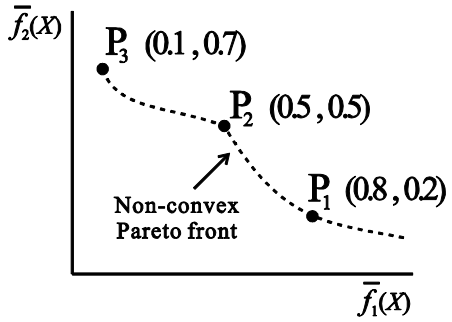

Figure 4.7. Representation of a non-convex Pareto front

Simple algebraic calculations were done for the objective functions and the Pareto-optimal solutions under several weights are shown in Table 4.1. In addition, the length variance in the solutions is shown.

Table 4.1. Comparison of Pareto-optimal solutions in Figure 4.7

Weight	WS	AWS*	MMWS
0.99	P_1	P_1	P_1
0.9	P_1	P_1	P_1
0.7	P_1	P_1	P_1
0.5	P_1	P_2	P_2
0.4	P_3	P_2	P_2
0.3	P_3	P_3	P_3
0.1	P_3	P_3	P_3
0.01	P_3	P_3	P_3
l_{avg} [-]	0.86	0.44	0.44
Length variance, 10^{-4} [-]	---	2.63	2.63

* After one refinement

From the results in Table 4.1, it can be seen that the MMWS and the AWS objective function after one refinement obtained the same solutions. Thus, the MMWS is better than the WS to obtain Pareto-optimal solutions. Because the WS approach was able to find two Pareto-optimal solutions,

its l_{avg} is calculated as the distance between point P_1 and P_3 while its variance cannot be calculated. Because the AWS and MMWS approaches were able to find the three Pareto-optimal solutions, its l_{avg} is calculated as the distance between point P_1 and P_2, defined as l_1 and the distance between P_2 and P_3 , defined as l_2, divided by two while its variance is calculated from the distances $l_1$and l_2.

In the following part of this chapter, the MMWS which can readily find Pareto-optimal solutions in non-convex regions is combined with the adaptive algorithm presented by Kim and de Weck[12] which can find a better density of the distribution in the Pareto front to generate an adaptive min-max weighted sum (AMMWS) approach. Equation 19 represents the AMMWS to optimize two objective functions.

$$
\begin{aligned}
&\min_X WF = \max\left\{ w_1 \overline{f}_1(X) \ , \ (1-w_1)\overline{f}_2(X) \right\} + \rho \sum_{k=1}^{n} w_1 \overline{f}_1(X) + (1-w_1)\overline{f}_2(X) \\
&s.t. \\
&\overline{f}_1(X) \le P_1^{\overline{f}_1} - \delta_1 \\
&\overline{f}_2(X) \le P_2^{\overline{f}_2} - \delta_2 \\
&X^{lo} \le X \le X^{up} \\
&h(X) = 0 \\
&g(X) \le 0 \\
&0 \le w_1 \le 1
\end{aligned}
\qquad (19)
$$

The typical WS, the proposed AWS[12], the typical MMWS[11] and our proposed AMMWS will be considered in solving several MOO. Later, a comparison between these approaches will be done to assess which alternative represents better the Pareto front in more complex and bigger optimization problems.

4.7 Optimization of two objectives in distillation sequences

This section presents two case studies to synthesize distillation sequences where heat integration and compressor addition are possible. The MILP problems were formulated with the above-mentioned method and solved by IBM ILOG OPL® under the following conditions: 10 years of payout time and 8000 hours of operation per year. Table 4.2 shows a list of utilities and heat transfer coefficients used in the case studies. The data presented in Table 4.2 is equivalent to the data for utilities and heat transfer coefficients presented in Chapters 2 and 3, but ammonia is also considered as cooling utility.

Comparisons among the optimal sequences on the Pareto front were addressed from the viewpoint of the *TAC*, and *EC*, and their savings compared with a base case by solving Equation 20

$$\min_{i \in TK} U_2 = \max\left\{w\overline{TAC}_i, (1-w)\overline{EC}_i\right\} + \rho\left(w\overline{TAC}_i + (1-w)\overline{EC}_i\right) \tag{20}$$

where U_2 is the weighted objective function, which combines the two optimization criteria. $\overline{TAC}_i$ is the normalized *TAC* for the selected sequence i and $\overline{EC}_i$ is the normalized *EC* for the selected sequence i.

$\overline{TAC}_i$ and $\overline{EC}_i$ are expressed by the following equations

$$\overline{TAC_i} = \frac{TAC_i - TAC^*}{TAC^N - TAC^*} \tag{21}$$

$$\overline{EC_i} = \frac{EC_i - EC^*}{EC^N - EC^*} \tag{22}$$

where TAC^* and TAC^N are utopia point and Nadir point of *TAC*, and EC^* and EC^N are utopia point and Nadir point of *EC*, respectively.

Table 4.2. Data for utilities and heat exchange coefficients for all the examples[23]

Utility	Temperature [K]	Cost [$/MWh]
Ammonia, (AM)	255	51.32
Chilled Water†, (CHW)	278	14.40
Cooling Water†, (CW)	305	0.914
Steam at 446 kPa, (S1)	420	11.17
Steam at 1135 kPa, (S2)	459	18.93
Steam at 3202 kPa, (S3)	511	29.43

Heat transfer coefficients [kW/(m^{2}K)]

Condenser: 0.6, Reboiler: 1, Heat exchanger: 0.5

† 20 K Rise

4.7.1. Case study 1: Separation of a ternary mixture

A ternary mixture of Cyclopentane, Benzene, and Toluene is investigated in the first case study. This mixture has relative volatility close to 3 between adjacent components and does not exhibit azeotropic behavior or any major nonlinearity, which implies their separation is not difficult. Therefore, the thermodynamic model was the Wilson equation[13] to calculate the activity coefficients in the liquid phase, and the Redlich-Kwong equation[14] to calculate the fugacity coefficients in the vapor phase. In this case study all the sequences shown in Figure 4.1 were simulated at three different pressures: 122, 304, and 507 kPa. The linking flows of thermally coupled sub-sequences were optimized at 304 kPa, and recompression of vapor streams was done at 304 and 507 kPa. The feed flow rate is 100 kmol/h, while the specifications for all the states are shown in Table 4.3. In order to clarify the difference of intermediate states obtained by a conventional column and a sloppy split column, the intermediate states obtained by a sloppy split column is shown by using lower cases, i.e., Ab and bC are intermediate states of SS sequence. The conventional column separating A and B from C will have states AB and C while the sloppy split separating AB and BC will have states Ab and bC.

Table 4.3. Specifications for all the states in case study 1 [mol%]

	ABC	AB	BC	Ab	bC	A	B	C
Cyclopentane (A)	10	*	1	*	1	96	*	*
Benzene (B)	60	*	*	*	*	*	92	*
Toluene (C)	30	1	*	1	*	*	*	96

*Not restricted

For this example, the WS, AWS, MMWS and AMMWS obtained the same global optimal solution, which minimized both *TAC* and *EC* as shown in Figure 4.8a. The optimal structure is a sloppy split sequence with vapor recompression in every column resulting in self-integration (X1 in the figure). In addition, it can be observed that cooling utilities are not used. External heat integration between condensers and reboilers is represented by X2, X3 and X4 in the same figure. Figure 4.8b is the suboptimal solution with vapor recompression of side and top streams. It is the PPL sequence and it adopts vapor recompression resulting in heat integration within the thermally coupled column (X1 in the figure). The Petlyuk column operating at 122 kPa in Figure 4.8c is the best sequence without vapor recompression or heat integration. When the optimal solution is drastically penalized with

high cost and high energy consumption, it can be removed from the Pareto front so as to find suboptimal solutions as those in Figures 4.8b and 4.8c.

For the sake of simplicity, hereinafter, the amount of energy exchanged between condensers and reboilers is indicated only once at either one of the heat exchangers denoted by X and a consecutive number.

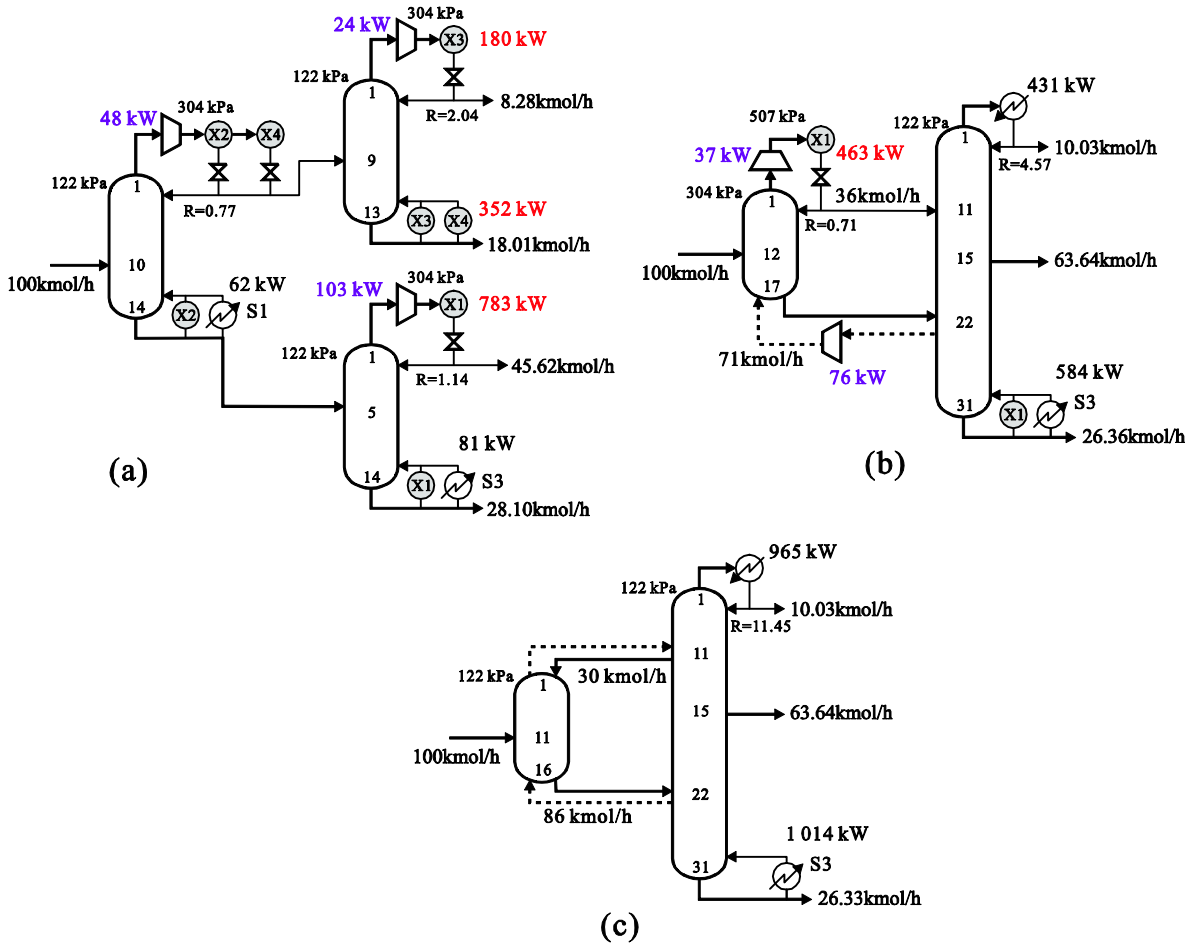

Figure 4.8. Solutions for case study 1: a) optimal solution,
b) suboptimal solution with vapor recompression, and
c) Petlyuk sequence at 121 kPa.
red: external heat integration, purple: work duty, black: utility

Where there are more than one condenser and/or reboiler, the adopted configuration placed them in parallel. It is a conceptual representation of the heat integration network; however, detailed

calculations are necessary at a later design stage to compare if a parallel configuration is better than a series configuration.

The global optimal solution and two suboptimal solutions were compared with the base case (sloppy split sequence without heat integration or vapor recompression at 122 kPa), and the results are shown in Table 4.4.

Table 4.4. Economic and energy savings of optimal solutions in case study 1

Solution	*TAC* [k$/y]	Economic savings [%]	*EC* [kW]	Energy savings [%]
Base Case	389.1	---	1 476	---
Figure 4.8a	229.4	41.0	666	54.9
Figure 4.8b	275.6	29.2	924	37.4
Figure 4.8c (PET)	310.5	20.2	1 014	31.3

For case study 1, a wide pressure range was assigned to the problem. Thus, the heat integration by changing the vapor pressure is effectively adopted in the optimal solution. In addition, the optimization results show that the thermally coupled columns shown in Figure 4.1d to 4.1g are more likely to realize heat integration than the Petlyuk column when pressure change is possible.

4.7.2. Case study 2: Four-Component mixture of Acetone, Ethanol, 1-Propanol and 1-Butanol

The second case study involves a mixture of Acetone (A), Ethanol (B), 1-Propanol (C), and 1-Butanol (D). This mixture is more difficult to separate because the relative volatility between acetone and ethanol is close to one. Furthermore, there is a quaternary azeotrope at pressures higher than 456 kPa, and a binary azeotrope between acetone and ethanol at pressures higher than 233 kPa. To avoid azeotropic behavior, the candidate columns were simulated at three pressure levels: 101, 152 and 202 kPa. As in section 4.7.1, the thermodynamic model was the Wilson equation[13] to calculate the activity coefficients in the liquid phase, and the Redlich-Kwong equation[14] to calculate the fugacity coefficients in the vapor phase. The linking flow rates of thermally coupled sub-sequences were decided on the basis of the optimization results at 152 kPa. Although the

azeotropic condition is avoided, the system still shows highly non ideal behavior. The feed flow rate is 200 kmol/h. The product specifications for all the states that separate the quaternary mixture are shown in Table 4.5 for conventional columns. For the SS sequence, the composition of the intermediate state is different even when the flow consists of the same components. Thus, the all the states for SS sequences are summarized in Table 4.6.

Table 4.5. Specifications of states for the sequence of conventional columns [mol%]

	ABCD	ABC	BCD	AB	BC	CD	A	B	C	D
Acetone (A)	15	*	0.5	*	0.5	*	97	*	*	*
Ethanol (B)	15	*	*	*	*	0.5	*	95	*	*
1-Propanol (C)	40	*	*	0.5	*	*	*	*	95	*
1-Butanol (D)	30	0.5	*	*	0.5	*	*	*	*	97

*Not restricted

Table 4.6. Specifications of intermediate states for the SS sequences [mol%]

	ABc	bCD	Ab	bC	Bc	cD
Acetone (A)	*	0.2	*	0.2	*	*
Ethanol (B)	*	*	*	*	*	0.2
1-Propanol (C)	*	*	0.2	*	*	*
1-Butanol (D)	0.2	*	*	*	0.2	*

*Not restricted

The original mixture and the intermediate streams were separated by a combination of the sharp and sloppy split conventional columns as well as thermally coupled columns shown in Figure 4.1.

For this example, the WS, AWS, MMWS and AMMWS obtained the same Pareto front. Two optimal solutions are obtained and shown in Figure 4.9. Both of them consist of a combination of conventional and thermally coupled columns. Figure 4.9a shows the sequence that realized heat integration and resulted in the lowest *TAC*. It consists of a PPL sequence that separates AB from C and D and a conventional column separating A from B. The conventional column supplies energy to the first column in the PPL sequence. Figure 4.9b realized vapor recompression in addition to heat integration, and this combination resulted in lower *EC*. It consists of a PPL sequence that separates A

and B from CD and a conventional column separating C from D. The conventional column supplies energy to the second column in the PPL sequence. In both cases the conventional column supplies energy to the thermally coupled column.

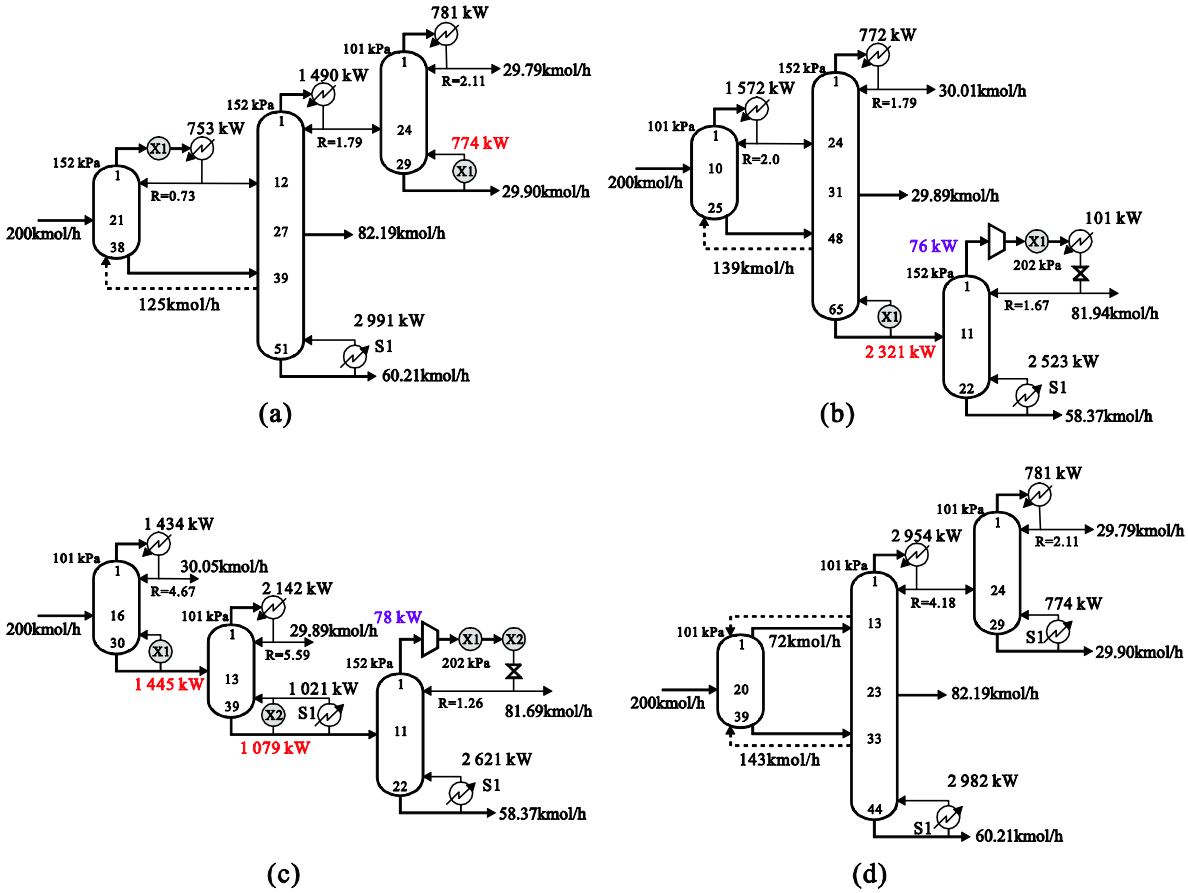

Figure 4.9. Solutions for case study 2: a) Pareto-optimal solution with the lowest *TAC*,
b) Pareto-optimal solution,
c) CC+HI sequence,
d) PET+CC sequence, and
red: external heat integration, purple: work duty, black: utility

In addition to two Pareto optimal solutions, simulation results of another three solutions are listed in Table 4.7. One is the best distillation sequence consisting of only conventional columns without heat integration. In such condition, the combination of SS and a conventional column minimizes *TAC*.

In this structure, the feed is separated into (AB/C/D) by SS and then a conventional column is used to separate A from B. This structure is expressed as Base Case in Table 4.7. Figure 4.9c is the case where the sequence consists of only CC. Heat integration and vapor recompression are considered to derive the optimal sequence, which minimizes the *TAC*. The result is also shown in Table 4.7 as CC+HI. In this case, the structure consists of the columns separating (A/BCD), (B/CD) and (C/D). Vapor recompression is also adopted in the last column. In Figure 4.9d, all sub-sequences in Figure 4.1 are considered but heat integration is not executed. In such condition, the combination of a conventional column and PET is selected as the best structure, which minimizes the *TAC*. In this case, the feed is separated to (AB/C/D) by a Pelyuk column, then a conventional column is used to separate (A/B). For case study 2, the feasible pressure range was very narrow. This feature limits the application of vapor recompression. However, vapor recompression can still realize the lowest *EC*.

Table 4.7. Economic and energy savings of optimal solutions in case study 2

Solution	TAC [k$/y]	Economic savings [%]	*EC* [kW]	Energy savings [%]
Base Case	743.2	---	5 202	---
Figure 4.9a	530.6	28.6	2 991	42.5
Figure 4.9b	554.9	25.3	2 750	47.1
Figure 4.9c (CC+HI)	674.0	9.3	3 877	25.5
Figure 4.9d (PET+CC)	548.3	26.2	3 756	27.8

4.7.3. Case study 3: Five-Component mixture of Propane, Isobutane, Butane, Isopentane, and Pentane

This five-component mixture was proposed by Rathore et al.[15] and it has been widely used to synthesize sequences with heat integration. The relative volatility between the isomers is close to one, which means these separations are more difficult than the rest. The used thermodynamic model was the Chao-Seader correlation[16] in the liquid phase and Peng-Robinson equation[17] in the vapor phase. Under the previous considerations, this mixture could be considered as ideal and it did not exhibit azeotropic behavior. Thus, simulations over a wide pressure range from 507 to 2027 kPa

were performed. The optimization pressure for complex columns was 1216 kPa. The feed flow rate is 907.2kmol/h and the feed composition of Propane, Isobutane, Butane, Isopentane, and Pentane namely A, B, C, D and E is 0.05, 0.15, 0.25, 0.20, and 0.35mol% whereas their product specification is 97, 97.6, 98.5, 95.3 and 99.4% molar purity respectively.

The candidate separation cuts were the separation of AB from CDE (AB/CDE) and ABC from DE (ABC/DE) by conventional columns. Each ternary mixture ABC and CDE was separated by the sequences shown in Figure 4.1. These separation cuts were selected because thermally coupled sequences are expected to separate the isomers BC and DE with less energy consumption. Another sharp split separations such as (A/BCDE), sloppy split separations such as (ABC/CDE) as well as thermally coupled separations such as (A/BC/DE) can also be candidate separation cuts to the superstructure, however, they are not included in this example because the number of rigorous simulations and the superstructure complexity drastically increase.

For this example, as the number of candidate sub-sequences and operating pressure increases, the Pareto front for the WS, AWS, MMWS and AMMWS was different in each case when *TAC* and *EC* were minimized simultaneously. The Pareto front of the four optimization methods is shown in Figure 4.10.

From Figure 4.10a it is shown that WS can only find few Pareto optimal solutions. In addition, those solutions are not distributed evenly. The Pareto-optimal solutions in MMWS from Figure 4.10b are more evenly distributed and one solution is found in non-convex region. These results agree with our previous demonstration in section 4.5 for the MMWS. The solutions for the AWS and AMMWS in Figures 4.10c and 4.10d, respectively, are better distributed in the pareto front and are found in the non-convex regions.

The solution obtained from the WS approach shows two regions with no information of the Pareto front; therefore, reliable information cannot be derived from this approach. The solution from the MMWS technique was able to find more Pareto-optimal solutions in the non-convex region close to the vertical axis. When the adaptive algorithm explained in section 4.6 is applied, more Pareto-optimal solutions were found. The AWS and the AMMWS had almost the same Pareto-optimal solutions, but, the AMMWS approach was able to find more Pareto-optimal solutions and the solutions were more evenly distributed in the pareto front.

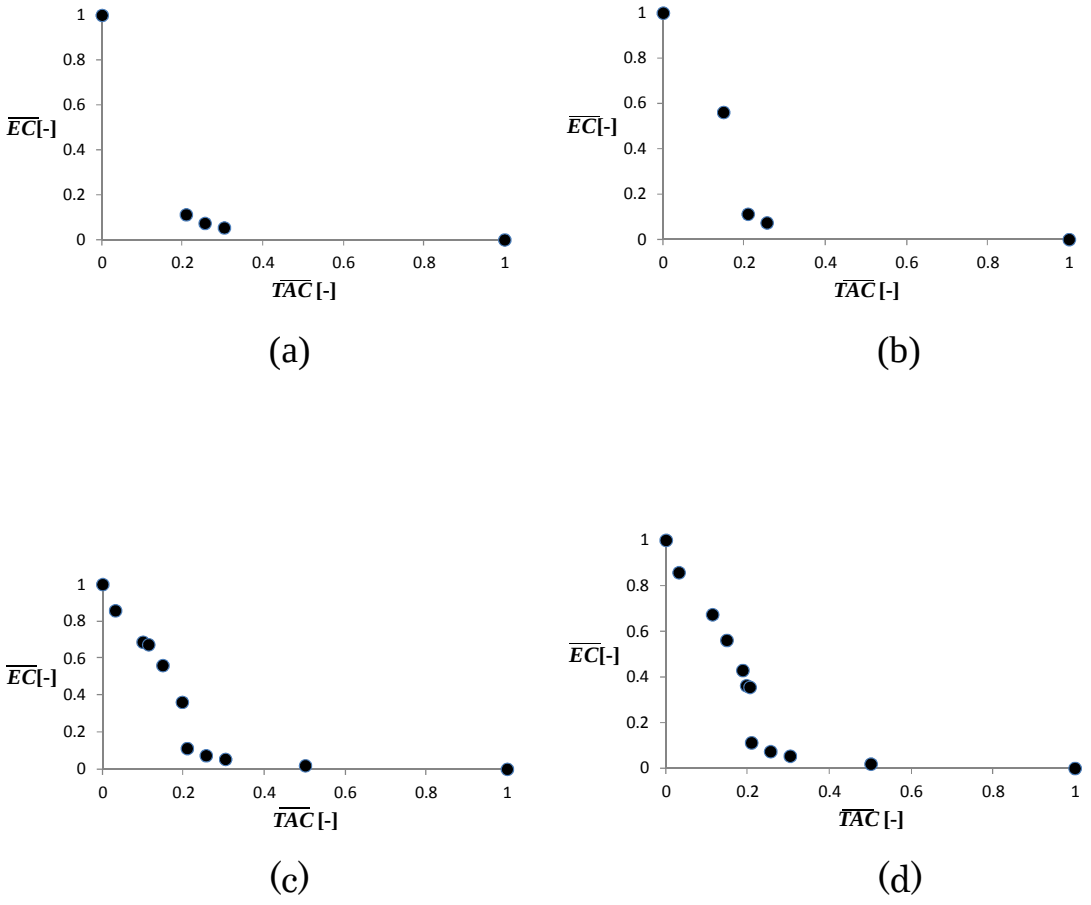

Figure 4.10. Pareto front solutions for case study 3: a) WS solution, b) MMWS solution, c) AWS solution, d) AMMWS solution

Table 4.8 shows the values for the parameters $n_{initial}$, ε, C, and δJ, and ρ, the average length and the length variance in the Pareto-optimal solutions for each weighted objective function. The length variance of the Pareto-optimal solutions is calculated to measure the evenness of the Pareto-optimal solutions. Values close to zero mean the Pareto-front is evenly distributed. The AWS shows better results in these values, but more refinements were necessary than the AMMWS approach.

Table 4.8. Average length and deviation between Pareto optimal solutions

Optimization approach	l_{avg} [-]	Length variance [-]	Iterations	Optimizations	Pareto-optimal solutions
WS	0.34	0.147	0	6	5
MMWS	0.43	0.080	0	6	5
AWS	0.17	0.019	2	21	11
AMMWS	0.16	0.018	2	21	12

$n_{initial}$ = 4, ε = 0.05, C = 2, δJ = 0.1 and $\rho = 10^{-4}$

Figure 4.11 shows four Pareto-optimal solutions when the AMMWS multi-objective optimization was solved. Figure 4.11a is a sequence of conventional columns with vapor recompression where column D/E supplies energy to column AB/C and column A/B, in addition column A/B used vapor recompression to avoid using expensive cooling utility. Figure 4.11b is a sequence with conventional and thermally coupled columns where column D/E realizes self-integration though vapor recompression and it also supplied energy to the thermally coupled sequence PCV. Figure 4.11c is a sequence of conventional columns with vapor recompression where column D/E realizes self-integration and supplies energy to column AB/C, in addition column ABC/DE supplies energy to column AB/C. Finally, Figure 4.11d is a sequence with conventional and thermally coupled columns with vapor recompression where column D/E realizes self-integration though vapor recompression and it supplies energy to the thermally coupled sequence PCV, column ABC/DE also supplies energy to the thermally coupled sequence PCV.

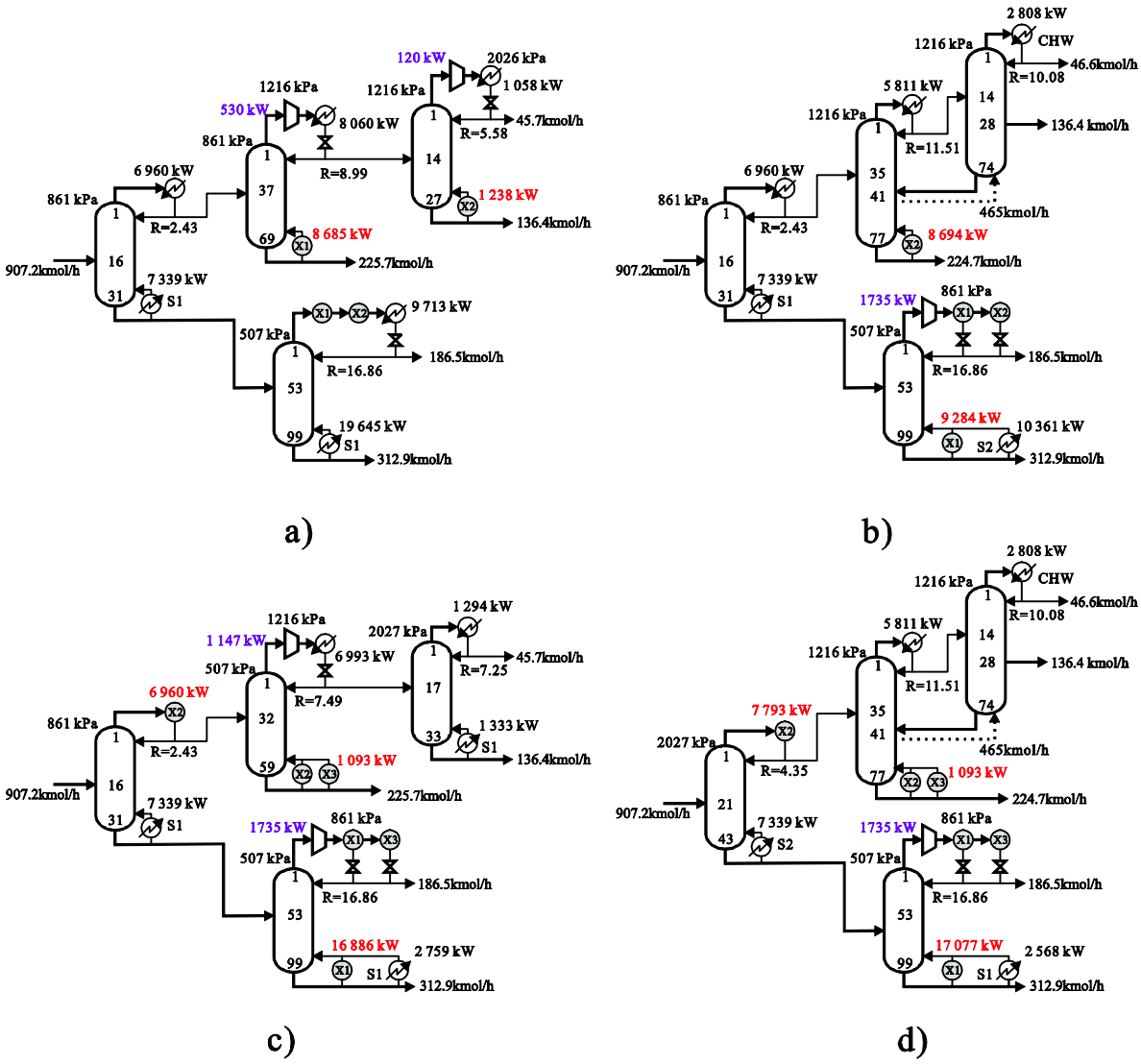

Figure 4.11. Pareto-optimal solutions for case study 3:
red: external heat integration, purple: work duty, black: utility

The Pareto-optimal sequences in Figure 4.11 were compared with the best sequence reported by[15], but operating at 861 kPa. The results for this comparison are reported in Table 4.9

Table 4.9. Economic and energy savings of optimal solutions in case study 3

Solution	*TAC* [k$/y]	*FC* [k$/y]	*OC* [k$/y]	Economic savings [%]	*EC* [kW]	Energy savings [%]
Base Case	10 209	4 446	5 763	---	29 033	---
Figure 4.11a	6 246	3 335	2 911	38.8	28 935	0.3
Figure 4.11b	6 836	4 005	2 831	33.0	22 906	21.1
Figure 4.11c	7 061	4 595	2 465	30.8	20 078	30.8
Figure 4.11d	7 451	4 789	2 663	27.0	15 930	45.1

A combination of only conventional columns, and conventional and thermally coupled columns with vapor recompression were Pareto-optimal solutions. The wide operating pressure range was effective to realize heat integration to avoid the use of expensive utility as well as to realize heat integration.

Figure 4.12 show a graphical representation of the trade-off between economic and energy savings for all the Pareto-optimal solutions in Figure 4.10d. The blue bars represent the economic savings in the Pareto-optimal solutions while the green bars represent the energy savings for the same solution. It is clarified how the improvement in energy savings can result from the worsening of economic savings and vice versa. These savings of the Pareto-optimal solution offer valuable information because it can readily be determine how much additional investment is necessary to attain less energy consumption, or how much additional energy consumption is necessary to reduce the investment in a distillation sequence.

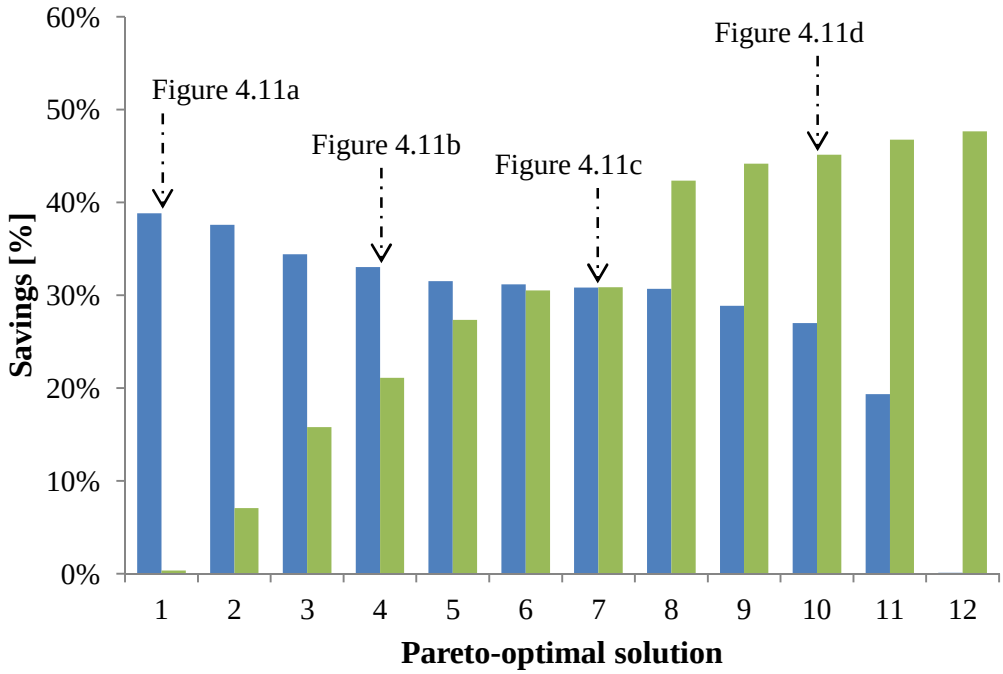

Figure 4.12. Trade-off between economic and energy savings for the Pareto-optimal solutions in case study 3.

4.8 Optimization of three objectives in distillation sequences

4.8.1 Case study 4: Environmental and economic optimization of distillation structures to produce anhydrous ethanol

Ethanol obtained from lignocellulosic materials has gained remarkable attention for new renewable fuels, but the ethanol-water mixture forms an azeotrope. Thus, the distillation of the ethanol-water mixture becomes energy-intensive and its separation requires azeotropic distillation either by pressure swing or extractive distillation. Several flow sheets have been proposed to reduce cost and energy consumption. [18, 19]

First, a conventional column is used to concentrate a diluted feed (5–8 wt%) obtained from lignocellulosic materials. For pressure swing distillation, two more columns are needed[13]: a stripping column that concentrates the mixture below its azeotrope (90–94 wt%), and a column operated at high pressure to surpass the azeotrope and to obtain fuel grade ethanol (>99.5 wt%). For extractive

distillation, three more columns are needed [18, 19]: a stripping column to concentrate the mixture below its azeotrope, an extractive distillation column to surpass the azeotrope by entrainer and to obtain fuel grade ethanol, and a column to recover the entrainer.

These alternatives offer several possible combinations of operating pressure or entrainer selection. In addition, to lower the fixed and operating costs several energy conservation methods such as external heat integration[19], internal heat integration[20] and thermal coupling distillation[21] have been studied.

For extractive distillation, although several entrainers have been suggested to reduce the impact on human health, their impact has not been quantitatively assessed. Furthermore, the optimal design to obtain sequences with minimum impact on global warming has not been addressed either.

In this section various distillation structures, entrainers, and energy conservation methods are taken up, and separation structures which optimize the total annual cost, impact on global warming and impact on human health are derived by solving a multi-objective optimization problem.

4.8.2 Superstructure formulation

A state-task network superstructure formulation is adopted to express all of the candidate structures that include conventional and complex columns where pressure swing distillation, extractive distillation, external heat integration and vapor recompression are possible. Figure 4.13 shows a general description of the proposed superstructure.

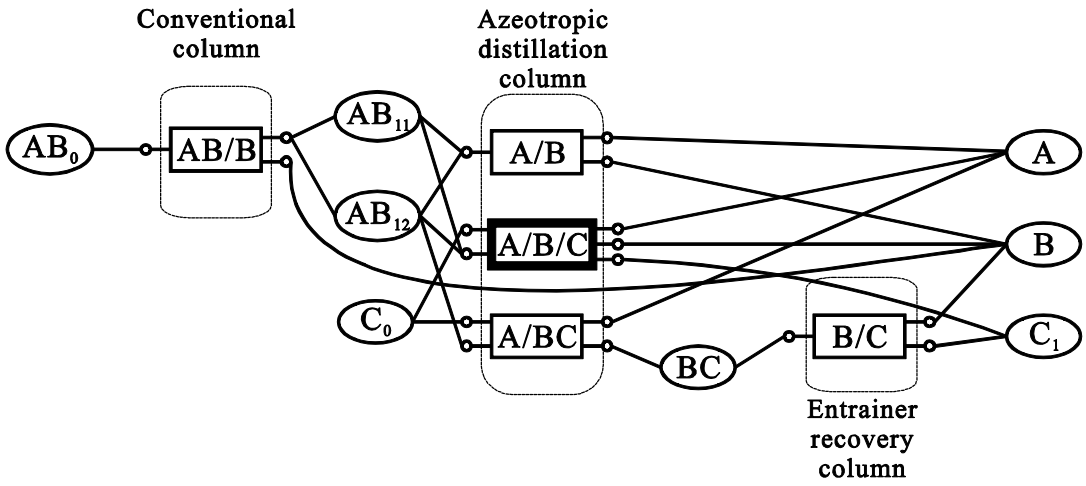

Figure 4.13. Conceptual superstructure representation.

An ellipse in Figure 4.13 is a state the composition of which is given in advance. A rectangle is a set of tasks, each of which has the same input and output states and operates at different discrete pressures. The bold rectangle represents a set of aggregated tasks, each of which consists of two thermally coupled columns. An aggregated task can separate ethanol (A), water (B), and the selected entrainer (C) simultaneously. Figure 4.14 shows the column structures treated in this research. Figure 4.14a is a conventional column (CC), Figure 4.14b is an extractive column (EC), and Figure 4.14c is a thermally coupled column with side rectifier (TCSR), which is expressed by aggregated tasks.

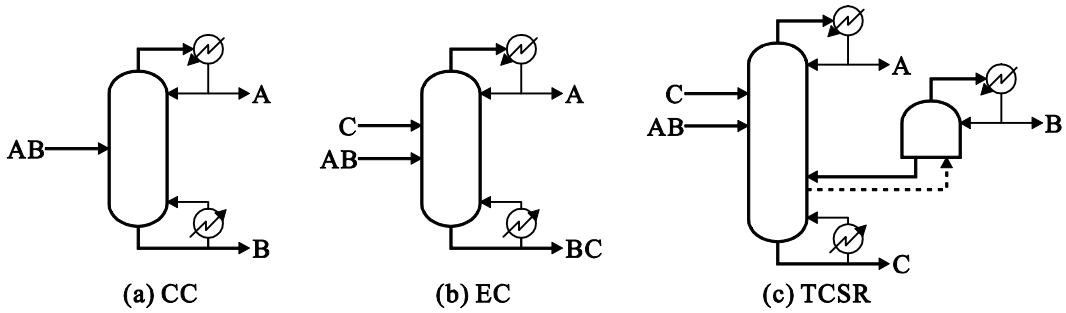

Figure 4.14. Column structures adopted in this study

4.8.3 Multi-objective optimization model

In this research, three candidates in Table 4.10 are studied as the entrainer. To avoid thermal decomposition and metal corrosion by the entrainer[22], the temperature and pressure ranges of the columns, which use an entrainer, are restricted and are shown in Table 4.10. The other columns are assumed to take one of the discrete pressures 101, 202, 304, or 405 kPa. Table 4.11 shows the specifications of states used in this research.

Table 4.10. Operating conditions for the studied entrainers

	Temperature range [K]	Pressure range [kPa]
Ethylene glycol, (EG)	453–530	101, 202, 304, 405
Propylene glycol, (PG)	453–540	101, 202, 304, 405
Glycerin, (GL)	453–555	51, 101, 202, 304

Table 4.11. Design specifications for all the states [wt%]

	AB0	AB11	AB12	BC	A	B	C1
Ethanol (A)	8	40	60	1	99.5	*	*
Water (B)	92	60	40	*	*	99	*
Entrainer(C)	0	0	0	*	*	*	99

* Differ in every task

The results of rigorous simulation are used to decide the design parameters in a distillation column such us the reflux ratio, number of stages, column diameter, condenser and reboiler duty, and compressor work duty, which are input in the optimization problem. Binary variables are introduced to express whether each task is adopted or not. Finally, the synthesis problem is formulated as a MILP problem.

The economical assessment is based on the total annual cost, *TAC*, which includes the fixed and the operating costs as shown in Equation 23

$$TAC = FC/PT + OH \cdot OC \tag{23}$$

where *FC* is the fixed cost which includes the costs of columns, trays, heat exchangers, compressors and vacuum operation if any, whereas *OC* is the operating cost which includes the costs of cooling, heating, and electricity usage. *PT* is the payout time and *OH* is the annual operation hours. Since compressors are expensive, their fixed and operating costs are included in the *TAC*. The equipment cost is calculated according to Seider et al.[23]

To conduct the environmental assessment, the score for human toxicity, *HT*, is derived by multiplying the amount of consumed/emitted chemical species by its characterization factors[24].

$$HT = OH \cdot \sum_{i \in TK} CF_i \cdot \alpha_i \tag{24}$$

where α_i is the amount of entrainer emissions for task *i*, and CF_i is the characterization factor. Values at the midpoint category or end-point category of damage level can be used as CF_i. The emission of entrainers in the wastewater and purge streams is treated in this research. *TK* is the set of tasks.

The impact of global warming, *GW*, is assumed as a sum of the amount of CO_2 emissions from steam generation, CE_{steam}, and that from electricity generation, CE_{elec}.

$$GW = OH \cdot CE_{steam} \sum_{\substack{i \in TK \\ j \in HU}} Q_{ext}^{i,j} + OH \cdot CE_{elec} \left(\sum_{j \in TK} W_{VR}^{j} Y^{j} + \sum_{d \in IDc} \sum_{\substack{i \in TKF_d \\ j \in TKP_d}} W_{comp}^{i,j} Y_{comp}^{i,j} \right) \tag{25}$$

The characterization factor[24] for each entrainer is 1.83x10^{-3} for ethylene glycol, 3.05 x10^{-5} for propylene glycol, and 1.42 x10^{-4} for glycerin in kg Chloroethylene in air per kg of entrainer while CE_{steam}[24] is 9.54 x10^{-4} and CE_{elec}[25] is 4.60 x10^{-4} in tons of CO_2 in air per kWh.

The synthesis problem is formulated as a multi-objective optimization problem, which minimizes the three criteria shown in Equations 23, 24 and 25. The weighted sum of multiple criteria is widely used, but it has two major drawbacks: it cannot find solutions in concave regions, and the optimal solutions are not evenly distributed on the Pareto front. To overcome these disadvantages a procedure combining a min-max weighted sum and an adaptive procedure[12] which is explained in section 4.6 is adopted. Equation 26 shows the min-max weighted sum adopted in this section.

$$\min_{i \in TK} U_3 = \max \left\{ w_1 \overline{TAC_i}, w_2 \overline{GW}_i, w_3 \overline{HT}_i \right\} + \rho \left(w_1 \overline{TAC_i} + w_2 \overline{GW}_i + w_3 \overline{HT}_i \right) \tag{26}$$

where U_3 is the weighted function of three optimization criteria, w_i is a weighting parameter chosen by a decision maker and ρ is a parameter usually set between 10^{-2} and 10^{-4}. $\overline{TAC}_i$ is the normalized *TAC* for the selected sequence *i*, $\overline{GW}_i$ is the normalized *GW* for the selected sequence *i*, and $\overline{HT}_i$ is the normalized *HT* for the selected sequence *i*. $\overline{GW}_i$ and $\overline{HT}_i$ are expressed by the following equations

$$\overline{GW_i} = \frac{GW_i - GW^*}{GW^N - GW^*} \tag{27}$$

$$\overline{HT_i} = \frac{HT_i - HT^*}{HT^N - HT^*} \tag{28}$$

where the superscript * is the utopia point, and the superscript *N* denotes the nadir point.

The problem specified by Table 4.11 is solved by the procedure explained above. The optimization was performed through IBM OPL ILOG® by using CPLEX®. By changing the weight w_i in Equation 26, various structures are obtained. Some structures appearing on the Pareto front are shown in Figure 4.15. Except the *HT* vertex, extractive distillation is selected whose entrainer is Propylene glycol.

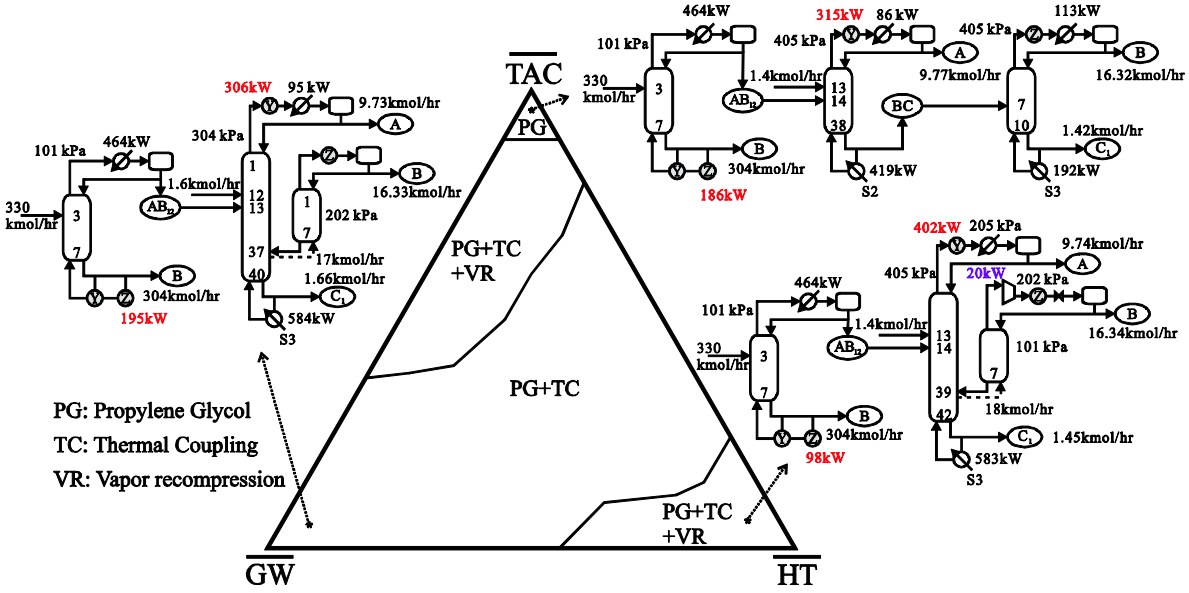

Figure 4.15. Multiobjective optimization solution and representative solutions.

Heat integration in conventional sequences is the best choice to minimize *TAC*; however, thermally coupling and vapor recompression are selected when the weights of *GW* and/or *HT* are increased. External heat integration is executed every case, thermal coupling and vapor recompression are additionally used to reduce CO_2 emissions and/or toxic discharges.

The synthesis procedure to obtain optimal flow sheets to produce anhydrous ethanol was proposed. Pressure swing distillation and extractive distillation were included as alternatives to separate the azeotropic mixture. In addition to the conventional column, thermally coupling columns were studied. A new procedure that combines a min-max weighted sum and an adaptive method was proposed to solve the multiobjective optimization problem.

Various structures were derived on the pareto front, but they were classified in several groups where propylene glycol was used as entrainer. A combination of conventional column structure with external heat integration showed the lowest total annual cost. When human toxicity and CO_2 emissions are taken into account, vapor recompression or thermally coupled columns become attractive. When showing the optimal structures on a multi-criteria space, the characteristics of the given separation problem become much clearer.

4.9 Conclusions

The synthesis problem of Pareto-optimal distillation sequences was addressed and solve for conventional and thermally coupled columns with or without vapor recompression when several objectives are considered. The optimal solution with minimum cost and the optimal solution with minimum energy consumption contradicts each other when compressors are included in the synthesis of distillation sequences. Multi-objective optimization techniques were applied to the separation of distillation mixtures from ternary to five-component separation processes.

The min-max weighted sum (MMWS) was adopted along with an adaptive algorithm to readily obtain Pareto-optimal solutions in non-convex regions of the pareto front. Distillation sequences with conventional and thermally coupled columns were dominant in the Pareto front.

When two objectives were considered, a worsening in economic savings resulted in an improvement of energy savings. Thus, the ratio of cost increment per unit amount of energy can be calculated to establish the trade-off between cost and energy in a mixture. When three objective functions were considered as optimization criteria, our newly proposed entrainer (Propylene Glycol) resulted in the best trade-off among cost, global warming and human toxicity to realize economically attractive and environmentally friendly flow sheets to obtain anhydrous ethanol.

Chapter nomenclature

C = constant of the adaptive algorithm

C_{col}^{i} = column cost of task i [k$]

C_{tray}^{i} = tray cost of task i [k$]

C_{heat}^{i} = cost of heating utility i [k$/kWh]

C_{cool}^{j} = cost of cooling utility j [k$/kWh]

C_{elec} = cost of electricity [k$/kWh]

C_{VR}^{i} = compressor cost to realize vapor recompression in streams to condensers of column i (or task i) [k$]

$C_{comp}^{i,j}$ = compressor cost which is installed to flow a vapor stream from column i (or task i) to column j (or task j) [k$]

$C_{ext}^{i,j}$ = heat exchanger cost per unit amount of heat exchanged between the rectifying section of task i and stripping section of task j [k$/kW]

CE_{elec} = amount of CO_2 emissions from electricity generation [ton of CO_2 in air/ kWh]

CE_{steam} = amount of CO_2 emissions from steam generation [ton of CO_2 in air/ kWh]

CF_i = characterization factor of entrainer for task i [kg Chloroethylene in air/kg of entrainer]

CU = set of cold utilities [-]

EC = energy consumption [kW/y]

$\overline{EC}_i$ = normalized energy consumption of sequence i [-]

EC^* = utopia point of the energy consumption [kW/y]

EC^N = Nadir point of the energy consumption [kW/y]

$f_k(X)$ = k-th objective function

$\bar{f}_k(X)$ = k-th normalized objective function

f_k^* = utopia point of a k-th objective function

f_k^N = Nadir point of a k-th objective function

FC = fixed cost [k$]

$FEED$ = set of tasks whose input stream is the original feed state [-]

$g(X)$ = functions in inequality constraints

GW = impact on global warming [ton of CO_2 in air/y]

$\overline{GW}_i$ = normalized impact on global warming of sequence i [-]

GW^* = utopia point of the impact on global warming [ton of CO_2 in air/y]

GW^N = Nadir point of the impact on global warming [ton of CO_2 in air/y]

$h(X)$ = functions in equality constraints

HU = set of hot utilities [-]

HT = human toxicity [kg Chloroethylene in air/y]

$\overline{HT}_i$ = normalized impact on human toxicity of sequence i [-]

HT^* = utopia point of the impact on human toxicity [kg Chloroethylene in air/y]

HT^N = Nadir point of the impact on human toxicity [kg Chloroethylene in air/y]

l_i = length of the i-th segment between two Pareto-optimal solutions [-]

l_{avg} = average length of all the segments

n = number of objective functions [-]

$n_{initial}$ = initial number of divisions [-]

OC = operating cost [k$/h]

OH = annual operation hours [h/y]

PT = payout time [y]

$P_i^{\tilde{f}_j}$ = value of the j-th axis for point P_i in Figure 4.6 [-]

$q_0^{c,i}$ = condenser heat duty before heat integration for task *i* [kW]

$Q_0^{r,j}$ = reboiler heat duty before heat integration for task *j* [kW]

$Q_{ext}^{i,j}$ = amount of heat exchanged between the top vapor stream of task *i* and the bottom liquid stream of task *j* [kW]

ST = set of all states excepting the feed and product states [-]

ST_C = set of all aggregated states [-]

TKF_s (TKP_s) = set of task whose output (input) flow connects state *s* or aggregated state *s* [-]

TAC = total annual cost [k$/y]

$\overline{TAC}_i$ = normalized total annual cost of sequence *i* [-]

TAC^* = utopia point of the total annual cost [k$/y]

TAC^N = Nadir point of the total annual cost [k$/y]

TK = set of tasks [-]

U_2 (U_3) = weighted objective function of two (three) optimization criteria

VR = set of tasks with vapor recompression [-]

w_k = weighting parameter of the *k*-th objective function [-]

$W_{comp}^{i,j}$ = compressor work duty for the stream from column *i* (or task *i*) to the column *j* (or task *j*) in a thermally coupled column (or an aggregated task) [kW]

W_{VR}^{i} = compressor work duty to increase the pressure of a stream to a condenser in column *i* (or task *i*) [kW]

WF = weighted objective function [-]

X^{lo} (X^{up}) = lower (upper) bound for a decision variable in a general optimization description

X^P = set of variables that derive Pareto-optimal solutions

$Y_{comp}^{i,j}$ = binary variable which become one if tasks *i* and *j* compose an aggregated task and are selected [-]

Y_{ext}^{i} = binary variable assigned to task *i*. It becomes one when task *i* is selected [-]

Greek letters

α_i = amount of entrainer emissions for task *i* [kg of entrainer/h]

δ= offset distance along the linearized Pareto front [-]

δ_1(δ_2) = horizontal (vertical) component of δ [-]

δJ = prescribed maximum length of δ [-]

ε = prescribed Euclidian distance between two Pareto-optimal solutions [-]

θ = angle of the offset distances parallel to the objective axes [rad]

ρ = optimization parameter in the MMWS and AMMWS approaches [-]

Reference literature

(1) Rangaiah, G. P. *Multi-objective optimization;* World Scientific: Singapore, 2009.

(2) Caballero, J. A.; Grossmann, I. E. Structural Considerations and Modeling in the Synthesis of Heat-Integrated-Thermally Coupled Distillation Sequences. *Ind. Eng. Chem. Res.* **2006,** 45, 8454-8474.

(3) Yiqing, L.; Xigang, Y.; Fenglian, D. Synthesis and heat integration of thermally coupled complex distillation system. *Int. J. Energy Res.* **2010,** 34, 626–634.

(4) Agrawal, R.; Fidkowski, Z. T. New Thermally Coupled Schemes for Ternary Distillation. *AIChE J.* **1999,** 45, 485-496.

(5) Agrawal, R.; Fidkowski, Z. T. More Operable Arrangements of Fully Thermally Coupled Distillation Columns. *AIChE J.* **1998,** 44, 2565-2568.

(6) Christiansen, A. C.; Skogestad, S.; Lien, K. Complex Distillation Arrangements: Extending the Petlyuk Ideas. *Comput. Chem. Eng.* **1997,** 21, S237-S242.

(7) Yeomans, H.; Grossmann, I. E. Optimal Design of Complex Distillation Columns using Rigorous Tray-by-Tray Disjunctive Programming Models. *Ind. Eng. Chem. Res.* **2000,** 39, 4326-4335.

(8) Turton, R.; Bailie, R.C.; Whiting, W.B.; Shaeiwitz, J.A. *Analysis, Synthesis, and Design of Chemical Processes*; Prentice Hall: Upper Saddle River, New Jersey, **2003**.

(9) Iwakabe, K.; Nakaiwa, M.; Huang, K.; Nakanishi, T; Røsjorde, A.; Ohmori, T.; Endo, A.; Yamamoto, T. Performance of an internally Heat-Integrated Distillation Column (HIDiC) in separation of ternary mixtures. *J. Chem. Eng. Japan* **2006**, 39, 417–425.

(10) Horiuchi, K.; Yanagimoto, K.; Kataoka, K.; Nakaiwa, M.; Iwakabe, K.; Matsuda, K. Energy saving characteristics of the internally heat integrated distillation column (HIDiC) pilot plant for multicomponent petroleum distillation. *J. Chem. Eng. Japan* **2008**, 41, 771–778.

(11) Marler, R.T.; Arora, J.S. Survey of multi-objective optimization methods for engineering. *Struct. Multidisc. Optim.* **2004**, 26, 369–395.

(12) Kim, I.Y.; de Weck, O.L. Adaptive weighted-sum method for bi-objective optimization: Pareto front generation. *Struct. Multidisc. Optim.* **2005**, 29, 149–158.

(13) Wilson, G.M. A New Expression for the Excess Free Energy of Mixing. *J. Am. Chem. Soc.* **1964**, 86, 127.

(14) Redlich, O.; Kwong, J.N.S. On the Thermodynamics of Solutions V. An Equation-of-state. Fugacities of Gaseous Solutions. *Chem. Rev.* **1979**, 44, 223–244.

(15) Rathore, R. N.S.; Van Wormer, Kenneth A.; Powers, G. J. Synthesis strategies for multicomponent separation systems with energy integration. *AIChE J.* **1974,** 20, 491-502**.**

(16) Chao, K.C.; Seader, J.D. A General Correlation of Vapor-Liquid Equilibria in Hydrocarbon Mixtures. *AIChE J.* **1961**, 7, 598–605.

(17)Peng, D.-Y.; Robinson, D. B. A New Two-Constant Equation-of-state. *Ind. Eng. Chem. Fundam. 1***976,** 15, 59–64.

(18) Cardona Alzate, C. A.; Sánchez Toro, O. J. Energy Consumption Analysis of Integrated Flowsheets for Production of Fuel Ethanol from Lignocellulosic Biomass. *Energy* **2006**, 31, 2447-2459.

(19) Dias, M. O. S.; Modesto, M.; Ensinas, A. V.; Nebra, S. A.; Filho, R. M.; Rossell, C. E.V. Improving Bioethanol Production from Sugarcane: Evaluation of Distillation, Thermal Integration and Cogeneration Systems. *Energy* **2010**, 36, 3691-3703.

(20) Mulia-Soto, J. F.; Flores-Tlacuahuac, A. Modeling, Simulation and Control of an Internally Heat integrated Pressure-swing Distillation Process for Bioethanol Separation. *Comput. Chem. Eng.* **2011**, 35, 1532-1546.

(21) Hernández, S. Analysis of Energy-efficient Complex Distillation Options to Purify Bioethanol. *Chem. Eng. Technol.* **2008**, 31, 597-603.

(22) Rudenko, A. I.; Gershundi, A. N.; Kalabina, L.V. Some Characteristics of Ethylene Glycol as a Heat-transfer Agent for Closed Two-phase Systems, *J Eng. Phys. Thermophys.* **1997**, 70, 799-804.

(23) Seider, W. D.; Seader, J.D.; Lewin, D.R.; Widagdo, S. *Product and Process Design Principles;* John Wiley and Sons, Inc. 3rd International student edition, **2010**.

(24) Humbert, S. ; Margni, M.; Jolliet, O. IMAPCT 2002+: User Guide Draft for version 2.1, **2005**, http://www.sph.umich.edu/riskcenter/jolliet/IMPACT2002+/IMPACT2002+_UserGuide_for_v2.1_Draft_October2005.pdf

(24) Humbert, S. ; Margni, M.; Jolliet, O. IMAPCT 2002+: User Guide Draft for version 2.1, **2005**, http://www.sph.umich.edu/riskcenter/jolliet/IMPACT2002+/IMPACT2002+_UserGuide_for_v2.1_Draft_October2005.pdf

(25) **International Energy Agency. CO_2 emissions from fuel combustion.**

http://www.iea.org/co2highlights/co2highlights.pdf, visited August 1st 2012.

Chapter 5

Final remarks

5.1 Summary

The synthesis problem of distillation sequences has been widely researched because the urging need to find sequences which can realize low cost and low energy consumption. However, synthesis problems that consider internal heat integration, vapor recompression and thermally coupled distillation simultaneously and systematically remain unexploited. To find intensified distillation sequences by means of internal heat integration, vapor recompression and/or thermally coupled distillation, this presented thesis has proposed systematic methods to solve the unsolved synthesis problems.

The presented synthesis problems have the following three features:

1. Superstructure representations, which included from conventional columns (one feed and two product streams) to thermally coupled columns (multiple feeds and product streams) as eligible candidates to find the optimal distillation sequence. The proposed superstructures were based on the state task network representation. A state was defined in terms of a molar composition and its thermal condition while a task was defined as a distillation column operating at a predefined pressure where columns at different pressures were regarded as different tasks even though they can satisfy the same states.
2. Rigorous simulations of each task to readily deal with two crucial problems in distillation, which are the inherent nonlinearity owing to complex thermodynamic relations and non-convexity owing the product of molar composition by molar flow. Consequently, rigorous simulations were advantageous to obtain reliable data on the design (e.g, number of trays, diameter) and the operating conditions (e.g., reflux ratio, condenser and reboiler duty, and work duty) of each task which satisfies the already defined states even for the cases of non-ideal mixtures.
3. Mathematical programming formulation based on superstructure representations and reliable data obtained from rigorous simulations. Mathematical programming was the adopted optimization tool to find the best combination of tasks, which can result in the optimal distillation sequence in terms of total annual cost, energy consumption and/or environmental

impact. Hence the mass balance constraints were satisfied by the rigorous simulation, only connectivity constraints among tasks and energy balance constraints for all the tasks were necessary to solve the optimization problems, which were formulated as Mixed Integer Linear Programming (MILP) problems.

Moreover, the combination of the aforementioned three features is systematic, needs few rigorous simulations, and is compiled in a commercial optimization software without too much effort. Thus, it is also remarkably more advantageous than typical trial-and-error approaches or the execution of only mathematical programming approaches. Trial-and-error approaches are not systematic and are impractical for the separation of multicomponent mixtures in industrial practice because an excessive number of simulations are required. Mathematical programming approaches are systematic, but they are based on assumptions (e.g., short-cut methods, 100% tray efficiency, ideal or nearly ideal mixture, etc.) to avoid, at some extent, the inherent nonlinearity and non-convexity in distillation. In addition, the engineer must have strong mathematical and computational skills to obtain a solution, which in most cases requires long computation time.

Summarizing, the combination of the three features requires far less rigorous simulations than trial-and-error approaches and far less computation time than only mathematical programming based approaches.

The combination of superstructure representations, rigorous simulations and mathematical programming is the main originality in this thesis to solve the synthesis problems where external heat integration, internal heat integration and vapor recompression are possible in conventional and/or thermally coupled columns.

The assessment of the adopted energy conservation methods and the development of new concepts introduced to comprehensibly address the synthesis problems will be covered in turns for each chapter.

Chapter 2 dealt with the synthesis problem, which included external and internal heat integration in conventional columns where the use of compressors was not allowed. Internal heat integration significantly differs from external heat integration in two aspects. Firstly, external heat integration is defined by the match between a vapor stream to the condenser of one column and a liquid stream to the reboiler of another column while internal heat integration is defined by the match of any of the stages in the rectifying section of a column to any of the stages in the stripping section of another column, but excluding the match between a condenser and a reboiler. Such difference results in an exceedingly increased combinatorial problem, which makes more difficult to obtain the best heat integration network. Secondly, in external heat integration, the net reduction of condenser and reboiler duty in the two columns is equal to the amount of energy exchanged; however, in internal heat integration, the net reduction of condenser and reboiler duty in the two columns depends on the location of the match between stages and the amount of energy exchanged. These characteristics

make even more important the selection of the best heat exchange network. Because of the two main differences between external and internal heat integration, the synthesis problems in previous researches have been limited to two columns while the synthesis problem for more than two columns remains unexploited. In chapter 2 the concept of “compensation term” was developed to systematically obtain external and internal heat integration networks among several columns. With a reduced number of simulations, the effect of side condensers in the net reduction of condenser duty and the effect of side reboilers in the net reduction of reboiler duty can be estimated effectively. The compensation terms resulted from the heat removed/supplied in all stages of all the tasks were added to the first the optimization level to find the best heat exchange network between two columns. Then, the amount of heat exchanged and the overall compensation term for each pair of columns were added to the second optimization level as a parameter to find the best distillation sequence among several columns. At each optimization level, only one objective function was assessed. At the first optimization level the net reduction of reboiler duty for each pair of columns was minimized while at the second optimization level the total annual cost of the best sequence among columns was minimized. In addition, for comparison reasons, the optimization procedure was performed for the case the concept of “compensation term” was not considered, this case was regarded as the Column Grand Composite Curve (CGCC) approach. Later, from simple energy and mass balances, calculations of the reflux ratio and reboil ratio after internal heat integration were derived for the optimal sequences. The optimization results from the proposed approach and the CGCC approach were compared with those results from the execution of rigorous simulations.

Chapter 3 dealt with the synthesis problem, which included external heat integration, internal heat integration in conventional and thermally coupled columns, but the use of compressors was allowed through vapor recompression. The inclusion of vapor recompression into the synthesis problem offers appealing futures because vapor streams to condensers can be at higher temperature resulting in more heat integration possibilities than only external heat integration. The concept of “aggregated task” was developed to represent thermally coupled columns in the synthesis problem. In addition, recompression of vapor streams between thermally coupled columns can enhance their “thermal flexibility” resulting from more heat integration possibilities within thermally coupled columns which is unlikely to happen in typical thermally coupled columns because they operate only at one fixed pressure. The concept of “thermal flexibility” regards to thermally coupled columns, which operate at different pressures. The expensive equipment and electricity cost of compressors have limited the implementation of vapor recompression in practice. Because these costs cannot be neglected, they are explicitly included in the optimization procedure. The concept of “compensation term” was applied also to thermally coupled columns in this chapter. Three synthesis problems were addressed in this chapter: external and internal heat integration in conventional columns, external heat integration and vapor recompression in conventional and thermally coupled columns, and

external heat integration, internal heat integration and vapor recompression in thermally coupled columns. For the first and third synthesis problems, a similar optimization procedure to the one in Chapter 2 at the first optimization level was proposed while for the second synthesis problem, an optimization procedure similar to the second level in Chapter 2 was proposed. In all the synthesis problems the equipment cost and the electricity cost of compressors was included. As a result, connectivity constraints for compressors and terms for vapor compressors in the energy balance constraints and in the objective function were added. At each optimization level, only one objective function was assessed. At the first optimization level the net reduction of reboiler duty for each pair of conventional or thermally coupled columns was minimized while at the second optimization level the total annual cost of the best sequence among columns which can realize vapor recompression was minimized. Later, from simple energy and mass balances, calculations of the reflux ratio and reboil ratio after internal heat integration were derived for the optimal sequences. The optimization results from the proposed approach were compared with those results from the execution of rigorous simulations.

The results from the proposed optimization procedure and those from only rigorous simulations in Chapters 2 and 3 showed some differences when the concept of “compensation term” was adopted, but still the difference was not large. This means that the proposed optimization procedures can result in tight lower bounds for the feasible optimal solutions from rigorous simulations. However, the result from the CGCC-approach had large deviations when compared to the result from rigorous simulations; therefore, the CGCC-approach was not adopted in Chapter 3. In Chapter 2, the combination of external and internal heat integration in conventional columns realized the minimum total annual cost while in Chapter 3, thermally coupled columns without heat integration realized the minimum total annual cost. In Chapter 3, the best solutions without compressors showed lower total annual cost than the best solutions where the use of compressors was enforced. To obtain suboptimal solutions, the optimal solution in each case was penalized and additional constraints were added.

As the number of tasks and states in a superstructure increases the complexity of the problem also increases, but still the computation time was little, between few seconds to few minutes. In addition, as the number of energy conservation methods increases, the possibility to obtain solutions with less energy consumption also increases; therefore the economic assessment is not enough to determine which solution is not only optimal in terms of total annual cost, but also in terms of energy consumption. The results in Chapter 3 showed that the economic optimal solution differs from the energy optimal solution. Moreover, a worsening in the economic savings can result in improving the energy savings. Because of that, Chapter 4 dealt with the optimization of two or more objective functions.

The synthesis problems in distillation have been primarily focused on minimizing the cost or maximizing the profit in distillation sequences, but when several energy conservations methods are included, the optimization of only one objective is not enough to cope with the increasing worldwide restriction on energy usage, global warming and waste disposal of toxic chemicals. Thus, multi-objective optimization offers a solution to find the best trade-off between two or more objective functions.

The energy consumption from steam or electricity is explicitly included in the economic optimization when the total annual cost is to be minimized, however, the obtained solutions do not warranty that the economic optimal solution and the energy optimal solution are the same. To get energy optimal solutions a new objective function was defined in Chapter 4.

The independently optimization of the synthesis problem to find the economic optimal and energy optimal distillation sequences can obtain, at most, two solutions. Because the energy prices are closely related to the global financial market, its cost in the near future is uncertain. To obtain more information about the trade-off between economic and energy optimal solutions, multi-objective optimization was carried out. The optimization results will show, at least one solution but, in most cases a pareto front whit several optimal distillation sequences. From this information, it will be easier to make a better decision on which distillation sequence is the best choice to be realized in an industry.

Chapter 4 dealt with the synthesis problem, which included external heat integration and vapor recompression in conventional and thermally coupled columns. The concept of “aggregated state” was derived. In Chapter 3, three thermally coupled columns with the same topology were adopted, but in Chapter 4, five thermally coupled columns with different topology were adopted. When a section of a thermally coupled column can be moved to another column, the resulting thermally coupled column is not thermodynamically equivalent if pressure change is allowed between columns. As a consequence, the concept of “aggregated state” was developed to identify thermally coupled columns with modified topology. The inclusion of vapor recompression into the synthesis problem has a positive effect because solutions with less energy consumption can be obtained, but it also has a negative effect because the expensive equipment cost and electricity cost of compressors result in solutions with higher total annual cost. To readily assess the trade-off between total annual cost and energy consumption, four multi-objective optimization approaches were adopted. The first approach was the weighted sum approach (WS) because it has been widely used to solve multi-optimization problems, but it has two drawbacks: it cannot find Pareto-optimal solutions in non-convex regions of the Pareto front, and the pareto front is not well distributed. To find solutions in nonconvex regions, the min max weighted sum (MMWS) was adopted as second approach. This second approach was able to find solutions in nonconvex regions, but still the Pareto-optimal solutions were not well distributed. To find well distributed pareto fronts, and adaptive algorithm

was adopted. The third approach combined the weighted sum and the adaptive algorithm (AWS) and the fourth approach combined the min max weighted sum and the adaptive algorithm (AMMWS). These approaches were executed for three case studies, which minimized two objective functions: the total annual cost and the energy consumption. Then, the four approaches where extended for a case study, which minimized three objective functions: the total annual cost, the global warming impact, and the impact of toxic releases into the environment. The pareto front obtained from the AMMWS approach was studied in detail to analyze the Pareto-optimal solutions because it was able to obtain more Pareto-optimal solutions with the minimum average length and length variance in the pareto front. The solutions in the pareto front included conventional and thermally coupled columns with vapor recompression. The economic optimal solution always realized external heat integration while the energy optimal solution always realized vapor recompression in addition to external heat integration when two and three objective functions were minimized. The optimization results for the separation of a five-component mixture showed economic savings up to 39% and energy savings up to 48%. The optimization results for the production of anhydrous ethanol showed that propylene glycol was the entrainer with the best trade-off between economic and environmental optimization criteria.

Table 5.1 summarizes the type of synthesis problem, candidate columns, number of objective functions, and other information.

Table 5.1. Summary of the synthesis problems in each chapter

	Chapter 2	Chapter 3	Chapter 4
Type of column	Conventional	Conventional and thermally coupled	Conventional and thermally coupled
Type of heat integration	Internal External	Internal External	External
Compressor	No	Yes	Yes
Objective	Single	Single	Multiple
Case study	3 components	3 components	3 components 4 components 5 components
Concept developed	Compensation term	Thermal flexibility Aggregated task	Aggregated state

5.2 Future work

The presented ideas and algorithms in this thesis extended the feasible region of optimal solutions in the synthesis problem of distillation columns. Thus, the future work will be in three directions:

Synthesis problems of distillation columns

The synthesis problems in Chapters 2 and 3 dealt with ternary mixtures, but the presented ideas in this chapters are not limited to such case. The synthesis problems will be researched for more than three-component mixtures.

The synthesis problem of internal heat integration by means of compressors between rectifying and stripping section will be proposed by taking into account the concept of "compensation term" to realize optimal sequences where heat integrated distillation columns (HIDiCs) are candidates in the superstructure representation. Apply the synthesis problem to the case of ternary and more than three-component mixtures.

In Chapter 3, thermally coupled columns where limited to those that have the same topology as the Petlyuk column; however, thermally coupled columns with modified topology will be researched and included in the synthesis problem of external heat integration, internal heat integration and vapor recompression.

Mathematical programming

The synthesis problem of external and internal heat integration in conventional columns in Chapters 2 and 3 showed that the calculated the reflux ratio resulted in negative values, which means the solution from optimization procedure could be infeasible. Therefore, as a future work, calculations of the reflux ratio and reboil ratio will be included in the first optimization level to warranty the obtain solutions are feasible.

The synthesis problem of external and internal heat integration in conventional columns in Chapters 2 and 3 was solved in two optimization levels; however, the simultaneous optimization of the internal heat integration network between a pair of columns and the best distillation sequence among several columns will be researched.

The first optimization level in the synthesis problems in Chapters 2 and 3 assumed that the heat exchange network is done in a cascade way starting from the top of a rectifying section or ending at the bottom a stripping section. Thus, a reformulation of the mathematical programming problem will be done to obtain heat exchange network which are not restricted to be in a cascade way.

Dynamic analysis

One of the challenges in the synthesis problem is to obtain the distillation sequence which is optimal from the economic and operational point of view. Set a controllability index in the synthesis problem can be helpful to find distillation sequences, which are likely to be controllable.

The control properties of the generated solutions with internal and external heat integration will be assessed and to explore a trade-off between the amount exchanged through internal heat integration and the controllability of the optimal solution.

The control properties of the generated solutions with external heat integration and vapor recompression will be assessed and to explore a trade-off between the work duty in the compressor and the controllability of the optimal solution.

Energy optimal solutions are unlikely to be implemented in practice owing to an excessive and complex interaction between process streams, heat exchangers, and controllers. Thus, to implement in practice a distillation sequence, the worsening of energy savings might result in the improving on economic savings and on cotrollability, although a detailed design will be carried later.

Acknowledgment

I would like to express my gratitude to Professor Shinji Hasebe for being a great mentor and for all the time and for all I've learnt from him. I would also like to thank him for accepting me into the Department of Chemical Engineering at Kyoto University to conduct my research on Process Systems Engineering.

I would like to thank Professor Manabu Kano, his dedication and his example of hard work has been always a motivation for me to try my best and to chase my dreams.

I would also like to thank Professor Tamon and Professor Miyahara for their very helpful comments and corrections during the elaboration of this thesis.

I would like to thank my family in Mexico because they always have supported me in the pursuit of my dreams and happiness. They are the reason I have tried my best during these years in Japan. To my Father (Rafael) and Mother (Ma. Esther) who are a great example of commitment, discipline, honesty, respect, and love. To my bother (Victor M.) who inspires me whenever we talk with his revolutionary mind. To my lovely sister (E. Rocio) for all her love towards the family and for all the happiness she projects with her beautiful smile.

I have been in Japan for more than three years, during this time I had the chance to meet many people from all over the world, and to get a better understanding of the Japanese culture and language. I would like to thank all the nana-koza staff and members, and all my dear friends in Kyoto University who made my stay more enjoyable, and to my Japanese host mother (Naoko H.) who was always willing to help make my stay better.

I thank God for allowing me to feel the joy of being alive.

Research achievements

Journal publications

1. J.R. Alcántara-Avila, M. Kano, S. Hasebe: Multiobjective optimization for synthesizing compressor-aided distillation sequences with heat integration, *Ind. Eng. Chem. Res.*, **51**, 5911- 5921 (2012). (Chapter 4)
2. J.R. Alcántara-Avila, M. Kano, S. Hasebe: Intensification of distillation sequences by combining internal and external heat integration, (Submitted at *Ind. Eng. Chem. Res.*). (Chapter 2)
3. J.R. Alcántara-Avila, M. Kano, S. Hasebe: Environmental and economic optimization of distillation structures to produce anhydrous ethanol, (Submitted at *Comput. Chem. Eng.*). (Chapter 4)
4. J.R. Alcántara-Avila, S. Hasebe: Synthesis of heat integrated columns (HIDiC) in distillation sequences, (To be submitted). (Chapter 3)

International conferences

1. J.R. Alcántara-Avila, M. Kano, S. Hasebe: Two-Level Approach for Synthesizing Externally and Internally Heat Integrated Distillation Sequences, *APCChE 13th*, Taipei, Taiwan, October 5-8 (2010). (Chapter 4)
2. J.R. Alcántara-Avila, M. Kano, S. Hasebe: Multiobjective optimization for synthesizing compressor-aided distillation sequences with heat integration, *AMIDIQ 2011*, Riviera Maya, Mexico, May 3-6 (2011). (Chapter 4)
3. J.R. Alcántara-Avila, M. Kano, S. Hasebe: Environmental and economic optimization of distillation structures to produce anhydrous ethanol, *ESCAPE 22*, London, UK, June 17-20 (2012). (Chapter 4)
4. J. Cabrera-Ruiz, J. G. Segovia-Hernández, J. R. Alcántara-Avila, S. Hernández: Optimal dynamic controllability in compressor-aided distillation schemes using stochastic algorithms, *ESCAPE 22*, London, UK, June 17-20 (2012). (Collaborative research)

Domestic conferences

1. J.R. Alcántara-Avila, M. Kano, S. Hasebe: Economically and energetically optimal synthesis of complex distillation sequences, *The society of Chemical Engineers, Japan, 43rd Autumn meeting*, Nagoya Institute of Technology, Nagoya, September 14-16 (2011). (Chapter 4)
2. J.R. Alcántara-Avila, M. Kano, S. Hasebe: Intensification of distillation sequences by combining external and internal heat integration, *The society of Chemical Engineers, Japan, 77th Annual meeting*, Kogakuin University, Tokyo, March 15-17 (2012). (Chapter 2)
3. J.R. Alcántara-Avila, S. Hasebe: Intensification of heat integrated distillation columns (HIDiCs) through external heat integration, *The society of Chemical Engineers, Japan, 44th Autumn meeting*, Tohoku University, Sendai, September 19-21 (2012). (Chapter 3)